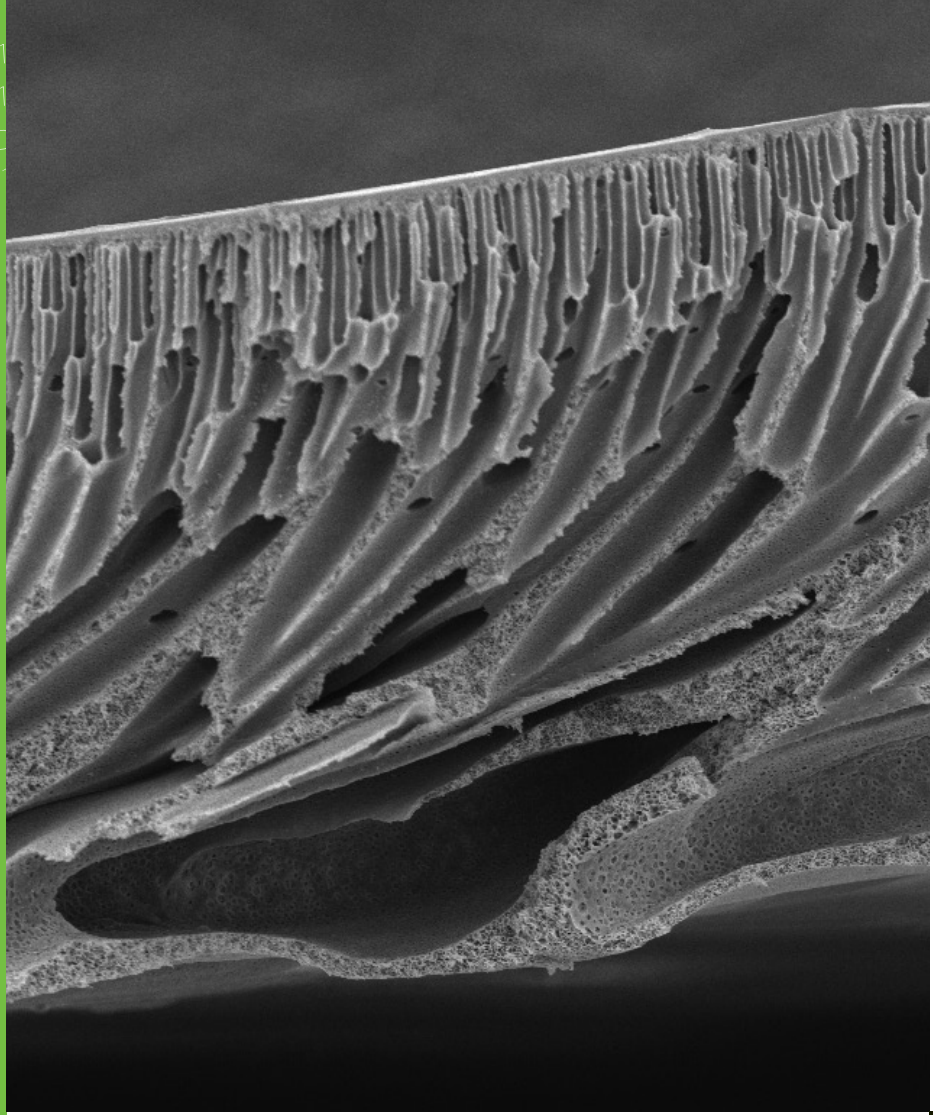

SCIENCE • TECHNOLOGY • RESEARCH HIGHLIGHTS • VISIONS

Dissertation
66

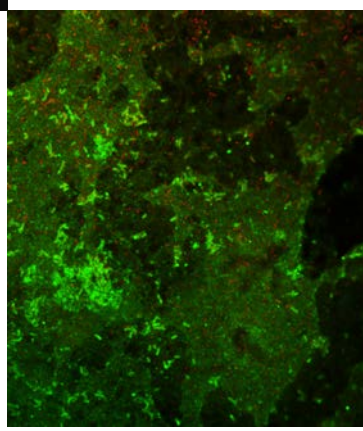

Polymer hybrid thin-film composites with tailored permeability and anti-fouling performance

Juha Nikkola

VTT

VTT SCIENCE 66

Polymer hybrid thin-film composites with tailored permeability and anti-fouling performance

Juha Nikkola

Thesis for the degree of Doctor of Science to be presented with due permission for public examination and criticism in Auditorium RG202, at Tampere University of Technology (Tampere, Finland), on the 31st October, 2014, at 12 noon.

ISBN 978-951-38-8163-4 (Soft back ed.)
ISBN 978-951-38-8164-1 (URL: http://www.vtt.fi/publications/index.jsp)

VTT Science 66

ISSN-L 2242-119X
ISSN 2242-119X (Print)
ISSN 2242-1203 (Online)

JULKAISIJA – UTGIVARE – PUBLISHER

VTT
PL 1000 (Tekniikantie 4 A, Espoo)
02044 VTT
Puh. 020 722 111, faksi 020 722 7001

VTT
PB 1000 (Teknikvägen 4 A, Esbo)
FI-02044 VTT
Tfn +358 20 722 111, telefax +358 20 722 7001

VTT Technical Research Centre of Finland
P.O. Box 1000 (Tekniikantie 4 A, Espoo)
FI-02044 VTT, Finland
Tel. +358 20 722 111, fax +358 20 722 7001

Cover image: Marjo Ketonen and Mari Raulio

Grano Oy, Kuopio 2014

Preface

This thesis was produced at VTT Technical Research Centre of Finland. Some of the experimental parts were done by using the facilities at Department of the Material Science at Tampere University of Technology in Finland, at Nanyang Technological University in Singapore and at Singapore Membrane Technology Centre in Singapore.

The work was part of research projects PLASTEK1 (2005–2007), PLASTEK2 (2007–2009) and FRONTWATER (2010–2015) funded by Tekes – the Finnish funding agency for technology and innovation, VTT and Finnish industry.

I am sincerely grateful to my supervisor, Professor Jyrki Vuorinen from the Department of Materials Science at Tampere University of Technology for the enormous time and effort spent in guidance and advice. I also want to express my gratitude to my instructor at VTT, Professor Chuyang Y. Tang, for valuable guidance and introduction to membrane technologies. My sincere thanks go to the pre-examiners for their valuable comments and advice.

I am deeply grateful to my current and former colleagues at VTT and especially, to Dr. Kalle Nättinen, Mr. Juha Mannila, Ms. Riitta Mahlberg, Ms. Marjo Ketonen, Ms. Sini Eskonniemi, Mrs. Ulla Kanerva, Mrs Lisa Wikström, Mr. Jarmo Siivinen, Dr. Hanna-Leena Alakomi, Dr. Mari Raulio, Dr. Hanna Kyllönen and Mr. Pekka Taskinen. Furthermore, I am grateful to my current and former team leaders Dr. Marke Kallio, Mr. Amar Mahiout, Mr. Tomi Lindroos, Mr. Janne Hulkko and technology managers Dr. Erja Turunen, Dr. Aino Helle, Dr. Tarja Laitinen, Dr. Tuulamari Helaja at VTT. Also, sincere thanks go to Dr. Jing Wei, Dr. Yining Wang and Mr. Xin Liu at Nanyang Technological University. I would also like to thank all my co-authors who have made contributions to the included publications.

Finally, I would like to thank my parents Maria-Lea and Heikki Nikkola as well as my sister Kirsi for all the support and care needed to undertake this journey. Most of all, I would like to thank my wife Jonna for giving all the strength, faith and love, which was really needed. My lovely son Jaki, you are the reason I go on.

Espoo, October 2014

Juha Nikkola

Academic dissertation

Supervisor	Professor Jyrki Vuorinen Department of Materials Science, Tampere University of Technology, Finland
Instructor	Professor Chuyang Y. Tang VTT Technical Research Centre of Finland, Finland
Reviewers	Professor Mika Mänttäri Lappeenranta University of Technology, Finland
	Dr. Dirk Vangeneugden VITO, Belgium
Opponents	Professor Mika Mänttäri Lappeenranta University of Technology, Finland
	Professor José María Kenny University of Perugia, Italy

List of publications

This thesis is based on the following original publications which are referred to in the text as [P1–P6].The publications are reproduced with kind permission from the publishers.

[P1] K. Nättinen, J. Nikkola, H. Minkkinen, P. Heikkilä, J. Lavonen, M. Tuominen, Reel-to-reel inline atmospheric plasma deposition of hydrophobic coatings, Journal of Coatings Technology and Research, 8 (2011) 2, 237–245.

[P2] J. Nikkola, Raising the barriers, European Coatings Journal, 1 (2011) 41–47.

[P3] T. Hirvikorpi, M. Vähä-Nissi, J. Nikkola, A. Harlin, M. Karppinen, Thin Al_2O_3 barrier coatings onto temperature-sensitive packaging materials by atomic layer deposition, Surface and Coatings Technology, 205 (2011) 21–22, 5088–5092.

[P4] J. Nikkola, H.-L. Alakomi, C. Y. Tang, Bacterial anti-adhesion of coated and uncoated thin film composite (TFC) polyamide (PA) membranes, Journal of Coating Science and Technology, 1 (2014) 1–7.

[P5] J. Nikkola, X. Liu, Y. Li, M. Raulio, H.-L. Alakomi, J. Wei, C. Y. Tang, Surface modification of thin film composite RO membrane for enhanced anti-biofouling performance, Journal of Membrane Science, 444 (2013) 192–200.

[P6] J. Nikkola, J. Sievänen, M. Raulio, J. Wei, J. Vuorinen, C. Y. Tang, Surface modification of thin film composite polyamide membrane using atomic layer deposition method, Journal of Membrane Science, 450 (2014) 174–180.

Author's contributions

[P1] Contributed to the coating trials, conducted the AFM characterisation, supervised and analysed the characterisation results (SEM and FTIR) and was the co-author in the manuscript.

[P2] Designed and synthesised the sol-gel coatings, planned and conducted the coating trials, applied the coatings on the selected substrates, conducted the AFM characterisation, supervised and analysed the other characterisation results (SEM, contact angle of oleic acid and OTR) and was the main author of the manuscript.

[P3] Designed and conducted the synthesis of sol-gel hybrid coatings, planned the lab-scale sol-gel coating trials, applied the sol-gel coatings on the selected substrates, conducted the AFM characterisation, analysed the characterisation results (water contact angle, OTR, WVTR) and was the co-author of the manuscript.

[P4] Conducted the AFM characterisation, supervised and analysed the other characterisation results (water contact angle, surface energy and microbiological studies) and was the main author of the manuscript.

[P5] Designed and fabricated the PVA coatings, planned the lab-scale coating trials, applied the coatings on the selected substrates, conducted the AFM and FTIR characterisation, supervised and analysed the other characterisation results (SEM, water contact angle, surface energy measurements, microbiological studies, separation studies) and was the main author of the manuscript.

[P6] Designed and supervised the fabrication of ALD coatings, planned the lab-scale coating trials, conducted the AFM and FTIR characterisation, supervised and analysed the other characterisation results (SEM, water contact angle, surface energy measurements, microbiological studies, separation studies) and was the main author of the manuscript.

Contents

List of abbreviations and symbols

ALD	Atomic-layer-deposition
Al_2O_3	Aluminium oxide
APD	Atmospheric plasma deposition
BO	Biaxial orientation
BOPP	Biaxially oriented polypropylene
CA	Cellulose acetate
CFU	Colony-forming unit
DBD	Dielectric barrier discharge
DIZ	Diffusion inhibition zone
GLYMO	3-Glycidyloxypropyltrimethoxysilane
HMDSO	Hexamethyldimethoxysiloxane
H_2O	Water
EPS	Extracellular polymer substances
EtOH	Ethanol
EVOH	Ethylene vinyl alcohol
MF	Microfiltration
MIP	Microwave induced plasma

NaCl	Sodium chloride
NAMS	(3-(2-Aminoethylamino)propyltrimethoxysilane
NF	Nanofiltration
LBL	Layer-by-layer deposition
LDPE	Low-density polyethylene
OTR	Oxygen transmission rate
PA	Polyamide
PE	Polyethylene
PECVD	Plasma enhanced chemical vapour deposition
PES	Polyethersulfone
PET	Polyethylene terephthalate
PEG	Polyethylene glycol
PHMG	Polyhexamethylene guanidine hydrochloride
PLA	Polylactic acid
PP	Polypropylene
PVA	Polyvinyl alcohol
PVDC	Polyvinylidene chloride
RF	Radiofrequency
R_{RMS}	Root-mean-square roughness
RO	Reverse osmosis
SG	Sol-gel
SiOx	Silicon oxide
TEOS	Tetraethoxysilane

TFC	Thin-film composite
TMA	Trimethylaluminium
UF	Ultrafiltration
WVTR	Water vapour transmission rate
WV	Water vapour

Parameters

P	Permeability coefficient
S	Solubility coefficent
D	Diffusion coefficient
q	Quantity of permeant
A	Area
t	time
l	Thickness
Δp	Partial pressure difference
J_v	Water flux
Q_p	Volumetric flow rate of permeate
A_m.	Membrane area
ΔP	Applied pressure
$\Delta \pi$	Osmotic pressure
R_m	Hydraulic resistance of the membrane
η	Viscosity
R_g	Universal gas constant (R_g = 8.31 J/mol K)

T	Temperature
C	Molar concentration
C_f	Concentration of feed solution
C_p	Concentration of permeate solution
R	Rejection of a membrane
A	Water permeability coefficient
B	Solute permeability coefficent
R_f	Hydraulic resistance caused by fouling
R_c	Hydraulic resistance caused by coating

1. Introduction

Economic pressures and competition have created a need for superior performance and multifunctional properties of materials. The ever-increasing demand for new product properties makes it challenging to achieve the required features when using traditional materials. Therefore, new material combinations (i.e. hybrid or composite materials) are intended to meet these challenges, providing added value for the existing products or creating novel spinoffs.

The difference between hybrid and composite materials is narrow, and in some cases the terms overlap. Hybrid material can be defined as a combination of materials, which are composed of at least two different materials, usually inorganic and organic [1]. Indeed, hybrid material is typically a blend, multilayer or nanostructured material. Moreover, composite is a consolidation of materials, in which the matrix material is further enhanced using particles, fibres or coatings.

In recent years, significant progress has been made in the choice of materials and in the manufacturing routes for nanocomposites. Totally new properties can be obtained using only nanoscale fillers [2]. For example, carbon nanotubes and fibres have been studied for reinforcement in nanocomposites [3]. Among the nanocomposite research, the modification of bulk material has gained most attention. Nevertheless, the fabrication of such materials in the form of thin films can also provide special features. For example, a thin-film composite (TFC) structure can be expected to tailor the permeability of polymeric films applied in various industrial applications, ranging from non-permeable packaging to semi-permeable membranes. TFCs usually have a three layer structure, containing a support, a core and a skin layer.

Permeation is described as diffusion of a permeate (e.g. liquid, gas, ions or particles) from a high concentration to a low concentration [4]. Permeability is the measured material permeation property, describing the penetration of permeate through a solid interface [4]. Tailored permeability of a material usually indicates the creation of a barrier against a permeate [5]. These barrier layers can be semi- or non-permeable structures. The former is a mesoporous bulk material or coating layer, which rejects the desired gases, vapours, liquids, ions or particles, and is permeable for the targeted substance, while the latter is a nonporous bulk material or a coating layer, which rejects the targeted substances.

Food and pharmaceutical packaging is a typical example, where non-permeable features are desired. Food packaging is needed to protect the items of food from various exposures. New developments aim to improve the barrier properties or to create antimicrobial activity to prevent the microbiological spoilage of food [6]. Furthermore, recyclable and renewable materials are considered to increase the sustainability of packaging by replacing the existing metal or polymer coatings. Therefore, various new polymers, biopolymers, nanoparticles and coatings have been studied [6]. Another recent trend in packaging material development is leading towards high barrier performance with a minimal amount of material [6]. Therefore, there is a need for functional coatings on paper, paperboard and plastic laminates for special or enhanced properties in the field of paper converting.

A water treatment membrane is used in various filtration processes to provide purified water or other liquids. A membrane is a typical example of a semi-permeable structure [7]. The membranes used in reverse osmosis (RO) and nano-filtration (NF) have a nearly nonporous structure [8]. The commercial RO and NF membranes are based on either cellulose acetate (CA) or polyamide (PA) TFC. The latter is composed of polyethersulfone (PES) cast on non-woven as a core and a support layer, which is further coated with PA as a skin layer. The fouling of membranes, such as colloidal fouling (inorganic and organic) or biofouling, is a critical issue in pressure-driven membrane processes [9]. The routes for low-fouling membranes include new polymers or their combinations, and incorporation of nanoparticles, biocides or pore-forming agents [10]. In addition, various anti-fouling coating approaches have been presented in the literature [10]. The optimal surface properties have, however, remained undetermined. Further research is, therefore, needed to identify the connection between membrane surface properties and the accumulation of biofilm.

Figure 1 presents the materials and processes of this thesis. Firstly, the aim was to fabricate a TFC with tailored permeability. Secondly, the aim was to enhance the anti-fouling performance of a TFC-PA. Industrially applicable and novel coating methods were used so as to fabricate TFCs by using roll-to-roll or batch processes. Inorganic, inorganic-organic and organic surface chemistries were created using coating methods such as sol-gel (SG), atmospheric plasma deposition (APD), atomic-layer-deposition (ALD) and polyvinyl alcohol (PVA) based dispersion. These were deposited either as skin layers on a low-density polyethylene (LDPE) or a polylactic acid (PLA)-coated board or as a top-coating on a TFC-PA membrane.

The scientifically novel contribution of this thesis is as follows. The thesis contributes to the development of novel TFC structures using various coating methods. The novel TFC structures provide new alternatives or improvements for the existing barrier materials in food packaging. In addition, the developed anti-fouling coatings tackle the critical challenge of membrane fouling and introduce new low-fouling TFC-PA membranes for water treatment.

The effects of coating chemistry and composition of the multilayer structure were studied in order to find optimal permeability. In particular, the difference between 2- and 3-dimensional oligomeric sol-gel coating layers was of interest. Non-polar polymers (e.g. LDPE) are known for their low-adhesion to coatings or

inks. Therefore, it was essential to study the effect of plasma-assisted deposition and pre-treatment on the adhesion between the coating layers and the substrate. The polymer surfaces (e.g. PLA) can be relatively rough and therefore challenges can be expected when applying a uniform and nano-sized coating layer. Consequently, the effect of a primer layer was also needed to study the deposition of an extremely thin ALD layer.

In membrane technologies for water treatment, the permeability is targeted to remain unmodified after applying a top-coating. For example, the permeability of a membrane may be reduced when an additional anti-fouling coating layer is used. In this thesis, organic and inorganic anti-fouling coatings were developed for TFC-PA membranes with bacterial anti-adhesion and antimicrobial performances. Firstly, the effect of the surface physiochemical properties on the attachment of bacteria was of interest. The correlation between surface polarity and bacteria repellence was demonstrated by using PVA and ALD coatings. In addition, for the first time the ALD method was studied as a surface modification of TFC-PA membranes. Secondly, the anti-fouling performance was further enhanced by the combination of a biocide effect with the desired surface properties. The PVA-based antimicrobial coatings were investigated in order to overcome an uncontrolled leaching of biocides.

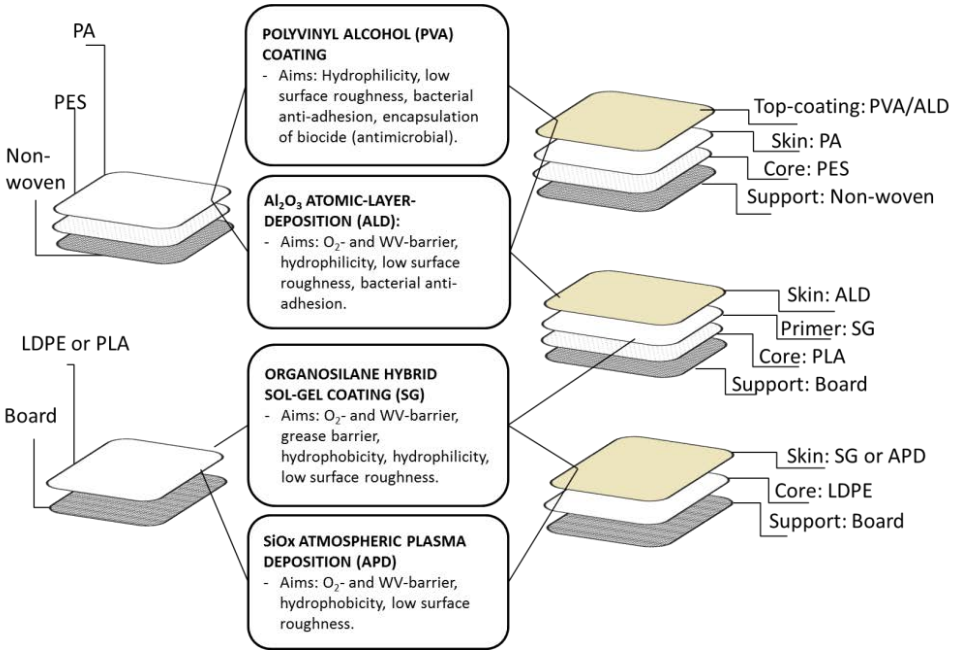

Figure 1. The schematic presentation describes the materials and processes of the PhD thesis, which investigates various coating technologies in order to tailor the permeability and anti-fouling performance of thin-film composites.

2. Advanced surface modification of polymeric substrates

The surface modification of a polymeric material can occur as a result of a chemical or a physical reaction [11]. In addition, a coating layer may attach to a substrate by mechanical interlocking.

The chemical reaction can occur through grafting-to or grafting-from methods, when appropriate chemically reactive groups can be found on the surface. The linkage or coupling directly to the existing end groups of the surface is called the grafting-to method [12]. This does not cause changes in the bulk material. In some cases, surface activation is needed prior to the coating deposition. The grafting-from method involves a chemical reaction of the coating to the solid surface, after it has been physically activated [12]. In general, the surface activation involves controlled degradation of the surface, using high energy radiation, such as electron beam, plasma or ultraviolet (UV) radiation.

The chemical bonding of the coating on the substrate is not necessary in every case. A coating application is also possible through physical adsorption, where the coating is attached by electrostatic forces [11]. Layer-by-layer deposition (LBL) is a common method to produce an electrostatically adhered coating. In addition to chemical and physical bonding, the coating can be attached by mechanical interlocking. In this case, the coating is attached on a rough or porous structure of the substrate [11]. Moreover, the attachment of the coating may be a combination of a chemical or physical reaction with mechanical interlocking.

2.1 Atmospheric plasma pre-treatment of polymers

Corona and plasma treatments of polymers are known to enhance their wettability and adhesion to coatings, inks and adhesives [13]. Moreover, a hydrophilic surface tends to provide better adhesion than hydrophobic ones [11]. The surface energy can be tailored according to the need using different treatment gases or chemicals. Figure 2 presents schematically the difference of plasma-activation and plasma deposition.

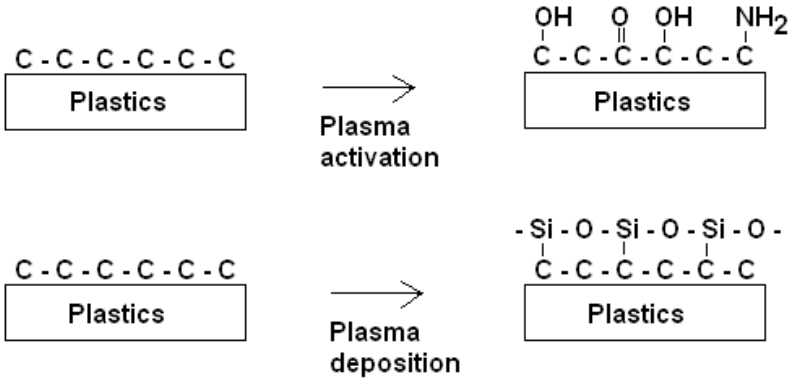

Figure 2. Plasma activation and plasma deposition [P1].

Corona treatment is one of the oldest industrial methods of polymer surface activation. Various plasma technologies have been developed in order to overcome some of the limitations of the corona technology [14]. In comparison to plasma technologies, surface-activation effect of the corona is less stable, and tailoring of plasma chemistry with different monomers or gases is limited. Dielectric barrier discharge (DBD), radio frequency (RF) and microwave induced plasma (MIP) technologies have been developed so as to generate plasma treatment for batch application [15]. In recent years, cold or non-equilibrium atmospheric pressure plasmas have been developed to produce new functionalities of heat-sensitive substrates [16,17]. Figure 3 shows an example of atmospheric plasma pre-treatment unit. In comparison to vacuum plasma treatments, less effort has been put into atmospheric pressure plasma developments as pre-treatments for coatings and deposition methods.

Both vacuum and atmospheric plasma technologies have been used for surface activation of various polymers [13]. In particular, the modification of surface energy and hydrophobicity by plasma or corona pre-treatment is necessary, when using non-polar plastic substrates, such as polypropylene (PP) or polyethylene (PE). Comparative studies have been carried out for screening the different pre-treatment methods to enhance the adhesion of a sol-gel coating on polyolefin [18]. The plasma pre-treatment showed a stronger effect on the adhesion of the sol-gel coating in comparison to chemical acid etching. When the pre-treatment was not used, the sol-gel coating delaminated during the curing process. Besides the increased surface hydrophilicity, a short-term (e.g. 15–30 s.) plasma treatment may reduce the surface roughness of polymers [19]. This may be attributed to cleaning of the surface by plasma flame. On the other hand, a long-term (e.g. 5 min.) plasma treatment time has been shown to increase the surface roughness [19]. Furthermore, high-temperature vacuum plasma treatment may already degrade the polymer surface, also causing undesired changes in the bulk material. In some cases, the increased surface roughness may enhance the adhesion of a coating.

However, the surface roughness should not exceed the thickness of the coating layer. Low-temperature atmospheric plasma treatment may overcome these challenges. Moreover, atmospheric plasma has resulted in a strong increase in the surface energy, while the surface roughness was not affected [19]. Atmospheric plasma experiments have been shown to create durable hydrophilicity for improved adhesion between polymer surfaces and additional coating layers [20].

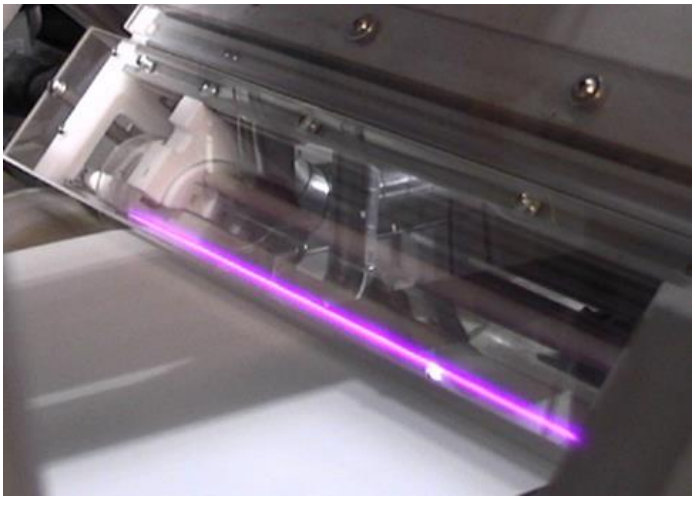

Figure 3. An example of atmospheric plasma pre-treatment unit.

2.2 Atmospheric plasma deposition of thin coatings on polymers

Recently, atmospheric plasma deposition (APD) of functional coatings on plastic films has gained increasing attention [16]. The main advantages of atmospheric plasma systems are the possibility of using different treatment gases and gas mixtures as well as deposition of chemicals [14]. In addition, the processing is more flexible and feasible, because there is no need to use a vacuum reactor or other low pressure systems.

An example of a plasma deposition unit and its configuration is described in Figure 4. Plasma deposition or plasma enhanced chemical vapour deposition (PECVD) is typically based on dielectric barrier discharge (DBD) plasma [16]. The two general types of PECVD methods are direct (glow) and remote (afterglow). In the direct method, the monomer is fed together with the plasma gas to the discharge area, resulting in reaction of the monomer. In the remote method, the monomer is fed and activated in the downstream of the discharge and, thus, only the carrier gas is fed through the discharge. Deposition of various molecules or compounds is allowed. Furthermore, the substrate has a enough long distance from the discharge, enabling treatments of heat-sensitive materials, such as polymers.

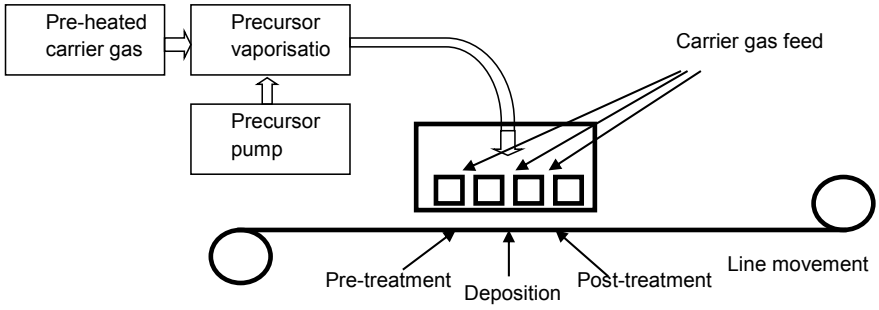

Figure 4. An example of atmospheric plasma deposition (APD) unit configuration [P1].

Fabrication of a hydrophobic silicon oxide (SiOx) coating layer on polyester terephthalate (PET) film has been the target in most of the studies [21]. For example, hexamethyldisiloxane (HMDSO) has been used as an SiOx source. In addition, glass-like coatings have been produced using tetraethoxysilane (TEOS) monomer with oxygen-helium carrier gas [22]. The TEOS monomer was used to enhance the abrasion resistance properties of the polymer surface. Furthermore, inorganic-organic hybrid coatings have been produced on PET to replace polyvinylidene chloride (PVdC) barrier coatings with atmospheric plasma deposited hybrid coatings [23]. In addition, polymeric coatings have been deposited on PP using the atmospheric plasma method [24].

The effects of APD conditions have been studied by analysing the surface properties of a coating [21]. For example, the increase of monomer flow rate has improved the hydrophobicity of coatings deposited on PET substrate. The use of lower flow rates may have led to a thinner or a discontinuous coating. In addition, the experiments have shown that the SiOx coating became more silica-like (SiO_2), when the air concentration was increased in the argon carrier gas [21].

2.3 Hybrid coatings synthesised using the sol-gel route

The sol-gel process involves the evolution of inorganic networks in a continuous liquid phase through the formation of colloidal suspension and following gelation of the sol [25]. The sol-gel process can be used to manufacture various materials, including coatings, powders, monoliths, capsules, fibres or aerogels. The main advantages of the sol-gel thin films are the homogeneity and purity of the end-products formed at relatively low temperatures.

Metal or non-metal alkoxides are used as monomers in a typical sol-gel synthesis for coatings. The sol-gel synthesis is based on controlled hydrolysis and condensation reactions. Reaction 1 represents the hydrolysis, where M is usually silicon, zirconium or titanium and n generally equals four [25]. Hydrolysis acts as a rapid initial reaction of sol-gel processes, where reactive alkoxide groups (-OR, where R is e.g. CH_3, CH_3CH_2, $CH_3(CH_2)_2$) react with water molecules to form hydroxyl groups (-OH). After the initiation of the reaction, the hydrolysed alkoxides

easily react with each other, forming dimers through the condensation reaction. Water or alcohol is obtained as a by-product, depending on the reaction mechanism. The condensation reactions are described with reactions 2 and 3.

$$M(OR)_n + H_2O \rightarrow M(OH)(OR)_{n-1} + ROH \quad (1)$$

$$M(OH)(OR)_{n-1} + M(OR)_n \rightarrow (OR)_{n-1}MOM(OR)_{n-1} + ROH \quad (2)$$

$$2\,M(OH)(OR)_{n-1} \rightarrow (OR)_{n-1}MOM(OR)_{n-1} + H_2O \quad (3)$$

The alkoxide monomers have a different reactivity, which is related to the partial charge of the metal or the non-metal alkoxide [25]. The reactivity of the monomers in hydrolysis and condensation reactions can be accelerated or hindered by using catalysts or by increasing or decreasing the reaction temperature.

Sol-gel coatings can be applied on various surfaces to provide functional properties. Easy-to-clean, self-cleaning as well as anti-fouling coatings have been developed by using sol-gel chemistry. The surface chemistry (e.g. polarity) and topography (smooth or rough) can be modified based on the performance requirements. Furthermore, active agents such as biocides can be incorporated to the sol-gel coating matrix.

Figure 5 presents schematically the basis of sol-gel processing of thin coatings. A variety of different types of thin films and coatings can be synthesised by using the sol-gel technology. In general, the sol-gel thin films can either be pure inorganic or inorganic-organic hybrid materials. Different wet chemical coating methods can be used depending on the targeted approach. Drying of the applied coating is an important step, where solvents and water are evaporated in order to avoid cracking in the final curing stage. Typically, the thickness of inorganic layers is from 20 nm to 200 nm. The film thickness of the inorganic sol-gel thin film as a one-layer system cannot be raised much more, due to possible cracking behaviour.

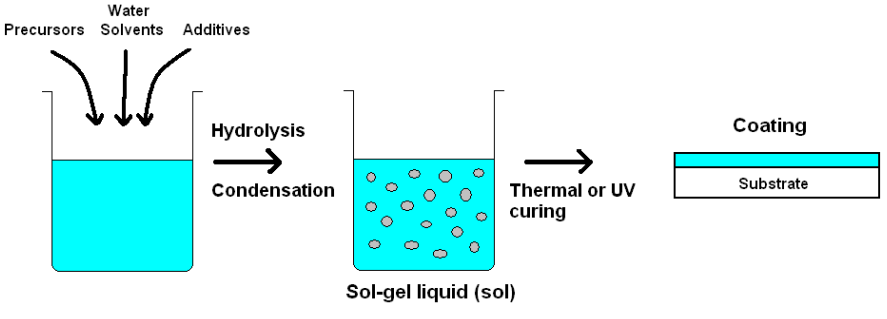

Figure 5. Schematic presentation of sol-gel processing of thin coatings.

From the late 1980s, there has been an increasing interest in preparing inorganic-organic hybrid coatings using sol-gel syntheses [26]. The basic idea is to introduce

organic components into the nanostructured glass-like (e.g. SiO_2) or ceramic (e.g. ZrO_2, Al_2O_3) network. Thus, the hybrid coating is not as fragile as the pure inorganic coatings. Therefore, the coating thickness can be increased from tens of nanometres up to tens of micrometres. The hybrid coatings are typically two or three dimensional (2D or 3D) oligomer structures [26]. For example, TEOS can be used to form the inorganic Si-O-Si backbone. TEOS bonds via hydrolysis and condensation reactions to organically modified alkoxysilanes, which can contain variety of different functional groups that can be used to provide hydrophilic, hydrophobic or even antimicrobial behaviour. This route can be used to create a 2D oligomeric structure. The 3D oligomeric hybrid structure is synthesised quite similarly as the 2D structure. The main difference is the use of silane coupling agents, which are organically modified alkoxysilanes or polymeric monomers, containing reactive groups (e.g. amino, isocyanate, vinyl, acryl, mercapto, methacryl or epoxy). These are able to polymerise, when induced using initiators, catalysts, cross-linkers, heat or radiation (e.g. UV or plasma) [16]. The 3D oligomer structure may improve the mechanical properties, elasticity and plasticity of the end-product. In addition, the highly cross-linked hybrid structure may be favourable for creating enhanced barrier performance.

Recently, the sol-gel technology has evolved to the next level and a few attemptions to produce sol-gel coatings in inline process have been presented [16,23,P2]. Furthermore, the development of inorganic-organic hybrid structures makes it a potential choice to apply the sol-gel coatings on flexible paper, board or plastic film surfaces. The possibility to include functional groups and tailor-made the surface chemistry makes the sol-gel technology even more desirable.

2.4 Atomic-layer-deposition of inorganic thin coatings on polymers

Atomic-layer-deposition (ALD) is a chemical vapour deposition (CVD) technique based on cyclic and self-terminating gas–solid reactions. ALD can be considered as an advanced version of CVD technology. ALD technology enables the manufacturing of several different kinds of inorganic materials such as oxides, nitrides, sulphides and others with thickness down to the nanometre range [27]. Moreover, polymeric and inorganic-organic hybrid films have been manufactured by using ALD technology [28].

One of the most studied ALD processes is deposition of Al_2O_3 thin films, which are prepared using trimethylaluminium (TMA, $Al(CH_3)_3$) and water or ozone as monomers [28]. The self-terminating reaction of TMA with water is also considered to be an ideal example of ALD process. The TMA monomer is highly reactive as well as thermally stable. The $Al(CH_3)_3$-H_2O process involves switches from methyl- to hydroxyl-terminated aluminium as presented by the side reactions in equations 4 and 5. Methane is obtained as a gaseous reaction product and it does not diminish the growth-per-cycle (GPC) of the Al_2O_3 thin film. Furthermore, the overall reaction of $Al(CH_3)_3$-H_2O process is presented in equation 6.

$$Al\text{-}OH + Al(CH_3)_3\ (g) \rightarrow Al\text{-}O\text{-}Al(CH_3)_2 + CH_4\ (g) \quad (4)$$

$$Al\text{-}CH_3 + H_2O\ (g) \rightarrow Al\text{-}OH + CH_4\ (g) \quad (5)$$

$$2\ Al(CH_3)_3\ (g) + 3\ H_2O\ (g) \rightarrow Al_2O_3\ (s) + 6\ CH_4\ (g) \quad (6)$$

Figure 6 presents the ALD device used in this thesis. In a typical Al_2O_3 ALD process, vaporized TMA and H_2O monomers are fed as pulses one-by-one into a vacuum chamber. Between the monomer pulses, an inert gas purge (e.g. N_2) is used so as to remove unreacted monomers and by-products. After the gas purge, the saturated surface layer of the TMA can react with H_2O, which is again subjected to a gas purge in order to complete the first ALD cycle [27]. These cycles can be repeated according to the desired film thickness or coating functionality.

Recent advances in ALD technology have increased its potential to produce functional thin films on flexible and temperature-sensitive polymeric materials [29]. ALD has also been applied to coat various fibrous polymers [30,31,32,33]. Although the ALD process is mainly carried out in batches in its current state, the development of a slow-speed roll-to-roll ALD technology is underway [34].

Figure 6. An example of atomic-layer-deposition (ALD) device.

3. Non-permeable packaging films

3.1 Permeability

Permeates (e.g. liquid, gas, ions or particles) diffuse from high concentration to low concentration [4]. The phenomenon is called permeation. The penetration of a permeate through a solid interface is described by permeability. Permeability is the material permeation property [4]. The transfer of permeate molecules through a material is a process that includes sorption, desorption and migration [4]. In general, the permeate molecules attach onto a material surface by a sorption mechanism. Migration occurs, when the attached molecules diffuse through the material. Finally, diffused molecules detach to the environment by desorption on the other side of the material.

Diffusion, solubility and permeability are the main parameters used to describe the mass transfer for a material [4]. The mass transfer of molecules can be described by the permeability coefficient (*P*) of the material [4]. The permeability coefficient, *P*, can be calculated using a solubility coefficient (*S, solubility*) and a diffusion coefficient (*D, diffusivity*). The permeability coefficient, *P*, is the volume of vapour (*q*) passing through a unit area of the polymer in a time unit, with a pressure difference unit across the polymer:

$$P = S * D = \frac{q*l}{A*t*\Delta p} = \frac{(quantity\ of\ permeant)\ x\ (film\ thickness)}{(area)\ x\ (time)\ x\ (partial\ pressure\ difference)} \quad (7)$$

where, *S* is a thermodynamic term describing the volume of vapour per unit volume of polymer per unit pressure, *D* is a kinetic term indicating the velocity of the molecule in the specific material. Respectively, *q* is the quantity of the permeant transferred by a unit of area (*A*) in a specific time (*t*), *l* is the thickness of the material, and Δ*p* is the partial pressure difference.

The barrier performance of packaging material can be determined using various barrier measurements [35]. In general, the molecules diffusing into and through the packaging material are detected. For example, the measurement of gas and water vapour transmission is of interest due to their effect on the shelf-life of the packaged product. The oxygen transmission rate (OTR) is the quantity of oxygen (O_2) molecules passing through an area in a certain time period under specified conditions of temperature, humidity and pressure [35]. The OTR measurement is

based on the O_2 flux diffusing through the sample, which is detected using an electrochemical (non-coulometric) or a coulometric oxygen sensor. In the literature various units have been used to report permeability of gases [35]. The most commonly used unit for permeability of gases in barrier polymers is (cm^3 mil) / (m^2 day atm). Respectively, the water vapour transmission rate (WVTR) determines the amount of water vapour transmitted through an area in a certain time under specified conditions of temperature and humidity [36]. There are many standard procedures for measuring WVTR using gravimetric methods [37,38]. The most commonly used unit for permeability of water vapour in barrier polymers is (g mil) / (m^2 day). OTR and WVTR values are reported in the literature as normalised to a layer thickness of 1 mil (1 mil = 25.4 µm).

3.2 Traditional packaging materials

Microbiological contamination is one of the major causes of food losses in the world [39]. Food packaging has been part of the food supply chain for decades. Among the traditional preservation systems, packaging technologies have an important role in securing food safety [40]. Furthermore, barrier films are needed in pharmaceutical packaging applications.

Packaging has to protect the substance from various environmental exposures, including oxygen, moisture, light, microbes and dust. Moreover, packaging material has certain requirements in terms of its usability (e.g. fresh outlook or decorative), technical aspects (e.g. sealability, easy opening, applicability for food contact, recyclability or refilling) and reasonable price [39].

Paper and paperboard (i.e. board) are so-called traditional packaging materials. They have several advantages, which make their use as food packaging extremely favourable. Paper and board meet the needs, because they have the required usability and technical properties, which enable their cost-effective use in a wide range of packaging structures. Furthermore, they can be coated, laminated or impregnated to improve their barrier properties and to extend their functional performance, such as heat sealability, heat resistance, barrier, grease resistance or product release. For example, board can be extrusion-coated using polymeric coatings made of polyethylene (PE).

Other traditional polymeric packaging materials include polypropylene (PP), polyamide (PA), polyethylene terephthalate (PET) and ethylene vinyl alcohol (EVOH) [16]. Furthermore, packaging performance can be further enhanced using surface treatments such as, polyvinylidene chloride (PVdC), wax, silicone or fluorocarbon based coating. Coatings can be applied by flexo, soft bar, foam, curtain and spray coating methods, including optional pre-treatments by plasma or corona and post-treatments/curing by cold or hot air drying, IR-drying or UV-curing.

Recently, bio-based and renewable coating materials have been introduced as a sustainable alternative to the petroleum-based polymeric materials [41]. For example, polylactic acid (PLA) has been applied to some extent in commercial

products. In addition, other bio-based materials, such as starch, xylan, chitosan and cellulose, have been investigated [41].

3.3 Developments of barrier films for packaging application

The polymers may have a variety of oxygen (O_2) and water vapour (WV) barrier properties, which are affected by their chemical structure, crystallinity and orientation [5]. Concerning the O_2 permeability, the presence of polar groups in polymer chains often increases the chain rigidity and decreases the specific free volume. This can further increase its packing density and therefore, increase crystallinity in the polymer. As a result, the permeability of gaseous molecules is reduced through the polymer [5]. For example, a PLA contains more polar groups than an LDPE, and lower O_2 permeability has been measured for PLA in comparison to LDPE. Respectively, PET and PA have lower O_2 permeability in comparison to PP [42]. On the other hand, the polymer chain flexibility affects on the gas permeability. The non-polar methyl ($-CH_3$) attached PP structure decreases the mobility of chains and decreases the gas permeability. Thus, PP has somewhat lower permeability compared LDPE [5]. Concerning the WV permeability, the hydrophobicity of a polymer has an effect [5]. The non-polar structure shows repellence of polar water molecules. This partly explains the lower water vapour permeability of PP and PE in comparison to the other substances.

The stretching of amorphous and semicrystalline polymer films can improve their barrier properties. For instance, biaxial orientation (BO) of PET, PP and PA reduces both the O_2 and WV permeability [43]. Furthermore, lamination and extrusion coating are two additional industrial processes for producing multilayer barrier structures [41]. Several polymeric layers can be coated to form a high barrier material. For example, EVOH is typically extrusion-coated as one layer in the 3- or 5-layer system. Use of EVOH has led to a slight improvement in the barrier properties [41]. The drawback of multilayer lamination is the increase in the coating thickness and, therefore, the increase of net weight of the packaging.

Active packaging materials have been widely studied and patented in recent years [40]. Active packaging materials include various types of functional systems, for example, oxygen, carbon dioxide and ethylene scavengers, carbon dioxide and ethylene emitters, moisture scavengers, ethanol emitters and absorbing systems as well as antimicrobial packaging materials [2]. Currently, oxygen and moisture scavengers are commercially the most significant, but other techniques have been predicted to play an important role in the near future.

Another recent trend in packaging materials is the change towards new functionalities using nanosized materials, such as nanoclays [2]. In addition, new surface treatments and coating technologies have been introduced to traditional packaging materials. The novel thin coating technologies may provide thinner barrier films. The replacement of conventional coating materials such as polyolefins, EVOH, fluorocarbons and silicones, typically several microns thick, by nanoscale coatings has the evident benefits of both a reduction of consumed materi-

als and negative effects on recyclability. Furthermore, these new coating methods may replace the existing metallisation treatments in the future.

Recently, sol-gel hybrid coating and ALD technologies have shown promising barrier performance enhancement, when deposited on polymeric film or polymer (e.g. PLA or LDPE) coated board [44,45,P2,P3]. Among the ALD-coated PLA-board specimens, Al_2O_3 ALD coating showed better barrier performance than SiO_2 [45]. Concerning the LDPE-board, the studies revealed that ALD-coating did not show as good barrier performance as shown for PLA-board [45]. This can be explained by the difference between the reactivity of the PLA and LDPE surfaces. Therefore, corona or plasma pre-treatment or primer layers could be used to improve the film growth or adhesion.

Some of the commercially available approaches include deposition of silicon oxide (SiOx) or aluminium oxide (AlOx)-based inorganic coatings on a polymer film for barrier property improvements [46]. The SiOx coating has been shown to reduce O_2 and WV permeability of PET [47]. Furthermore, the oxygen and water vapour barrier of a BOPP film can be enhanced by deposition of nanometre thick inorganic AlOx layer [46]. However, the inorganic coating layers may be fragile and delaminate from the flexible polymer surface.

To overcome the delamination issue, thin-film composite (TFC) concepts have been developed, where thin organic and inorganic coating layers are separately deposited on polymers. The TFC concept for enhanced O_2 barrier properties has already been presented in the late 1990s by Haas et al [48]. They deposited hybrid sol-gel on a PP film, which was followed by the deposition of a SiOx layer. In addition, enhancement of barrier properties has been obtained with TFC structure of an AlOx and a few micrometre thick acrylate coating. Recently, a combination of sol-gel hybrid coating and ALD technologies has also shown promising barrier performance enhancement, when deposited on polymeric films or polymer coated boards [P3].

4. Semi-permeable thin-film composite membranes

4.1 Reverse osmosis (RO) membranes

Membrane filtration technology is used in various industries to provide purified water from sources including, mining, biorefinery, brackish, processing, or seawater [7]. Moreover, the membrane filtration technology is utilised in microfiltration (MF), ultrafiltration (UF), nanofiltration (NF) and reverse osmosis (RO) [8]. These methods have been applied in water and wastewater treatment, desalination and water re-use since the late 1960s.

Reverse osmosis (RO) membranes are nonporous systems which retain particles and low molecular weight species such as salt ions, micropollutants, pesticides and pharmaceuticals [8]. The commercial RO membrane materials are either cellulose acetate (CA) or thin-film composite (TFC) membrane, which consists of polyamide (PA) as a selective layer and polyethersulfone (PES) cast on nonwoven as a support layer [8]. The traditional CA membranes were developed in the late 1950s and commercialized in the early 1960s. CA has formerly been widely used, but nowadays TFC-PA membranes are more common. The TFC-PA membranes offer several advantages over the CA membranes, such as improved retention, increased productivity at lower operating pressures, great structural stability, and the ability to produce two to three times more purified water per unit area than CA membranes [49].

Both of the TFC-PA and CA membranes have one common challenge restricting their usage in industrial processes: fouling. Membrane fouling has an unwanted effect on membrane separation efficiency as well as on energy consumption [9]. Membrane permeability declines, resulting in unstable water flux behaviour, and therefore feed pressure should be increased in order to stabilize the process [50].

4.2 Permeability of reverse osmosis (RO) membranes

Permeability of a membrane is important for applications in water and wastewater treatment. In general, there is a strong trade-off between water permeability and

salt rejection. The more water permeable membrane tends to have lower salt rejection and higher solute permeability [8].

An adequate water flux is essential because of its relationship to the membrane productivity and process economics. Water flux is defined as a mass (or a volume) passing through a membrane unit within a given duration of time [8]. The pure water flux J_v is typically defined as:

$$J_v = \frac{Q_p}{A_m} \tag{8}$$

where Q_p is the volumetric flow rate that permeates through the defined membrane area A_m. In the literature the typical unit for water flux is L/m^{2}h.

The effect of the applied pressure (ΔP) and the osmotic pressure ($\Delta\pi$) of the solution on the permeate flux should be taken into account in the pressure-driven membrane systems [8]. Therefore, Darcy's law can be commonly determined according to the following equation:

$$J_v = \frac{(\Delta P - \Delta\pi)}{\eta R_m} \tag{9}$$

where R_m is the hydraulic resistance of the membrane and η is the viscosity of the permeating water. R_m can be determined for a membrane according to its water permeability (A):

$$R_m = \frac{1}{\eta A} \tag{10}$$

The applied pressure ΔP, i.e. the trans-membrane pressure (TMP), is the difference between the applied pressure on the feed water side and the pressure of permeate water [8]. The osmotic pressure, $\Delta\pi$, of the solutions can be determined by the van't Hoff equation:

$$\pi = R_g\, T \sum C \tag{11}$$

where R_g is the universal gas constant (R_g = 8.31 J/mol K), T is the absolute temperature given in Kelvin degrees, and C is the molar concentration of dissolved substances. In addition to the water flux, solute retention is one of the most important performance parameters for a membrane process. The retention ability of a membrane in water applications is expressed by the membrane rejection. Membrane rejection (R) can be determined by:

$$R = \frac{C_f - C_p}{C_p}\, x\ 100\ \% \tag{12}$$

where C_f and C_p are the concentrations (via conductivity measurements) of the feed and permeate solutions, respectively. Based on the literature, the solution-diffusion model is the most widely used transport model for RO membranes [8]. It is assumed that both solvent and solute absorbs into the rejection layer and diffuses through the nonporous layer [8]. Therefore, the water flux, J_v, through an RO membrane corresponds to the applied pressure (ΔP-$\Delta\pi$). Respectively, solute flux, J_s, through an RO membrane corresponds to the concentration difference (ΔC) across the membrane.

$$J_v = A(\Delta P - \Delta\pi) \tag{13}$$

where A is the effective water permeability of an RO membrane.

$$J_s = B(\Delta C) \tag{14}$$

where B is the effective solute permeability of an RO membrane. A more fundamental property describing the real salt permeability of an RO membrane is the solute permeability coefficient (B) [8]. The solute permeability coefficient can be determined from the water flux and rejection test results via:

$$B = A(\Delta P - \Delta\pi)(\frac{1}{R}\text{-}1) \tag{15}$$

4.3 Fouling of reverse osmosis (RO) membranes

Membrane fouling occurs when particles and solutes accumulate on the mass transfer boundary layer of the membrane and they begin to impede the solvent flow through the membrane [9]. Fundamentally, the fouling layer increases the hydraulic resistance on the membrane surface and, therefore, Darcy's law for water flux (J_v) can be determined according to [8]:

$$J_v = \frac{(\Delta P - \Delta\pi)}{\eta(R_m + R_f)} \tag{16}$$

where, R_f is the hydraulic resistance caused by fouling. After the initiation of the fouling macromolecules, proteins, gels or particles will continue adsorbing on the membrane surface [9]. The types of membrane fouling are classified into colloidal (inorganic and organic) and biological fouling (i.e. biofouling). Inorganic fouling (i.e. scaling) is occurred by deposition of major ions on membrane surface including calcium, magnesium, barium, bicarbonate, sulphate and inorganic salts. This causes pore-blocking and reduction of the water flux. The scaling is mainly avoided chemically by using antiscalants and pH control to pre-treat the feed solution before the separation process. Organic fouling typically involves attachment of proteins and humic acid on the membrane surfaces. Several researchers have studied the effects of the surface properties on the organic fouling tendency of the commercial RO membranes [51,52,53].

Biofouling is generally initiated by adhesion and accumulation of the microorganisms, which is followed by primary colonization and logarithmical growth [54]. In addition, a number of the microorganisms, such as bacteria, can be detected within the network of extracellular polymer substances (EPS). It is difficult to completely eliminate biofouling and, therefore, it is problematic for all membranes, especially in RO and NF processes [54]. The biofouling tendency of commercial membranes has been studied by several research groups [55,56,57]. Moreover, a few studies have concentrated on the interaction between bacteria and the surface properties of a variety membranes [58,59,60,61]. These previous studies have revealed that bacterial anti-adhesive behaviour varies between the different membranes.

The membrane surface properties have been shown to play an important role in affecting biofilm formation [62]. Studies have shown that membrane surface properties such as hydrophobicity, surface roughness and surface charge have an effect on the reduction in fouling [63]. Most of the commercial RO membranes are hydrophilic rather than hydrophobic. For example, it has been shown that TFC-PA and CA membranes have water contact angle values between 20–60º [62]. The TFC-PA membranes for RO processes are typically aromatic or semi-aromatic. Fully aromatic PA membranes are formed by 1,3-benzenediamine (m-phenylenediamine) and trimesoyl chloride (1,3,5-benzenetricarbonyl chloride) [64]. Respectively, the semi-aromatic poly(piperazinamide) membranes are formed by piperazine and trimesoyl chloride [64]. However, it is difficult to conclude whether the RO membrane has a hydrophilic nature based on chemical structure. Some of the commercial TFC-PA membranes are coated with an additional thin polyvinyl alcohol (PVA) layer in order to introduce a hydrophilic and smooth surface [64]. The water contact angle value of a fully aromatic PA membrane is reduced significantly by applying the PVA coating. On the other hand, the PVA coating layer has only a minor effect on the semi-aromatic membranes [64].

4.4 Development of low-fouling thin-film composite membranes

The development of new anti-fouling RO membranes has gained increasing attention [10]. In many cases, an anti-fouling membrane is achieved by combining the surface physiochemical properties, such as increased hydrophilicity, lowered surface roughness and neutralised surface charge [10]. These physiochemical anti-fouling properties are commonly referred to as anti-adhesion surfaces. In addition, antimicrobial surfaces have been presented as an active anti-fouling approach. Several different ways have been used to modify a membrane material itself or its surface by an additional coating layer.

The membrane material has usually been modified using polymer blends or composites, which consist of another polymer or some additives including titanium dioxide (TiO_2) or silica (SiO_2) nanoparticles and biocides (e.g. silver, copper, zinc or quaternary ammonium) [65]. In several approaches, improved water flux through a membrane is achieved by incorporating pore-forming agents, such as

silica, zeolites, carbon nanotubes and aquaporin protein into the skin or membrane layer [66].

Various different surface treatments have been developed for RO membranes. These include: 1) surface grafting of antimicrobial groups, 2) contact active amphiphilic, microbe-repelling or anti-adhesive polymers, 3) functional coating methods (LBL, casting, dipping, soaking or spraying) or 4) reactive coating methods (CVD, sputtering, UV and plasma immobilization) [10]. An ideal fouling-resistant coating would be an ultrathin, highly water-permeable surface layer that does not significantly increase the resistance to water flux [11]. The additional coating layer may indeed increase the hydraulic resistance of the membrane surface and the flux can thus be determined using Darcy's law:

$$J_v = \frac{(\Delta P - \Delta \pi)}{\eta(R_m + R_c)} \tag{17}$$

where, R_c is the hydraulic resistance caused by the coating. For example, the water flux through the membrane may be reduced, if the top-coating layer is much more hydrophobic, denser or thicker in comparison to the PA rejection layer.

The surface modification occurs mostly on the outermost surface of a membrane. For example, the CA membrane surface bears several hydroxyl groups for the chemical bonding. Furthermore, low concentrations of the amino or carboxylic groups can be found in TFC-PA membranes. Most of the polymeric membranes are, however, chemically rather stable and thus the controlled activation of the membrane is complicated or even impossible without changing the polymer bulk material morphology. Therefore, grafting-from approaches have been used in order to increase the reactive area of the surface and, furthermore, to increase the coverage of applied surface modification [11]. For example, the silylation of surfaces by using functional alkoxy- or chlorosilanes is one of the well-known methods for introducing reactive groups (amino, isocyanate, aldehyde, epoxide or carboxyl) onto a solid surface. The silylation layer is typically only molecular with a thickness of about 1 nm. In addition, physical activations (ion, plasma or UV) have been used to improve the adsorption of the coupling agents on the membrane surface.

Concerning the development in low-fouling TFC-PA membranes, the research groups have applied their surface treatments to either commercial or experimental TFC-PA membrane. The different treatments can be divided into passive (e.g. hydrophilication and lowering surface roughness) and active (e.g. antimicrobial) fouling prevention approaches as well as methods focusing on flux improvement [10]. Most of the studies have focused on the deposition of hydrophilic polymer brushes, which have either anionic or non-ionic behaviour [67,68,69]. For example, polyethyleneglycol (PEG), methacrylate acid (MA), polyethyleneglycolmethacrylate (PEGMA) and copolymers of N-isopropylacrylamide and acrylic acid (P(NIPAm-co-AAc)) have been applied on TFC RO membranes for repellence of bacteria and protein [70,71,72]. Some of the approaches have focused on plasma-assisted grafting of molecular layers. Also, plasma deposition has been used to fabricate

the coatings [73,74]. Silane coupling agents have recently been used to create hydrophilic and hydrophobic surfaces on TFC-PA membrane. This approach showed a flux decline of the TFC-PA membrane, because of increased hydrophobicity by the silane coupling agents. On the other hand, the use of silane coupling agents significantly increased the salt rejection of the TFC-PA membrane [75,76,77]. A few research groups have investigated atomic-layer-deposition (ALD) technology as surface modification of porous polymeric and ceramic membranes, which are used in microfiltration and ultrafiltration [78,79,80,81,82]. These studies suggested that ALD processing parameters, such as temperature and the number of ALD cycles, have a clear impact on membrane performance. For example, they have shown an effect on the pore size of membranes, which has affected solute permeability and rejection properties [80,81]. Furthermore, hydrophilic and low surface roughness polymeric membranes have been obtained by using TMA based ALD technology [79]. This could increase the potentiality of the ALD method to create low-fouling membrane surfaces. However, hydrophilicity and low surface roughness have typically been obtained using a relatively thick ALD coating, such as 300–500 ALD cycles [78,80]. In addition, change in the ALD processing temperature has an effect on the reactivity of TMA [31]. For example, the most hydrophilic membrane surface has been obtained at 150ºC [78].

5. Aims of the study

The aims of this research were to fabricate and modify thin-film composite structures with tailored permeability and anti-fouling performance. In particular, the interest was in studying the effects of pre-treatment, coating chemistry and multi-layer coating structure on the permeability of a thin-film composite (TFC). In addition, the thesis aimed to gain further understanding of the anti-fouling phenomena of coated TFC membranes.

This study was limited to industrially applicable coating methods by studying both roll-to-roll and batch processes. Inorganic, organic and inorganic-organic surface chemistries were created using coatings based on sol-gel (SG), atmospheric plasma deposition (APD), polyvinyl alcohol (PVA) and atomic-layer-deposition (ALD). These were deposited either as a skin layer on low-density polyethylene (LDPE) or polylactic acid (PLA)-coated board, or as a top-coating on a polyamide (PA)-based TFC membrane. Because of the variety of substrate materials, the coating application processes were investigated together with the surface properties obtained by a coating. The end-applications were targeted for food packaging [P1–P3] and for water treatment membranes [P4–P6]. The research questions of this study were as follows:

- Can TFC structure be fabricated with tailored permeability?
    - Does SiOx coating form on LDPE-board using atmospheric plasma deposition? [P1]
    - Does atmospheric plasma pre-treatment enhance the wettability and adhesion of sol-gel coatings deposited on LDPE-board? [P2]
    - Does 2-dimensional or 3-dimensional sol-gel network have different effect on the gas permeability of LDPE-board? [P2]
    - Do TFC structure-based sol-gel and ALD coatings reduce the gas and water vapour permeability of PLA-board? [P3]
- Does top-coating enhance the anti-fouling performance of TFC membrane?
    - Does the increase in surface polarity reduce the attachment of model bacteria? [P4–P6]

- Can an organic or inorganic coating layer create an anti-fouling effect on a TFC membrane without sacrificing the permeability of the substrate? [P5–P6]
- Can the anti-fouling effect be enhanced by combining hydrophilicity and low surface roughness with antimicrobial additives? [P5]
- What is the effect of ALD processing temperature and number of ALD cycles (i.e. film thickness) on hydrophilicity, surface roughness and permeability of TFC membrane? [P6]

6. Experimental procedures

6.1 Substrate materials

A variety of substrate materials were used in this thesis. These were polyamide (PA)-based thin-film composite (TFC) membranes and low-density polyethylene (LDPE) or polylactic acid (PLA) coated board. Table 1 summarises the substrate materials for the characterisation and coating deposition.

Table 1. The substrate materials used for the characterisation and coatings.

ID	Substrate material	Provider
LDPE-board	Low-density polyethylene coated (LDPE 15 g/m^2) board (210 g/m^2)	Stora Enso Oyj
PLA-board	Polylactide-coated (PLA 35 g/m^2) board (210 g/m^2)	Stora Enso Oyj
BW30	PVA-coated thin-film composite; polyamide (PA), polyethersulfone (PES), non-woven.	Dow FilmTec ltd.
SW30HR	PVA-coated thin-film composite; polyamide (PA), polyethersulfone (PES), non-woven.	Dow FilmTec ltd.
LE	Thin-film composite polyamide (PA), polyethersulfone (PES), non-woven.	Dow FilmTec ltd.
XLE	Thin-film composite polyamide (PA), polyethersulfone (PES), non-woven.	Dow FilmTec ltd.
NF90	Thin-film composite polyamide (PA), polyethersulfone (PES), non-woven.	Dow FilmTec ltd.

6.2 Atmospheric plasma deposition of SiOx coating

The plasma deposition was carried out in three continuous steps: pre-treatment, deposition and post-treatment, as described in Figure 4. The power of the plasma deposition unit was varied between 0.4–2.0 kW. The treatment width was 380 mm. Helium and argon were used as the carrier gas in the three carrier gas feeds of the equipment. The gas feed was 90 litres/min in the middle slit and 60 litres/min

in both side slits. In a typical plasma deposition experiment, the precursors were vaporized in the pre-heated carrier gas prior to the deposition. The SiOx source was hexamethyldisiloxane (HMDSO) precursor and it was used as such. The precursor (HMDSO) feed was 980 g/h. With the target of developing an industrially applicable plasma deposition method, the line speeds of 2, 5, 50, 100 and 200 m/min were used.

6.3 Synthesis and processing of sol-gel hybrid coatings

Three different kinds of sol-gel hybrid coatings were synthesised in this thesis. For the purpose of this study the coatings were named SG200, SG204 and SG206. The following alkoxysilane monomers (Figure 7) were used in this study: tetraethoxysilane ($Si(OC_2H_5)_4$, TEOS), octyltriethoxysilane ($C_{14}H_{32}O_3Si$, C8TES), 3-glycidyloxypropyltrimethoxysilane ($C_9H_{20}O_5Si$, GLYMO) and 3-(2-aminoethylamino)propyltrimethoxysilane ($C_8H_{22}N_2O_3Si$, NAMS). All the monomers were ordered from ABCR and used as such. SG200 (TEOS+GLYMO) was aimed to create a smooth primer layer for ALD layer. SG204 (TEOS+C8TES) was aimed to form a hydro- and oleophobic coating layer. SG206 (NAMS+GLYMO) was aimed to form a tight barrier coating layer. Table 2 summarises the sol-gel formulations synthesised and used in this thesis. All the coatings were prepared by dissolving the alkoxysilane monomers with a certain amount of ethanol (EtOH). The ethanol-silane mixture was vigorously mixed for 30 minutes using a magnetic stirrer. Then a solution of water (H_2O) and nitric acid (HNO_3) was prepared and added to the ethanol-silane mixture during mixing. The sol-gel solutions were mixed for 24 hours.

Table 2. The sol-gel (SG) formulations synthesised and used in the thesis.

	Coating ID /publication		
Monomer	SG200 / [P3] [wt-%]	SG204 / [P2] [wt-%]	SG206 / [P2] [wt-%]
TEOS	13.0	26.4	0
C8TES	0	10.5	0
GLYMO	29.5	0	7.8
NAMS	0	0	24.6
EtOH	45.9	46.8	50.9
H_2O (with HNO_3)	11.2 (0.4)	16 (0.3)	16.0 (0.7)

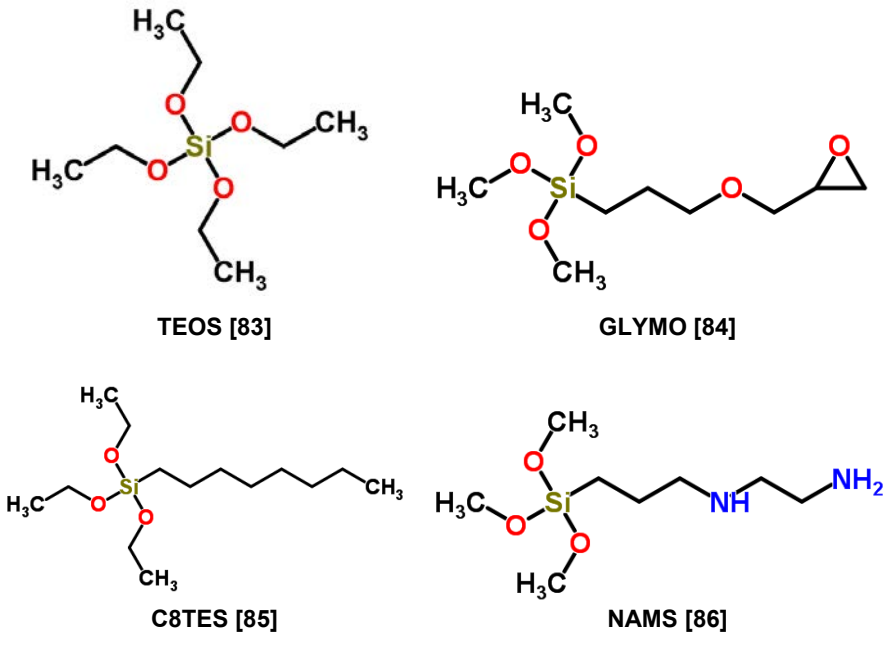

Figure 7. The chemical structures of the monomers used in the sol-gel hybrid coatings.

6.3.1 Sol-gel-coated LDPE-board

The sol-gel coatings, named SG204 and SG206 for this study, were spray-coated onto LDPE-board. The atmospheric plasma equipment with argon or helium treatment gases was used to activate the LDPE surface prior to deposition of the sol-gel coatings. The following parameters were used for the plasma-activation: treatment power 2 kW, treatment width 370 mm, air gap 1–2 mm and speed 100 m/min. The sol-gel hybrid coatings were spray-coated onto the plasma-activated LDPE surface using the line speed of 60 m/min. The coatings were thermally cured in a pilot coating line by using infrared and suspended heaters.

6.3.2 Sol-gel-coated PLA-board

The sol-gel coating, named SG200 for this study, was sprayed onto corona-treated A4-size PLA-board substrates and heat-treated at 120°C for 10 mins. Traditional corona treatment unit (ET1 from Vetaphone, Denmark) with a treatment time of 60 s was used to ensure wetting and adhesion properties between the coating and the PLA-board substrate.

6.4 ALD processing of Al_2O_3 coatings

6.4.1 ALD deposition on sol-gel-coated PLA-board

The ALD-Al_2O_3 depositions were carried out on the sol-gel coated PLA-board at 80°C using a Picosun SUNALE™ reactor (Picosun, Espoo, Finland). Trimethyl-aluminum (TMA, electronic grade purity, SAFC Hitech) and H_2O were used as precursors. The nominal thicknesses of the coating were estimated based on a growth rate of 0.1 nm/cycle [44,45]. In comparison to a silicon wafer, the ALD coatings have shown a minor variation in the actual film thickness, because of the difference in surface chemistry and roughness of different polymers.

6.4.2 ALD deposition on TFC-PA

The ALD-Al_2O_3 depositions were carried out in a Picosun SUNALE™ reactor on substrates that were 10×10 cm^2 in size. TMA and H_2O were used as precursors. Two different processing temperatures (70ºC and 100ºC) and three different ALD cycles (10, 50 and 100) were used to deposit the ALD coatings on the commercial LE-400 TFC-PA membranes. The coated membranes were named according to the coating cycles and temperature (e.g. c10_t70 denotes a membrane with 10 coating cycles at 70ºC). The precursor pulsing sequence was: 0.1 s TMA pulse, 10 s N_2 purge, 0.1 s H_2O, 10 s N_2 purge and the number of ALD cycles was adjusted according to the targeted Al_2O_3 coating thickness (0.1 nm/cycle).

6.5 Preparation and processing of PVA and PVA-PHMG coatings

The following chemicals were used for the membrane surface modification. PVA (molar weight 9000-10,000 g/mol, 80 % hydrolysed) polyvinyl alcohol was purchased from Sigma-Aldrich. PHMG, polyhexa-methylene guanidine hydrochloride ($C_7N_3H_{15}HCl$, Mw 8000-10,000 g/mol) was provided by Soft Protector Oy (Finland). The chemical structures are presented in Figure 8.

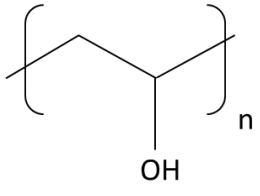

Polyvinyl alcohol (PVA)

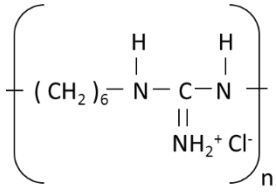

Polyhexamethylene guanidine hydrochloride (PHMG)

Figure 8. Chemical structure of polyvinyl alcohol (PVA) and polyhexamethylene guanidine hydrochloride (PHMG).

The preparation of the PVA coatings was carried out by mixing 2 wt-% of PVA into milliQ water at 60ºC. After complete mixing, the solution was cooled down to room temperature. The PVA-PHMG solutions were similarly prepared as described above, by adding PHMG to the PVA solution after the cooling step. PVA-PHMG solutions were prepared in ratios 95:5 and 99:1 (PVA:PHMG) with a total polymer content of 2 wt-%. The pure PHMG solution (2 wt-%) was prepared by mixing PHMG with milliQ water to reach the targeted concentration. PVA, PVA-PHMG and PHMG solutions were applied on the commercial LE-400 TFC-PA membrane coupons using the dispersion coating method with a K Control Coater K202 device (RK Print-Coat Instruments Ltd., United Kingdom). The device was equipped with a glass bed, and K202 coating bar No. 0 was used to cast the wet films with a thickness of 4 µm. The coatings applied were heat-treated at 110ºC for 2 minutes in order to evaporate the water and to increase the coating stability using thermal cross-linking [87].

6.6 Surface characterisation

A Perkin Elmer spectrum BX II FTIR (Fourier transform IR) system (USA) was equipped with vertical-ATR (Attenuated total reflectance) and KRS-5 (Thallium Bromoiodide) crystal [P3–P6]. ATR-FTIR measurements were carried out in order to analyse the surface chemistry. In a typical analysis 50 scans were collected from 500 to 4000 cm^{-1} at 4 cm^{-1} resolution. A background spectrum of pure KRS-5 was collected before running the samples.

The microscopic imaging was conducted using a scanning electron microscope (SEM) JEOL JSM-6360 LV equipment (USA) with 11 kV on high vacuum mode [P3–P6]. All SEM samples were sputter-coated with gold before imaging.

The surface topographies were characterised using non-contact mode atomic force microscopy (NC-AFM) [P1–P6]. The NC-AFM analysis was performed using Park Systems XE-100 AFM equipment (Suwon, South-Korea), with cantilever 905M-ACTA (AppNano Inc., USA). Typically, the scan rate was 0.4–0.6 Hz, and the measured area was 5x5 μm^2. Six replicate measurements were taken in order to determine the roughness values, average roughness R_a or root-mean-square roughness value R_{RMS}.

The contact angle measurements were taken using an Optical Tensiometer Theta T200 device (Biolin Scientific, Sweden) [P3–P6]. The measurements were taken in a controlled atmosphere (RH 50%, temperature 23ºC) and the results are given as an average of five parallel measurements. The water contact angle values are presented at the time point of 30 s from the moment the drop contacts the surface. The surface energy values were obtained by measuring the contact angle of three different probe liquids, namely water (H_2O, γ = 72.80 mN/m), di-iodomethane (CH_2I_2, γ = 50.80 mN/m) and formamide (CH_3NO, γ = 58.20 mN/m). The total surface energy values, as a summary of polar and dispersive surface energies, were determined from the measured contact angle data using Fowkes' theory [88].

6.7 Anti-fouling performance

Bacterial anti-adhesion

Biofilm formation was demonstrated by analysing the attachment of *Pseudomonas aeruginosa (P. aeruginosa)* on uncoated and coated membranes [P3–P6]. *P. aeruginosa* is Gram-negative, aerobic, rod-shaped bacterium, which is widely used as a model microbe for biofilm formation studies [55,58,89]. Therefore, *P. aeruginosa* was selected as model bacterium in this study so as to provide comparable data related to the attachment of bacteria.

A bacteria attachment test was carried out by submerging the membranes (Ø 4.7 cm) in a bacterial suspension consisted of standard seawater ASTM D1141-98 (2008) [90]. The suspension was inoculated overnight with a culture of *P. aeruginosa* (VTT E-96726) cultivated in 37°C Trypticase soy agar (TSA) broth solution, harvested by centrifugation (3000 rpm, 10 mins) and washed with phosphate-buffered saline (PBS) solution (10 mM). The cell density was approximately 1×10^8 CFU mL^{-1} determined by plate count on a TSA (37°C, 1 day). The 1 day exposure of membranes was conducted in a rotary shaker (75 rpm) at room temperature. The number of adhered cells on the membranes was determined after swabbing by plate count on TSA (37°C, 1 day), and it was intended to describe the anti-adhesion performance. Results are presented as colony-forming units per membrane area (CFU cm^{-2}). Three replicate membrane samples were examined for each membrane type.

Antimicrobial activity

The antimicrobial performance of uncoated and coated membranes was analysed using the colony-forming unit (CFU) test for the two rod-shaped model microorganisms, Gram-positive bacteria *Bacillus subtilis* (ATCC 6633) and Gram-negative bacteria *Escherichia coli* (ATCC 8739) [P5]. These bacteria are extensively used to investigate surface antimicrobiality [91,92]. Bacteria cultivation was conducted by following the instruction of the producer, ATCC (24 hour cultivation for *B. subtilis* in 30°C nutrient broth solution and 12 hour cultivation for *E. coli* in a 37°C nutrient broth solution, respectively). Bacterial cells were harvested by centrifugation (3,000 rpm, 10 mins) and washed twice with 0.9 % NaCl solution. Harvested bacterial cells were suspended in a 0.9 % NaCl solution to achieve a cell density of 1×10^7 CFU mL^{-1}. The membrane samples (Ø 1.27 cm) were immersed in Milli-Q water for 24 hours before the actual exposure to bacteria suspension. The respective membranes specimens were in contact with the bacterial suspensions for 24 hours. A serial dilution of bacterial suspensions was performed for the CFU test according to CLSI M07-A9 [93]. In the CFU test, 0.1 mL volume of diluents was inoculated and spread on a nutrient agar plate, and incubated for another 24 hours. CFU results were obtained from 3 measurements of 3 independent membranes, and each measurement was based on the results of 3 replicate agar plates.

A diffusion inhibition zone (DIZ) method was conducted to analyse the antimicrobial performance of the coatings in more detail [P5]. DIZ test of surface modified membranes were performed by following the CLSI document M2-A9 26:1 [94]. 100 µL bacterial inoculums were spread on the agar plates. Punched membrane discs (Ø 12.7 mm) were placed on the agar plates and incubated at 24 hour cultivation for *B. subtilis* at 30°C and 12 hour cultivation for *E. coli* at 37°C. The diffusion inhibition zones formed around the membranes were determined by visual observation.

6.8 Barrier performance and permeability

Grease barrier

The grease barrier performance of the specimens was studied by contact angle measurements with oleic acid using an Optical Tensiometer Theta T200 device [P2]. The contact angle was followed for 25 seconds to estimate the grease barrier effect.

The durability of the grease barrier effect and thus the adhesion of the coatings to the substrate were studied by measuring the contact angle of oleic acid before and after an abrasive wearing [P2]. The wearing test was carried out using a modified standard paint washing tester apparatus (modified standard DIN 53778), where a brush was used as an abrasive material (1000 abrasion cycles).

OTR and WVTR transmission

The oxygen and water vapour transmission rate (OTR and WVTR, respectively) values were measured for determination of the gas and vapour permeability of the barrier films [P3].

The OTR values were measured (Systech M8001or Mocon Oxtran 2/20) from two to three parallel samples using humid gases at 23°C and in 50% relative humidity. The size of samples was either 50 cm^2 or with masking 5 cm^2. 100% oxygen was used as the test gas.

The WVTR values were measured from two to three parallel samples according to the modified gravimetric methods ISO 2528:1995 and SCAN P 22:68 with a moisture gradient of 75% relative humidity (at 23°C).

Water permeability and salt rejection

Uncoated and coated membranes were tested in a lab-scale crossflow filtration setup in order to evaluate their water permeability and salt (NaCl) rejection according to Wang *et al*. [95]. Briefly, membranes were tested at a feed pressure of 27.6 bar (400 psi) using a feed water containing 10 mM NaCl. The temperature of the feed water was maintained at 23°C. Water flux of the membranes was determined by the gravimetric method.

The data obtained from the water flux (J_v) and the salt rejection (R) measurements was used to calculate water (A) and solute (B) permeability. These were

used to analyse the effect of coatings on the membrane separation performance. Water permeability (A) was calculated using the equation $A = J_v / \Delta P$. Solute permeability (B) was correspondingly calculated according to the equation $B = A(\Delta P - \Delta \pi) * (1/R - 1)$.

7. Results and discussion

7.1 Fabrication of thin-film composites with tailored permeability

7.1.1 Atmospheric plasma deposition of SiOx film on LDPE-board

Recently, several authors have presented their studies on novel atmospheric plasma equipment and surface activation or deposition [16–23]. However, the use of atmospheric plasma deposition in roll-to-roll process has not been widely reported [16]. In this work, the SiOx coating was plasma-deposited on LDPE-board using a pilot extrusion coating line equipped with an atmospheric plasma deposition unit [P1]. In general, the aim was to create SiOx coating on LDPE-board and to study its surface properties.

The appearance of the SiOx coating on the LDPE surface was confirmed using FTIR [P1]. The comparative analysis of the SEM images of both the plain LDPE surface and the plasma deposited LDPE surface showed that a coating of noticeable thickness is obtained. The processing marks were typically covered by the coating (Figure 9). However, when running at lower power or at higher line speeds, thinner coatings were obtained. The thinner coatings were visible on the surface, but these were not thick enough to cover the processing marks.

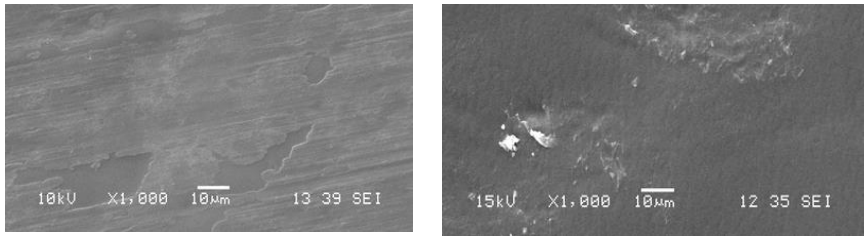

(a) LDPE-board (b) Plasma-deposited SiOx

Figure 9. SEM images of the LDPE surface without (a) and with (b) plasma deposited SiOx coating (modified from [P1]).

In addition to the SEM characterisation, the surface morphology of the plasma-deposited film was examined with AFM. Figure 10 presents the AFM images for uncoated (a) and SiOx-coated LDPE (b). The comparison of the AFM topography images showed covering of the LDPE surface by a SiOx layer. The plain LDPE showed typical crystallized and oriented morphology of LDPE [96]. The observed SiOx film did not show such a columnar well-defined growth structure of a HMDSO film obtained using vacuum RF plasma deposition [97]. However, the plasma-deposited SiOx film seemed to be a quite similar compared to previous achievements obtained by using atmospheric plasma deposition [98].

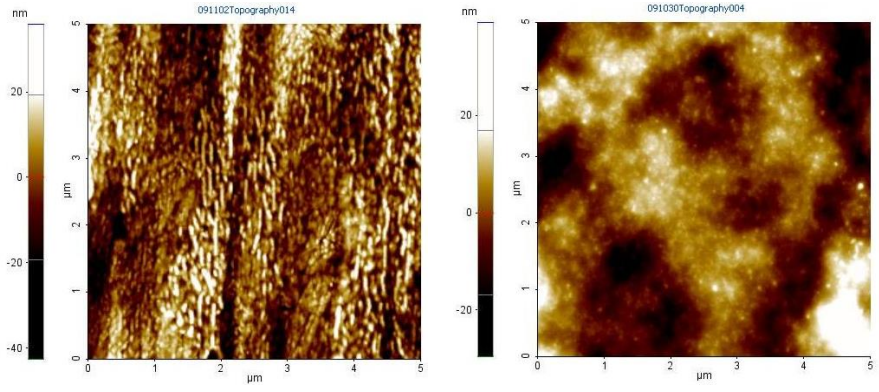

(a) LDPE-board (b) SiOx-coated LDPE-board

Figure 10. AFM topography of uncoated LDPE-board (a) and plasma deposited SiOx on LDPE-board (b).

Table 3 presents the surface roughness values of both the plain LDPE surface and the plasma-deposited LDPE surface. The decrease in Ra and R_{RMS} (=Rq) values showed that plasma deposition smoothed the average roughness of the LDPE surface.

Table 3. Surface roughness values of uncoated LDPE and SiOx plasma deposited LDPE (modified from [P1]).

Specimen	R_a (nm)	R_{RMS} (nm)
LDPE-board	12 ± 4	16 ± 5
SiOx Plasma deposited LDPE-board	8 ± 1	10 ± 2

SEM and AFM results indicated some non-uniform deposition of the SiOx coating layer. In this case, the water vapour transport may occur through the non-coated areas of the coating. This can partly explain why the WVTR measurements did not reveal considerable changes in water vapour permeability [P1]. The differences

between untreated, plasma-treated and plasma-deposited samples were within the limits of the standard deviation.

Further development of the plasma deposition process may improve the barrier performances. For example, more powerful plasma pre-treatment may be necessary to ensure better film formation. On the other hand, the LDPE surface is rather rough for deposition of uniform and dense thin films. Therefore, further research should focus on the effect of pre-treatment or primer layer in smoothing the LDPE surface prior to the plasma deposition. Moreover, a thicker SiOx coating layer might improve the barrier performance as well. However, it may lead to unwanted cracking of the inorganic coating layer. Therefore, a protective coating layer is possibly needed to improve the durability of the inorganic layer.

7.1.2 Atmospheric plasma-assisted sol-gel hybrid coating on LDPE-board

In relation to work on plasma-deposition of SiOx coatings, a pilot extrusion coating line was equipped with an atmospheric plasma pre-treatment unit. The main goal was to obtain high barrier effects for oxygen and grease by deposition of plasma-assisted sol-gel hybrid coatings on the LDPE-board [P2].

The sol-gel hybrid coatings consisted of either a 2-dimensional (SG204) or 3-dimensional (SG206) oligomer hybrid network. The SG204 coating was based on the 2D oligomer hybrid structure synthesised according to Figure 11, which illustrates the reaction between metal alkoxide (e.g. tetraethoxysilane, TEOS) and organically modified alkoxysilane (e.g. octyltriethoxysilane, C8-TES). Typically, some of the hydroxyl groups remain unreacted or react more slowly depending on the catalysis of the reaction [25]. These hydroxyl groups can enhance the bonding of the synthesised hybrid coating on substrates bearing hydroxyl or carboxyl groups. Therefore, the hydrophobic functional end-groups of the organically modified alkoxysilanes should align out from the substrate.

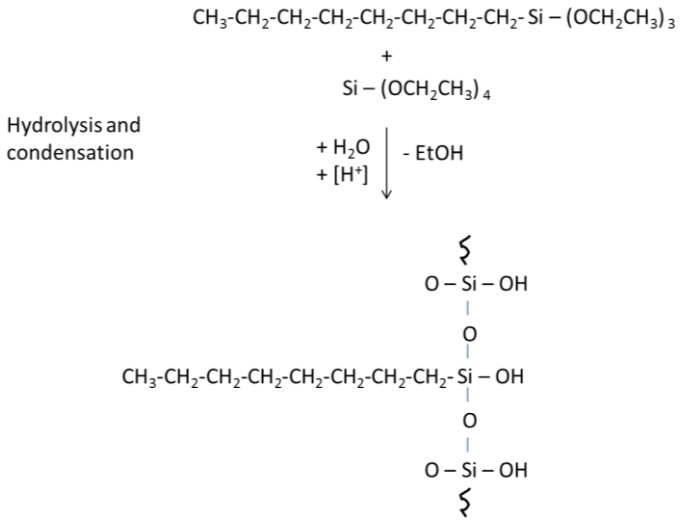

Figure 11. Synthesis of 2D oligomeric hybrid structure using sol-gel route.

The SG206 coating consisted of 3-glycidyloxypropyltrimethoxysilane and 3-(2-aminoethylamino) propyltrimethoxysilane. Figure 12 describes the synthesis route for formation of the 3D hybrid network, where an epoxy coupling reaction occurs between amino and epoxy groups, followed by methoxy group reaction through hydrolysis and condensation reactions to form the polysiloxane Si-O-Si bonds.

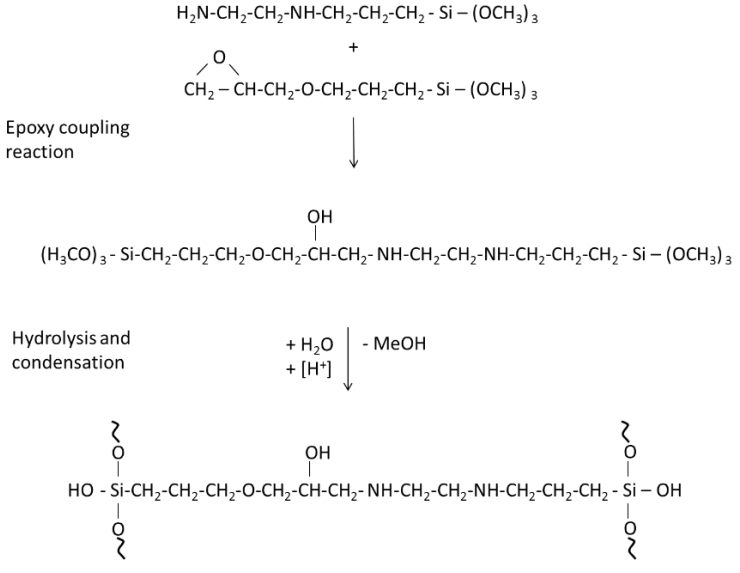

Figure 12. Synthesis of 3D oligomeric hybrid structure using epoxy coupling reaction and the sol-gel route.

The SEM analysis was used to characterise the structure and film thickness of the coated specimens. Figure 13 presents an SEM image of a cross-section of the SG206 coating deposited on the LDPE. The existence of the coating layer can be seen as a light grey colour. The coating thickness determined from the SEM image was approximately 1.3–1.5 µm. The SEM image indicated that the coating was uniform and dense. In addition, no film cracking was observed.

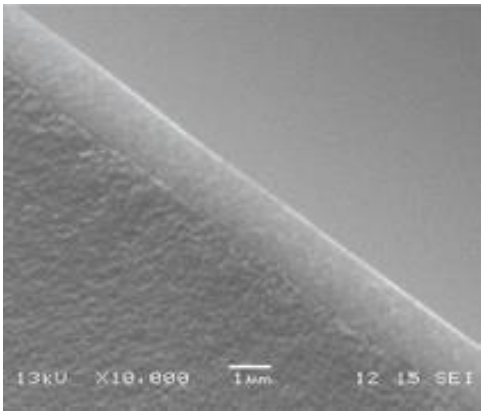

Figure 13. Cross-section SEM image of the SG206 coated LDPE-board.

Figure 14 presents the AFM topography images of (a) the uncoated LDPE-board and (b) the SG206-coated LDPE surface. Based on AFM images, the sol-gel coating formed a smooth and dense layer on the LDPE surface. Furthermore, the average roughness (R_a) value for the sol-gel-coated LDPE (0.4 nm) was evidently lower in comparison to that of the uncoated LDPE-board (5.1 nm).

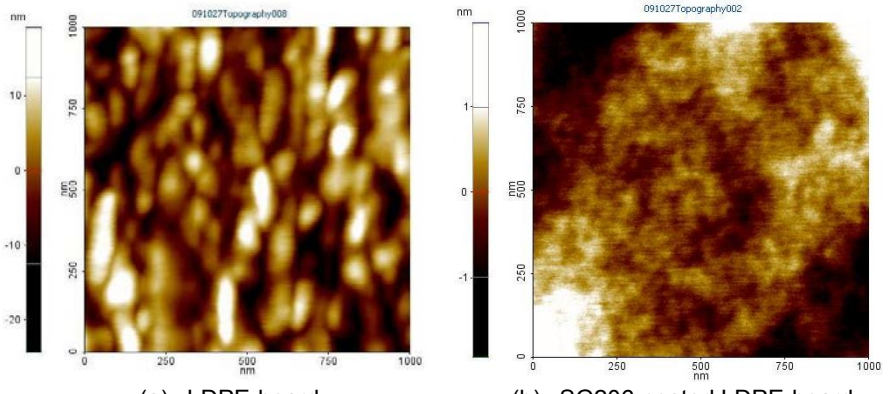

(a) LDPE-board (b) SG206-coated LDPE-board

Figure 14. AFM topography images of (a) the uncoated and (b) the SG206-coated LDPE-boards.

Oxygen barrier

The oxygen barrier performance of the two different hybrid sol-gel coatings was studied by comparing their oxygen transmission rate (OTR) values. The aim was to demonstrate the effect of an additional coating layer on the oxygen barrier performance of LDPE. The coating chemistry was expected to have an effect on the permeability properties of the coatings. In addition, the effect of plasma pre-treatment on spreadability and uniformity of the film was studied by comparing OTR values between the coatings deposited with and without plasma pre-treatments.

Figure 15 presents the OTR of the uncoated LDPE and sol-gel coatings (SG204 and SG206) with and without plasma pre-treatment. The oxygen transmission rate of the LDPE-board was approximately 8700 $cm^3/(m^2*atm*day)$. All the coated specimens had lower oxygen transmission in comparison to the uncoated LDPE-board. The comparison between the non-treated and the plasma-treated coatings showed some differences. The OTR values of the non-treated SG204 and SG206 coatings were 7100 and 6900 $cm^3/(m^2*atm*day)$. The OTR values of the plasma-pretreated SG204 and SG206 coatings were 7100 and 900 $cm^3/(m^2*atm*day)$, respectively.

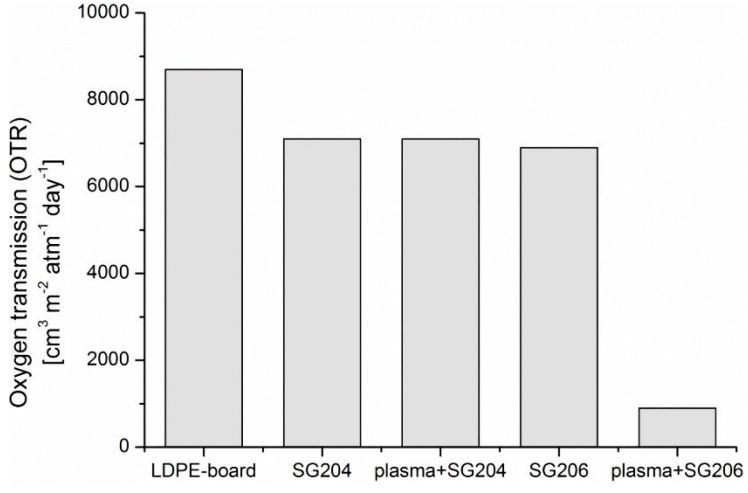

Figure 15. The oxygen transmission rates (OTR) of LDPE-board and sol-gel coatings SG204 and SG206 with and without plasma pre-treatment on the LDPE surface (modified from [P2]).

The differences in the barrier performance between the coatings can be explained by the coating chemistry. The SG206 coating formed a denser organic network, where epoxy groups reacted with the amino groups, forming the 3-dimensional network. The SG204 coating did not form a similar network, due to the lack of reactive groups for the cross-linking. The results indicate that the plasma pre-treatment did not affect the barrier performance of the SG204 coating, whereas

the plasma pre-treatment improved the oxygen barrier performance of the SG206 coating. The enhancement after the plasma pre-treatment was most likely due to the uniformity of the SG206 coating, resulting from the improved wetting.

Oleophobicity and grease barrier

Contact angles of oleic acid on the specimens were measured in order to investigate the oil repellence behaviour. In addition, a decrease in the contact angle values during the measurement time was expected to demonstrate the grease barrier performance. Figure 16 presents the contact angle of oleic acid for the uncoated and SG204-coated LDPE surface. The oleic acid droplets spread rapidly on the uncoated LDPE surface. The contact angle value was 10º for the uncoated LDPE after 25 s measurement time. In fact, the contact angle value decreased constantly during the measurement time, indicating possible absorption of the oil through or into the LDPE layer. In contrast, the contact angle value was a steady 45º for all the SG204-coated LDPE surfaces with or without plasma pre-treatment. In addition, the droplets were stable during the measurement time, indicating no absorption through the sol-gel coated surface.

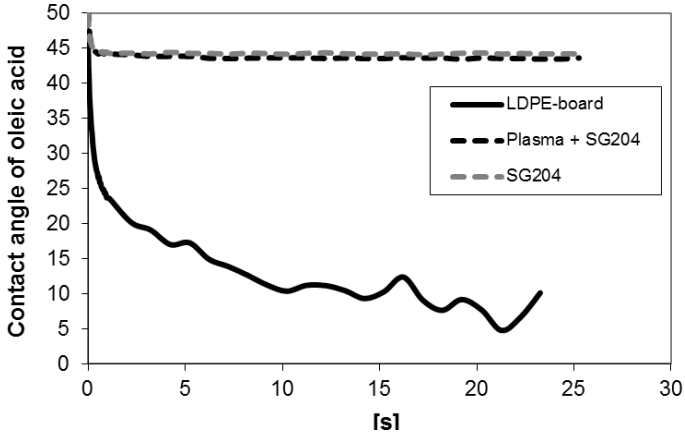

Figure 16. Contact angle values of oleic acid for the uncoated and the sol-gel (SG204)-coated LDPE surface with and without plasma pre-treatment (modified from [P2]).

The improved oil repellence performance might be attributed to the formation of long-tail hydrocarbon groups on the LDPE by the deposition of the SG204 coating. In addition, the smooth and dense surface structure of the sol-gel coating might have contributed to the oil repellence. The plasma pre-treatment did not affect the contact angle value of the coatings. This indicates that the coating had spread sufficiently on the LDPE even without the pre-treatment.

The effect of the atmospheric plasma pre-treatment on adhesion of the SG204 coating was studied, comparing the oil repellence behaviour before and after abrasive wearing test. Figure 17 presents the contact angles of oleic acid after the abrasive wearing for the uncoated LDPE and the SG204-coated LDPE with and without plasma pre-treatment. The contact angle values of the uncoated LDPE were remarkably lower after the wearing test. The contact angle values could not be measured after 3 seconds, indicating the rapid absorption of the oil through the abraded LDPE layer. In contrast, the sol-gel coated LDPE specimen revealed only a minor decrease in the contact angles. As expected, the contact angle values measured after the abrasive wearing showed some differences between the untreated and plasma pre-treated LDPE. The contact angle values of non-treated sol-gel coating decreased down to 20º. However, the contact angle value of 35º was measured for the plasma-treated sol-gel coating. The comparison between the abraded sol-gel coated samples with and without plasma pre-treatment suggested that the plasma pre-treatment enhanced the adhesion of the coating.

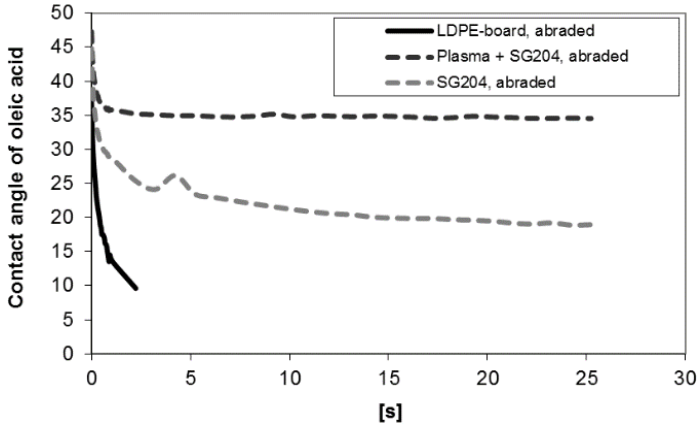

Figure 17. Contact angle values of oleic acid for uncoated LDPE and sol-gel coated LDPE specimens after the abrasive wearing (modified from [P2]).

7.1.3 ALD and sol-gel based thin-film composite on PLA-board

Thin-film composite (TFC) structures were aimed to enhance gas and water vapour barrier performance of PLA-coated board. The sol-gel (SG200)-based hybrid coating was intended to form a hydrophilic pre-barrier layer and additionally to smooth the surface roughness of the PLA surface. An inorganic ALD-Al_2O_3 layer was applied on the sol-gel layer in order to make a dense and nanosized barrier layer [P3].

Figure 18 presents AFM topography images of (a) PLA-board and TFC structures, (b) SG200/PLA-board, and (c) ALD/SG200/PLA-board. The TFC structure was formed by applying the SG200 coating on the PLA-board, which was followed by a coating of ALD-Al_2O_3 layer. Indeed, the SG200 coating, as a pre-barrier layer covered the larger valleys, pinholes and pores of the PLA surface, making it denser and smoother. Therefore, the surface is more favourable for the ALD based Al_2O_3 barrier layers, which was intended to give further densification of the surface.

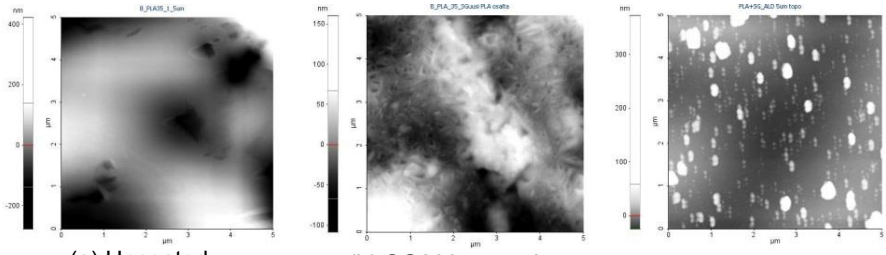

(a) Uncoated (b) SG200-coated (c) ALD/SG200-coated

Figure 18. AFM images of (a) uncoated PLA-board, and coated PLA-boards: (b) SG200 and (c) ALD/SG200.

Table 4 summarises the values for average surface roughness (R_a), water contact angle, OTR and the WVTR of uncoated, SG200-coated and ALD/SG200-coated PLA-boards. The R_a roughness results indicated that the SG200 coating reduced the R_a value making the PLA surface smoother. In addition, the SG200 coating reduced the water contact angle value indicating a more hydrophilic surface. The ALD-Al_2O_3 layer on top of the SG200 coating made the surface even smoother. However, some particle-like ALD growth as noticed, which has also been seen in other type of ALD experiments [78,79]. The total decrease in R_a was from 54 to 15 nm. Moreover, the water contact angle value dropped even further with the additional Al_2O_3 coating.

The high-barrier performance of the TFC structure was demonstrated using OTR and WVTR measurements. A minor improvement in the OTR and the WVTR values was obtained with the SG200 coating in comparison to plain PLA-board. A remarkable decrease in OTR and WVTR values was noticed after applying the ALD layer on top of the sol-gel layer. The lowest OTR and WVTR values of 2 $cm^3/(m^2*atm*day)$ and 2 $g/(m^2*day)$ were reached with the ALD/SG200 structure. Apparently, the obtained OTR and WVTR values of the ALD/SG200 were lower than those achieved for the ALD coating without the sol-gel (OTR: 6 $cm^3/(m^2*atm*day)$ and WVTR: 3 $g/(m^2*day)$).

Table 4. Values of water contact angle (WCA), average roughness (R_a) OTR and WVTR transmission of plain PLA-board and coated specimens SG200/PLA-board and ALD/SG200/PLA-board (modified from [P3]).

Specimen	R_a [nm]	WCA [o]	OTR [$cm^3m^{-2}atm^{-1}day^1$]	WVTR [$g\ m^{-2}day^{-1}$]
Uncoated PLA-board	54	71	400±9	75±2
SG200-coated PLA-board	27	58	310±2	44±2
ALD/SG200-coated PLA-board	15	52	2±1	2±1

7.2 Surface modification of thin-film composites with anti-fouling performance

7.2.1 Characterisation of uncoated and coated thin-film composites

The surface properties and their effect on bacterial anti-adhesion performance were studied using uncoated and coated polyamide (PA) thin-film composite (TFC) membranes [P4]. All the membranes were commercially available fully-aromatic TFC-PA membranes. Two of the TFC-PA membranes (SW30 and BW30) were coated using polyvinyl alcohol (PVA) coating, while the other three membranes (LE, XLE and NF90) were uncoated. Table 5 summarises the results on root-mean-square surface roughness (R_{RMS}), water contact angle and surface energies with total, polar and dispersive values. The PVA coated membranes (SW30HR and BW30) had a lower water contact angle and higher surface energy values in comparison to uncoated membranes (LE, XLE and NF90). Indeed, the most hydrophilic and highest surface energy was measured for the SW30HR membrane. In addition, SW30HR showed the highest polar surface energy value, among the characterised membranes. BW30 membrane had a slightly higher water contact angle and respectively, lower surface energy. Moreover, the polar surface energy of BW30 was somewhat lower than SW30HR. Based on the results, the PVA coating increased the polarity of the TFC-PA membrane surface.

Among the uncoated TFC-PA membranes, the LE membrane clearly had the lowest values for water contact angle and the highest for the surface energy respectively. The surface energy value for LE was almost at the same level with the coated membranes. However, comparison of polar surface energy values revealed that the LE membrane surface had a lower polarity. In contrast, among the characterised membranes the XLE and NF90 membranes showed most hydrophobic and non-polar surface properties. In fact, the highest value for water contact angle and respectively, the lowest value for surface energy were measured for the XLE membrane. Similarly, the NF90 membrane showed hydrophobic surface properties. The NF90 membrane had a slightly lower value for water contact angle value and a higher value for surface energy respectively in comparison to the XLE. However, the polarity of XLE membrane was higher compared to NF90 membrane.

The R_{RMS} roughness values for the coated membranes SW30HR and BW30 were somewhat lower in comparison to the uncoated membranes (LE, XLE and NF90). The slightly decreased roughness is most likely due to deposition of a very thin coating layer on the BW30 and SW30HR membranes. The coating layer might have filled the valleys of the PA selective layer. The high deviation in roughness may be explained by the uneven deposition of the coating. Among the uncoated TFC-PA membranes, LE and NF90 had a lower surface roughness than XLE. The uncoated membranes showed similarly high deviation of the roughness values. This can be explained by the differences in the formation of the PA selective layer, resulting in an uneven peak-and-valley surface structure.

Table 5. Summary of the results on water contact angle and surface energies.

Membrane	WCA [°]	Total surface energy [mN/m]	Polar surface energy [mN/m]	Dispersive surface energy [mN/m]	R_{RMS} [nm]
SW30HR	28 ± 5	66	24	42	70 ± 12
BW30	43 ± 4	56	19	37	57 ± 5
LE	53 ± 9	54	11	43	75 ± 23
XLE	76 ± 5	38	4	34	96 ± 21
NF90	70 ± 4	42	2	40	76 ± 12

Bacterial anti-adhesion performance

Figure 19 presents the results of the bacteria viability analysis of the membrane samples after a 24 hour exposure to *P. aeruginosa*. The attachment of the bacteria was evidently different between the membranes. Indeed, the decrease in the number of viable cells can be observed simultaneously with the increase of hydrophilicity and surface polarity (Table 5). The lowest amount of bacteria was attached to the most hydrophilic and polar SW30HR and BW30 membranes. Among the uncoated membranes, the LE membrane had a somewhat lower amount of attached bacteria in comparison to the XLE and NF90 membranes. Indeed, the amount of bacteria found on the uncoated membrane surface increased in the order: LE, XLE and NF90.

The correlation between the polar surface energy and the attachment of bacteria was investigated in order to gain further knowledge of the effect of the surface energy on the attachment of bacteria. Apparently, the polar surface energy values clearly correlated with the attachment of the bacteria. The amount of bacteria decreased identically with the increase of polar surface energy value. In addition, the type of surface roughness may somehow contribute to bacteria repellence. However, an exact conclusion cannot be presented due to the heterogeneous surface topography of the membranes.

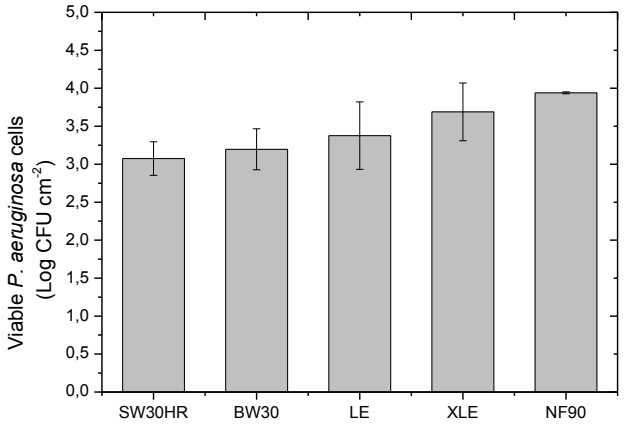

Figure 19. Viable *P. aeruginosa* cells on different membrane surfaces after 24 hour exposure.

7.2.2 PVA- and PVA-PHMG-coated thin-film composites

Anti-adhesion surfaces can be prepared using contact active amphiphilic, microbe-repelling or anti-adhesive polymers [67,68,69]. In addition, active antimicrobial coatings with bactericidal effects have been prepared using heavy metal nanoparticles, such as silver, copper and zinc [99,100]. However, the heavy metal-based antimicrobial coatings may have certain disadvantages: (1) uncontrolled leaching of the metal ions to the surroundings reduces the self-life of the anti-fouling membrane, and (2) these metal ions may raise questions concerning their safety to environment. In this regard, polymer based antimicrobial coatings may be favoured. The current study aimed to develop a surface coating method to enhance the anti-biofouling performance of TFC-PA RO membranes. Polyvinyl alcohol (PVA) and cationic polyhexamethyleneguanidine hydrochloride (PHMG) coatings were used to obtain hydrophilic and smooth surfaces to enhance membrane anti-adhesion properties [P5]. The PVA and PVA-PHMG coatings were coated on commercial LE-400 membrane. LE-400 is relatively high-permeable RO membrane and thus it was expected to be suitable for coating trials.

Surface chemistry of PVA and PVA-PHMG coatings

The surface chemistry of the PVA- and the PVA-PHMG-coated TFC-PA membranes was characterised using FTIR. Figure 20 shows the ATR-FTIR spectrum of the uncoated membrane and PVA-, PVA-PHMG- and PHMG-coated membranes in the range of 2000–500 and 4000–2600 cm^{-1}. The uncoated membrane showed the typical FTIR spectrum of fully aromatic PA membranes formed from m-phenylenediamine and trimesoyl chloride on top of a polyethersulfone (PES) support layer [64]. The peak at 1608 cm^{-1} was assigned to the C=O stretching (amide I band), and the peak at 1540 cm^{-1} was assigned to N-H bending (amide II band)

known to be typical for a secondary amide group [101,102]. Both the PVA- and the PVA-PHMG-coated membranes showed a strong peak at 1710 cm^{-1}, which was assigned as C=O stretching of carbonyl peak. The slightly broadened peak at around 1450–1420 cm^{-1} was due to the overlapping C-O-H in-plane bending and C-H bending vibrations. The minor broadening of the peaks at 1150–1070 cm^{-1} may be attributed to aliphatic C-O and C-C stretching. The peak at 1392 cm^{-1} was assigned as symmetric bending of CH_3 group [103]. The most evident peak of PHMG was the strong peak at 1650 cm^{-1}, which was identified as N-H bending (scissoring). A similar low intensity peak was noticed for the PVA-PHMG coating, although PHMG was added into PVA using relatively low amounts.

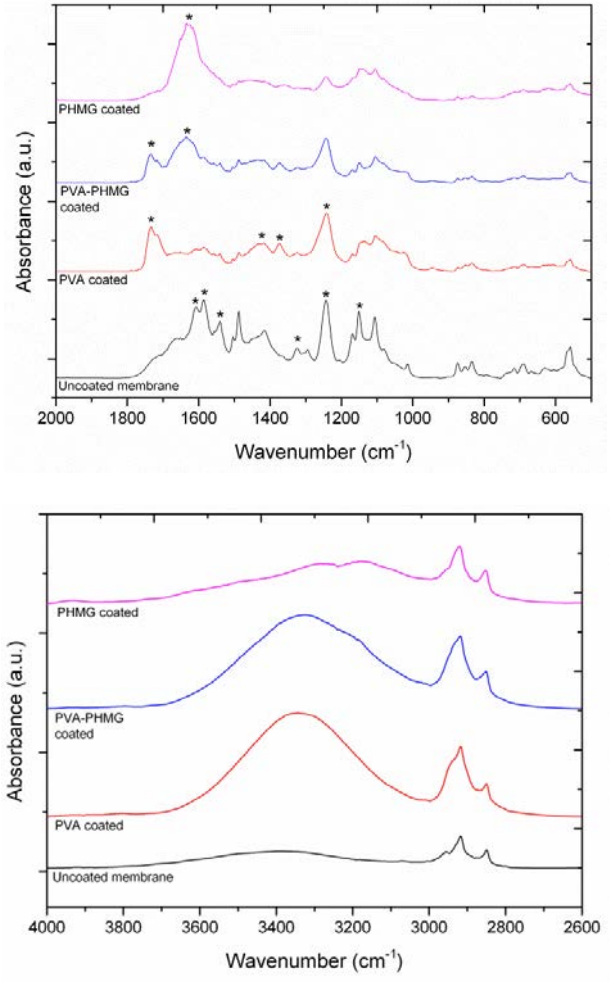

Figure 20. ATR-FTIR spectra of uncoated membrane and coated with PVA, PVA-PHMG (95:5) and PHMG. The peaks in the range of 2000–500 and 4000–2600 cm^{-1}.

Surface morphology and topography of PVA and PVA-PHMG coatings

The SEM characterization was performed to determine the coating thickness and to verify how the coatings were formed on the membrane. Figure 21 presents the SEM cross-section images of the uncoated and coated membranes. The SEM image of the uncoated TFC-PA membrane (a) clearly shows the PES support layer (thickness of ~150 μm). The SEM images (b, c and d) revealed that the coating thickness varied from approximately 80 nm to 250 nm. The detected coating thicknesses were within the optimal range (1–1000 nm) reported for RO membranes in the literature [104,105].

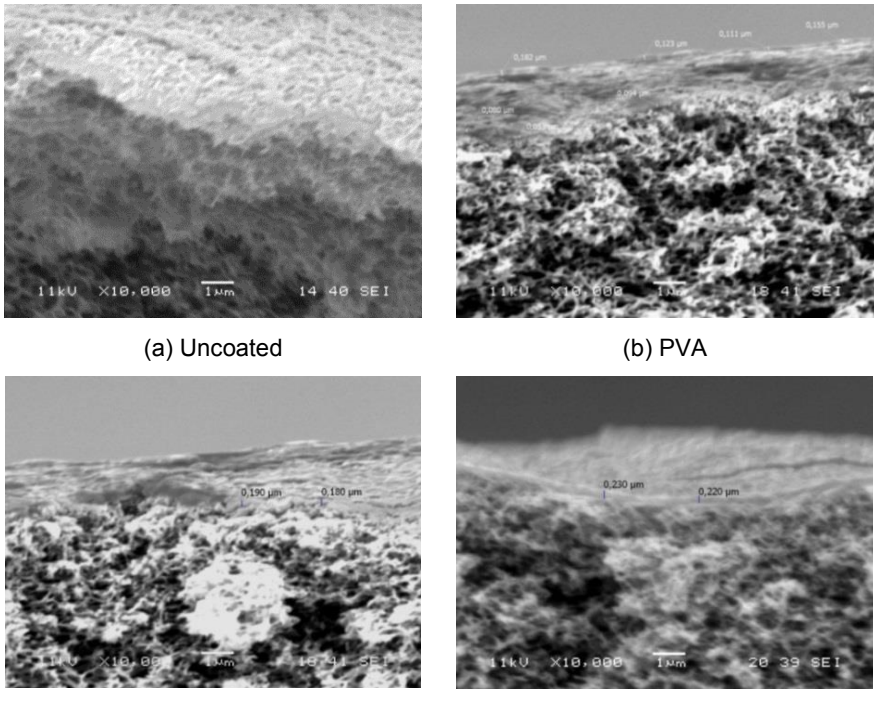

(a) Uncoated (b) PVA

(c) PVA-PHMG (95:5) (d) PHMG

Figure 21. SEM cross-section images (x10 000 magnification) of (a) the uncoated membrane and the coated membranes: (b) PVA, (c) PVA-PHMG (95:5) and (d) PHMG. The coatings thicknesses (80–250 nm) are marked in the specific SEM image.

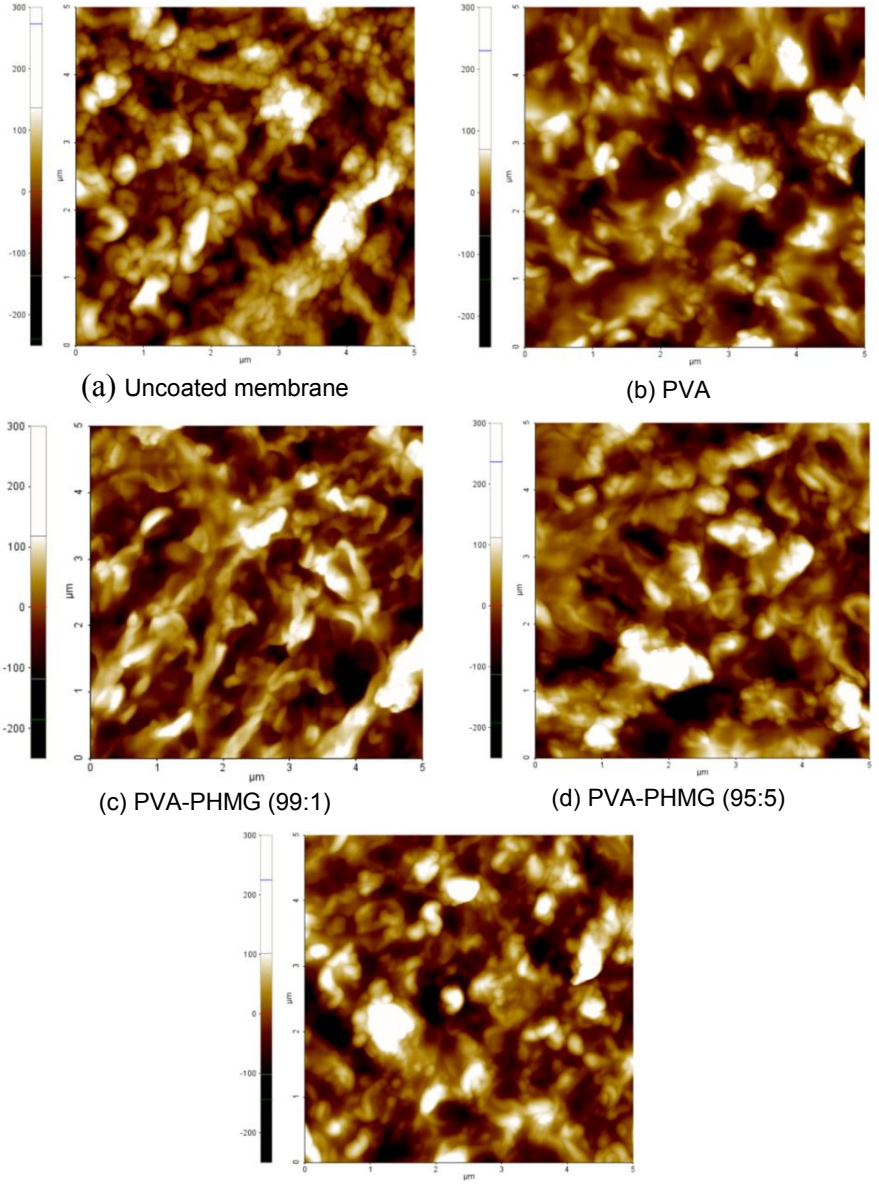

Figure 22. AFM images of the (a) uncoated membrane and the coated membranes: (b) PVA, (c) PVA-PHMG (99:1) (d) PVA-PHMG (95:5) and (e) PHMG.

Figure 22 presents AFM images of the uncoated and coated membranes. The uncoated membrane showed the ridge-and-valley as well as nodular surface texture, which is typical of TFC-PA membranes [106,107]. The AFM images of the PVA-, PVA-PHMG- and PHMG-coated membrane showed covering and smoothening of the nodular structure of the TFC-PA membrane, in good agreement with the SEM observations (Figure 21).

Table 6 presents the roughness parameter R_{RMS}. Comparison of the R_{RMS} values also indicated the smoothing of uncoated membrane surface (68 nm) after applying of the coatings. The PVA coating showed the lowest R_{RMS} value (43 nm) among the coatings. Furthermore, the results indicated that the PVA-PHMG (58 nm) and the PHMG (53 nm) coatings had a slightly rougher surface. The clear smoothing effect of the PVA coating is most likely due to the film forming capability [104,105].

Hydrophilicity and surface energies of PVA and PVA-PHMG coatings

Table 6 summarises the results of the water contact angle and the surface energies. The results revealed that the water contact value of the uncoated membrane (53º) was clearly reduced and respectively, the surface energy values were increased after applying the coatings. In addition, the surface polarity of coated membranes was higher compared to that of the uncoated membrane. The water contact angle values of the PVA (22º) and the PVA-PHMG (25º and 21º) coatings indicated formation of hydrophilic surface. The hydrophilic character of the PVA-based coatings originated from the dominant amount of hydroxyl groups as well as some residues of acetyl groups. a similar finding has been made for the commercial fully aromatic TFC-PA membrane coated with a PVA coating [64].

Table 6. Water contact angle, surface energy and surface roughness results for PVA- and PVA-PHMG-coated TFC-PA membranes. (modified from [P5])

		Surface energy			
Membrane	**WCA [º]**	**Total [mN/m]**	**Polar [mN/m]**	**Dispersive [mN/m]**	**R_{RMS} [nm]**
Uncoated LE-400	53 ± 9	54	11	43	68 ± 3
PVA	22 ± 2	60	20	40	43 ± 6
PVA-PHMG (99:1)	25 ± 3	60	19	41	55 ± 6
PVA-PHMG (95:5)	21 ± 2	60	22	38	58 ± 6
PHMG	16 ± 1	65	26	39	53 ± 2

Bacterial anti-adhesion performance of PVA and PVA-PHMG coated TFC-PA membranes

The attachment of the model biofilm-forming microorganism, *P. aeruginosa*, was studied in order to demonstrate the bacteria repellence performance of the uncoated and the coated membranes. The lower CFU values should indicate stronger bactericidal effects or bacteria repellence (anti-adhesion). Figure 23 illustrates the presence of P. aeruginosa on uncoated and coated membranes. In general, the CFU test revealed that a lower number of *P. aeruginosa* had adhered to the coated membrane surfaces than to the respective uncoated membranes.

Among the colony counts of the coated membranes, the PHMG coating clearly showed the lowest number of viable cells of bacteria. It was also observed that the PVA-PHMG-coated membranes attracted a lower number of the bacteria compared to the PVA-coated membrane. The unmodified PVA coating clearly showed a minor bacteria repellence effect when compared to the PHMG modified coatings. Nevertheless, the CFU results evidently showed that the PVA-coated membrane attracted less bacteria compared to the uncoated membrane.

As a result of the physiochemical anti-fouling performance, the PVA coating revealed anti-adhesion and bacteria repellence performance. The effect of the surface properties can be seen on the attachment of bacteria, because of the evident correlation between the increase in hydrophilicity (Table 6) and correspondingly, the decrease in the attachment of the bacteria. Furthermore, the lowered surface roughness might have contributed to the attachment of the bacteria. The results are related to the similar trend detected for the commercial membranes in Figure 16. However, PVA-PHMG and PHMG coatings also showed hydrophilic and smoother surface roughness compared to uncoated membrane. In fact, the attachment of the bacteria decreased by the increase in the PHMG content in the surface. This suggested that the strongest effect on the attachment of bacteria was obtained by combining the antimicrobial activity with the physiochemical anti-adhesion surface properties.

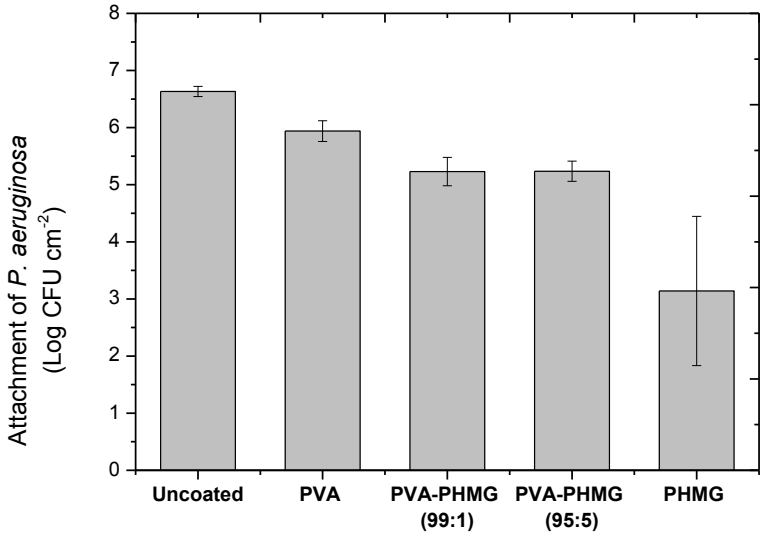

Figure 23. Attachment of *P. aeruginosa* on uncoated and coated membranes.

Antimicrobial performance of PVA and PVA-PHMG coated TFC-PA membranes

The membrane antimicrobial performance was studied by determining the number of the viable model bacteria, *E. coli* and *B. subtilis,* found on uncoated and coated membrane specimens. Figure 24 and Figure 25 present the CFU results of *E. coli* and *B. subtilis*, respectively. In Figure 24, the number of *E. coli* cells on the coated membranes was lower compared to that of the uncoated membrane. In addition, CFU test results of *B. subtilis* indicated similar behaviour, although the differences were not as significant (Figure 25). The trend in CFU changes was nevertheless consistent between the specimens. Furthermore, these CFU results showed a similar behaviour of the membrane specimens compared to the study of *P. aeruginosa*. The PHMG coating repeatedly showed the lowest number of viable cells of the bacteria, among the coated membranes. Similarly, the PVA-PHMG-coated membranes attracted a lower number of the bacteria when compared to the PVA-coated membrane. The results indicated that PHMG was somewhat more efficient against the Gram-negative *E. coli*. The unmodified PVA coating showed only minor repellence effect on these bacteria compared to the PHMG modified coatings. However, the CFU results showed that the PVA-coated membrane attracted less bacteria to some extent, in comparison to the uncoated membrane, indicating an enhanced anti-adhesion performance.

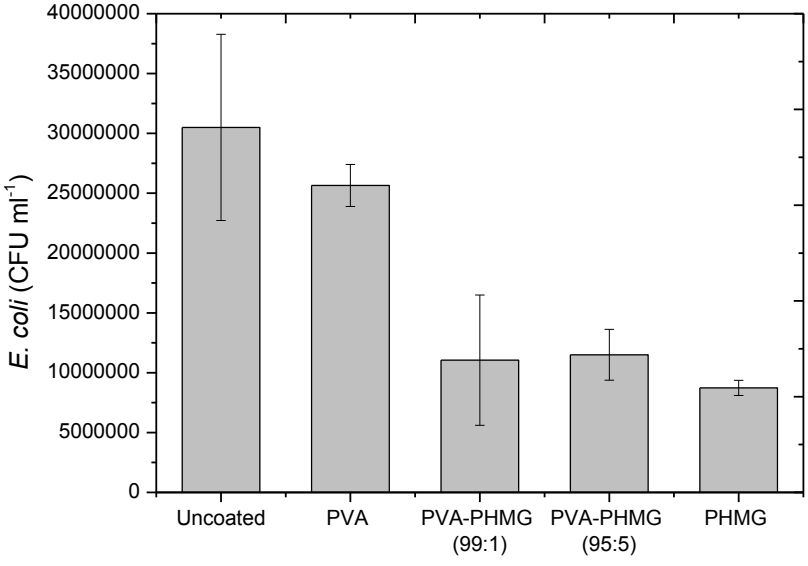

Figure 24. CFU results of *E. coli* on uncoated and coated membranes.

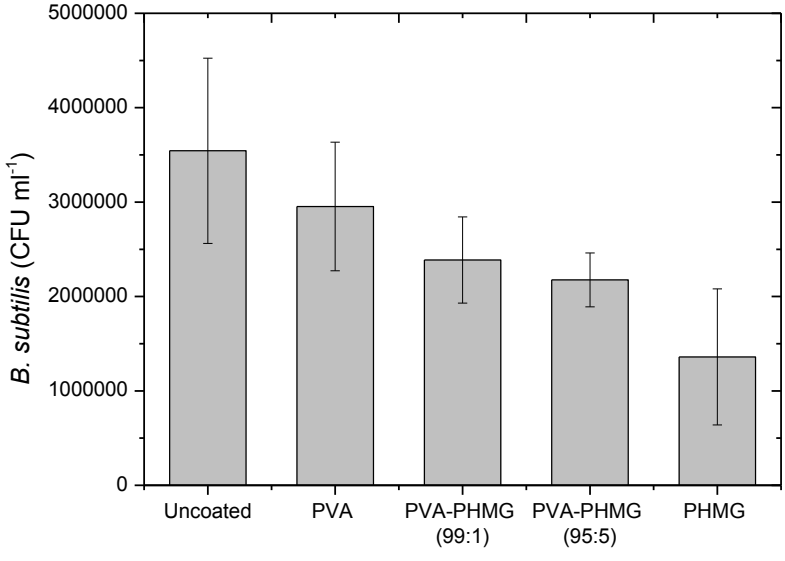

Figure 25. CFU results of *B. subtilis* on uncoated and coated membranes.

The diffusion inhibition zone (DIZ) test was conducted in order to further investigate the antimicrobial activity of the membrane specimens. An inhibition circle formed around a specimen would indicate antimicrobial activity and in addition, the leaching effect of the antimicrobial substance.

Figure 26 presents DIZ test results for Gram-negative *E. coli* bacteria and for Gram-positive *B. subtilis* bacteria. As expected, uncoated and PVA coated membranes did not show the formation of the inhibition circle against *E. coli* and *B. subtilis*; thus, the antimicrobial effect was not observed. The CFU results suggested that antimicrobial activity is obtained using PHMG. According to these results, the antimicrobial activity was more effective when the PHMG content was increased. However, the PVA-PHMG-coated membranes did not show the inhibition circle against the bacteria. Nevertheless, the results clearly showed that the pure PHMG coating formed the inhibition circle against both of the bacteria, *E. coli* and *B. subtilis*, indicating antimicrobial activity. PHMG is known to have antimicrobial performance [108,109]. The formation of a strong inhibition zone may also indicate leaching of the PHMG polymer, which might explain the lack of an inhibition circle in the case of the PVA-PHMG coatings. The decrease in the attachment of bacteria was obtained by adding low amounts of PHMG in the PVA coating. The FTIR spectra revealed only low intensity peaks assigned to PHMG (Figure 20). Furthermore, the SEM and the AFM analysis as well as the contact angle measurements suggested that PHMG had a minor effect on the PVA coating morphology, surface texture and hydrophilicity (Table 6). In that respect, PHMG might be somehow encapsulated or consolidated into the PVA coating matrix. This could explain the stability of the PVA-PHMG coating, allowing PHMG to be active against bacteria. In particular, our aim was to prevent biofilm formation by developing a bacteria-repelling anti-adhesion surface with a contact-killing antimicrobial property, without leaching of the antimicrobial agent. The target was reached with PVA-PHMG coatings.

E. coli ***B. subtilis***

(a) Uncoated membrane

(b) Uncoated membrane

(c) PVA

(d) PVA

(e) PVA-PHMG (95:5)

(f) PVA-PHMG (95:5)

(g) PHMG

(h) PHMG

Figure 26. DIZ photos of the Gram negative *E. coli* on (a) uncoated and coated membranes: (c) PVA, (e) PVA-PHMG (95:5), (f) PHMG. Respectively, DIZ photos of the Gram positive *B. subtilis* on (b) uncoated and coated membranes: (d) PVA, (f) PVA-PHMG (95:5) and (h) PHMG.

Water permeability and salt rejection of coated TFC-PA membranes

Table 7 summarises the values of water permeability (*A*), salt (NaCl) rejection (*R*) and salt (NaCl) permeability (*B*) of the uncoated and the coated membranes. The coating layers reduced the permeability properties compared to the uncoated membrane.

Among the coated membranes, the PVA coating reduced the water permeability by approximately 15%, and correspondingly the NaCl rejection showed a minor increase. However, the PVA coating decreased the NaCl permeability almost 55%. In comparison, the PVA-PHMG coatings led to a 45% and 58% reduction in water permeability. However, PHMG content did not have much effect on NaCl permeability of PVA coatings. The PHMG-coated membrane showed a 78% decline in water permeability. In fact, membranes with a higher PHMG percentage tended to reduce water permeability. Furthermore, the PHMG coating significantly reduced the NaCl rejection.

According to the calculation of NaCl permeability, the lower NaCl rejection could be contributed to the lower water flux (low water permeability or low pressure). Based on the equation 15 the salt permeability decreases, while the water permeability decreases. Furthermore, the salt permeability decreases, if the salt rejection increases. This explains the decrease in NaCl permeability of the PVA and PVA-PHMG (99:1) membranes with lower water permeability. Furthermore, the higher PHMG content tend to decrease the salt rejection, although the water permeability was decreased.

The detected decrease in permeabilities is reasonable. Some other investigations have typically shown a 50–80 % decrease in the water and NaCl permeability of

coated membranes [110]. Therefore, in conditions where higher pressure is applied or where the membrane has a reasonable permeability combination, the membrane is preferred in view of the better anti-fouling performance.

Table 7. Water permeability coefficient (*A*), salt (NaCl) rejection (*R*) and salt (NaCl) permeability coefficient (*B*) of the uncoated and the coated membranes.

Membrane	Water permeability coefficient (A) [L/m^2 h bar] [a]	Salt rejection (R) [%] [a]	Salt permeability coefficient (B) [L/m^2 h] [a]
Uncoated LE-400	4.35 ± 0.48	97.2 ± 1.2	3.47 ± 1.87
PVA	3.71 ± 0.31	98.5 ± 0.6	1.53 ± 0.51
PVA-PHMG (99:1)	2.39 ± 0.60	98.2 ± 0.6	1.26 ± 0.70
PVA-PHMG (95:5)	1.67 ± 0.25	95.8 ± 2.2	2.17 ± 1.28
PHMG	0.76 ± 0.48	91.6 ± 0.3	2.30 ± 1.29

[a] Water flux (J_v) and salt rejection (R) of the membranes were evaluated using 10 mM NaCl feed solution and applied pressure of 27.6 bar (400 psi) at 23 ºC.

7.2.3 ALD-coated thin-film composites

The ALD coating was intended to modify the surface properties of the TFC-PA membrane and thus to improve anti-fouling performance. Two different processing temperatures (70ºC and 100ºC) and three different ALD cycles (10, 50 and 100) were used to deposit the ALD coatings on TFC PA membranes. The increase of ALD coating thickness and temperature may negatively affect the RO membrane performance by tightening the rejection layer of a temperature-sensitive polymeric membrane. Therefore, further understanding of the ALD process is needed in order to overcome the current drawbacks and to develop a new low-fouling RO membrane using the ALD technology. To the best knowledge of the author, the ALD method has not been applied for modification of RO membranes, and therefore systematic study was needed to introduce ALD technology to the RO membranes [P6]. The ALD coatings were deposited on commercial LE-400 membrane.

Surface chemistry of ALD-coated TFC-PA membranes

FTIR was used to analyse the surface chemistry of the ALD-coated membranes. Figure 27 presents the FTIR spectra of the uncoated and the ALD-coated membranes in the range of 2000–500 cm^{-1}. The FTIR spectra of the ALD-coated membranes showed most of the significant peaks assigned for PA (1660, 1610, and 1540 cm^{-1}) and PES (1324, 1244 and 1180 cm^{-1}), although the intensities of these peaks were reduced compared to the uncoated membrane. The decrease in the peak intensities was more prominent for the thicker coating layers, which can be explained by the dilution effect due to the presence of the coating material. In

addition, the decrease in the peak intensity at 1660 cm^{-1} and 1540 cm^{-1} might be partially attributed to the reaction of the TMA precursor with C=O groups of PA (to produce C-O-Al bonds) [31,32] and N-H groups (to form Al-N bonds) [31,32], respectively. In addition, the coated membranes showed the appearance of a new low intensity peak at 1150 cm^{-1}, which may have originated from residues of unreacted Al-CH_3 groups of the TMA precursor [31,32].

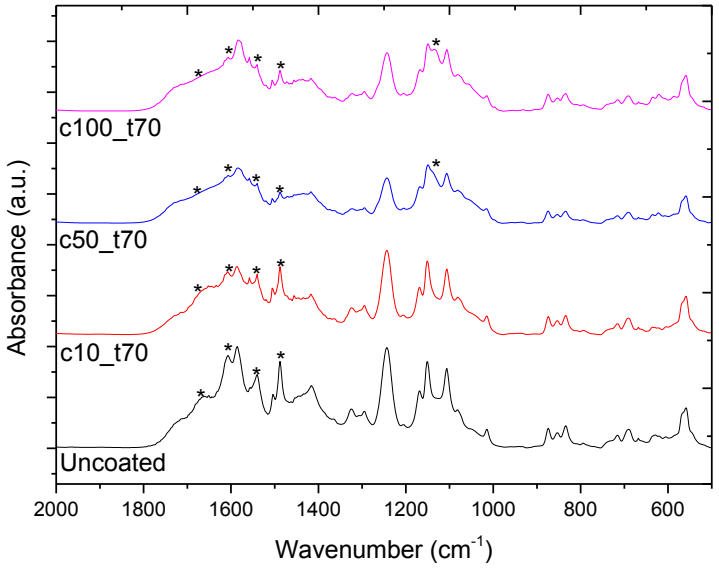

Figure 27. FTIR spectra of the uncoated and the ALD-coated (at 70ºC) specimens. The most significant peaks are marked with *.

Surface morphology and topography of ALD-coated TFC-PA membranes

The SEM characterization was performed to determine the surface morphology of the ALD-coated membranes. Figure 28 presents the SEM images of the uncoated and coated membranes. SEM images of the ALD-coated membranes (b–g) indicated some changes in the surface morphology compared to the virgin membrane (a). The membranes coated at 100ºC generally looked tighter when compared to those coated at 70ºC. Moreover, a tightening of the ALD coating layer can be noticed due to an increase in the coating thickness. The tightening could cause significant hydraulic resistance of the coating layer and a decrease in RO performance.

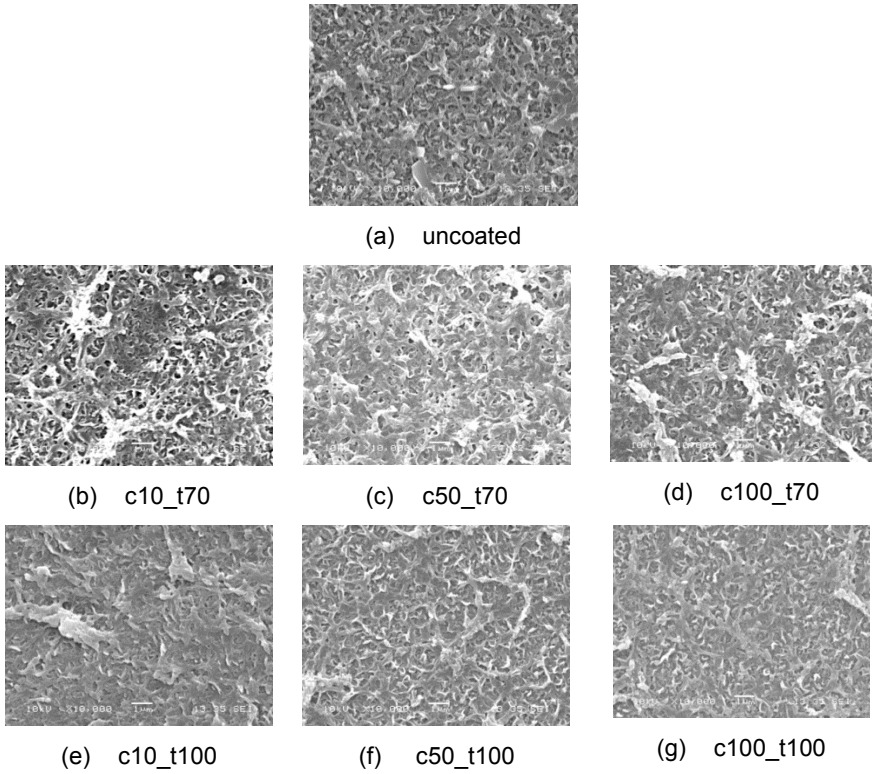

Figure 28. SEM images of the uncoated (a) and ALD-coated TFC-PA membranes using the number of ALD cycles (c) and processing temperatures (t) 70ºC (b–d) and 100ºC (e–g).

AFM was used to analyse the topography of ALD-coated membranes. Figure 29 presents AFM images of the uncoated and ALD-coated TFC-PA membranes. The uncoated membrane (a) showed a ridge-and-valley as well as nodular surface texture, which is typical of TFC-PA membranes [107]. The AFM images of the coated membranes indicated a particle-like topography of the ALD coating, which is typically obtained using a low number of ALD cycles [78,111].

Table 8 summarises the AFM roughness values. The R_{RMS} roughness value of the coated membranes declined significantly after 10 cycles, which may be due to the deposition of a few particles on the surface filling the valley areas. However, increase of the coating layer thickness significantly increased the R_{RMS} roughness of the coated membranes. Moreover, ALD coating layer with 100 cycles showed R_{RMS} values that were nearly identical to those of the uncoated membrane. A similar trend was observed with both of the temperatures. Indeed, the increase in surface roughness may be due to the particle-like ALD layers. Furthermore, the particle-like ALD layers may have grown on the ridges of the membrane surface,

which could then promote the surface roughness. A similar roughness increase has been also noticed when applying other type of ALD coatings [111].

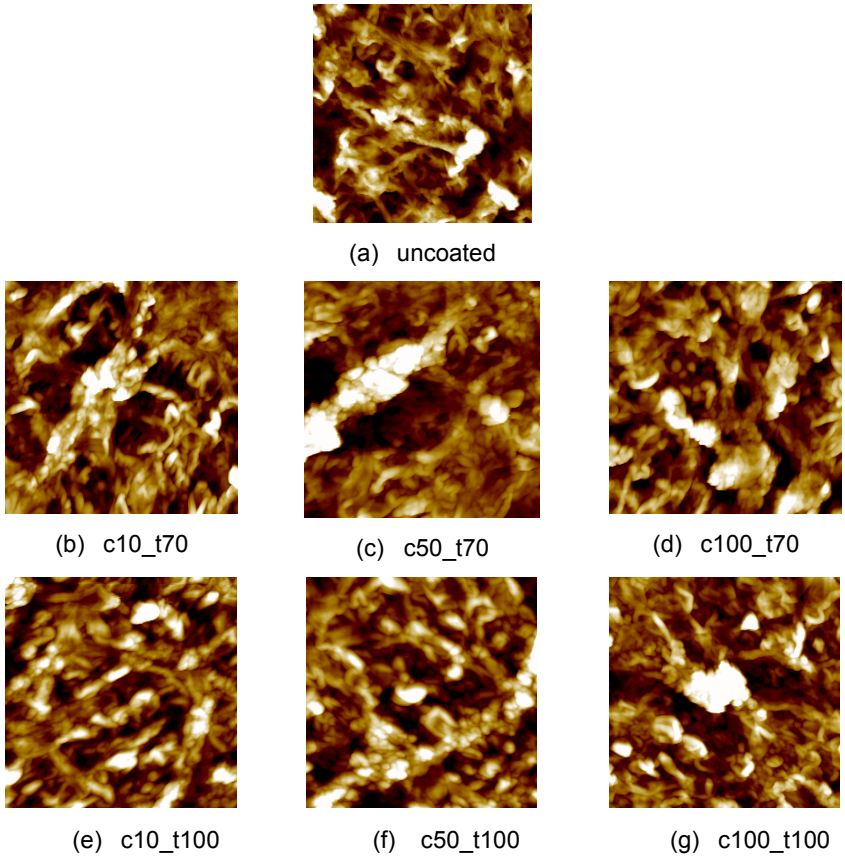

Figure 29. AFM images of the uncoated (a) and ALD-coated TFC-PA membranes using processing temperatures 70ºC (b–d) and 100ºC (e–g). Scan size 5x5 μm^2 and Z-range 250 nm.

Hydrophilicity and surface energies of ALD-coated TFC-PA membranes

Hydrophilic properties of the uncoated and the ALD-coated TFC-PA membranes were studied using water contact angle measurements. These results are summarised in Table 8. The membranes became more hydrophilic when a thin ALD coating layer was deposited on the membrane surface. The most hydrophilic membrane surface was obtained using 10 and 50 ALD cycles at 70ºC or 10 ALD cycles at 100ºC, having the water contact angles of ~ 15–30º compared to 53º for the uncoated membrane. This reduction in water contact angle can be attributed to the formation of a hydrophilic coating layer of Al_2O_3 with some residues of Al-OH

groups [111]. The membranes coated at 100ºC were generally less hydrophilic compared to those coated at 70ºC under otherwise identical conditions. This was probably due to the increase in reactivity and thus enhanced conversion of Al-OH to Al-O-Al at the higher temperature. Previous investigations have shown an increase in the reactivity of TMA precursor, when raising the temperature [31]. On the other hand, the number of ALD cycles was also seen to have an effect on water contact angles. The increase in hydrophobicity with the coating thickness might be due to the accumulation of hydrophobic alkyl residues (-CH_3) as the TMA was not completely converted to Al_2O_3. The existence of Al-CH_3 groups can be seen in FTIR spectra (Figure 27).

Table 8 also presents the surface energy measurement values. It was found that the surface energy was highly correlated to the contact angle – higher surface energy values were observed for membranes with lower contact angles. A closer analysis of the polar and non-polar components of the surface energy revealed that the increase in surface energy for the more hydrophilic membranes was mainly due to their higher polar contribution, whereas the non-polar contribution remained relatively constant. Once again, the increase in polarity may be attributed to the formation of Al-O-Al and Al-OH groups. The decrease in polarity for thicker coating layers may be due to the presence of significant amount of Al-CH_3 groups.

Table 8. Surface properties of ALD-coated TFC-PA membrane including water contact angle, surface energy and surface roughness results. (modified from [P6])

Membrane	WCA [o]	Total surface energy [mN/m]	Polar surface energy [mN/m]	Dispersive surface energy [mN/m]	R_{RMS} [nm]
Uncoated LE-400	53 ± 9	54	11	43	73 ± 7
c10_t70	16 ± 4	67	33	34	50 ± 5
c50_t70	27 ± 1	57	21	36	56 ± 4
c100_t70	66 ± 2	38	10	28	75 ± 1
c10_t100	27 ± 5	44	11	33	54 ± 3
c50_t100	84 ± 4	39	1	38	69 ± 2
c100_t100	92 ± 1	34	1	33	71 ± 2

Bacterial anti-adhesion performance of ALD-coated TFC-PA membranes

The attachment of the model biofilm-forming microorganism, *P. aeruginosa*, onto uncoated and ALD-coated membranes was studied in order to demonstrate bacteria repellence performance. The test was only performed for the ALD-coated membranes processed at 70ºC (t70), because of their promising surface properties in comparison to the membranes coated at 100ºC (t100). Figure 30 presents the

number of adhered *P. aeruginosa* cells on uncoated and coated membranes. In general, a lower number of the adhered *P. aeruginosa* was detected on the ALD-coated membrane surfaces compared to the uncoated. Up to two log units reduction in the number of adhered *P. aeruginosa* was detected on the thinner coatings with ALD cycles 10 (c10_t70) and 50 (c50_t70) compared to the uncoated membrane. The thicker coating with 100 ALD cycles (c100_t70) contained an almost equal number of viable cells as were detected on the uncoated membrane.

The ALD coating on the membrane created a surface with bacteria repellence performance, most likely due to the altered physiochemical properties of the membrane surface. The decrease in the number of adhered bacteria showed a strong correlation between the increase in surface hydrophilicity (Table 8) and the increase in surface polarity. For example, c10_t70 coatings (33.4 mN/m) had higher polarity compared to c50_t70 coatings (21.7 mN/m) and, fewer bacteria attached on former coatings. Moreover, c100_t70 coatings and uncoated membrane attracted bacteria in similar quantities and the surface polarity values of these were somewhat similar. The lower surface roughness of the thinner ALD coatings may have contributed to the attachment of the bacteria. Indeed, other researchers have shown that lower amount of *P. aeruginosa* bacteria were attached on model surfaces having nanotubular and nanotextured structure with a length of valleys and peaks 100–200 nm [112].

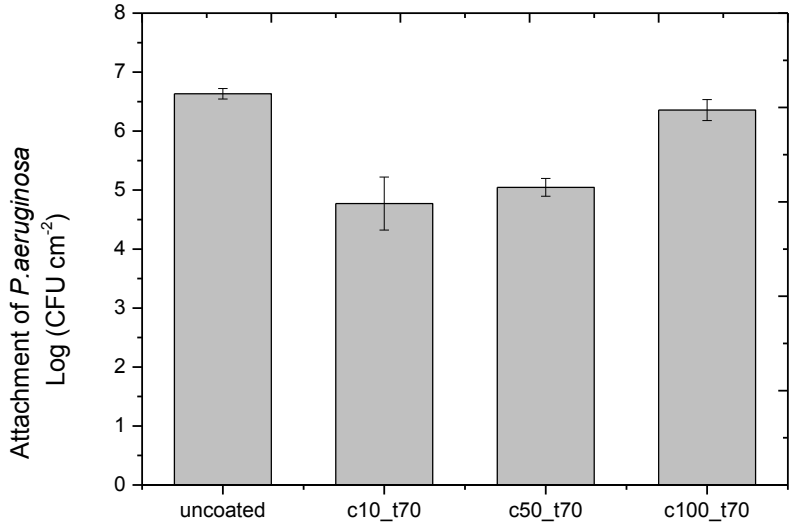

Figure 30. Attachment of *P. aeruginosa* bacteria on uncoated and ALD-coated (70ºC) membranes.

Water permeability and salt rejection of ALD-coated TFC-PA membranes

Table 9 summarises the values of water permeability (*A*), salt (NaCl) rejection (*R*) and salt (NaCl) permeability (*B*) of the uncoated and the coated membranes. These were measured only for the ALD-coated membranes processed at 70ºC.

Among the ALD-coated membranes, the thinner coatings with 10 and 50 ALD cycles (c10_t70 and c50_t70) did not show a significant effect on water permeability. Indeed, c10_t70 was marginally more permeable compared to the uncoated membrane. The sufficient water permeability of c10_t70 membranes could be explained by their hydrophilic character (Table 8) in addition to the low hydraulic resistance (R_c) due to the thin coating thickness. However, as a result of the ALD coating the NaCl rejection of these membranes was reduced and their NaCl permeability (*B)* was increased. This may indicate an impact of the ALD coating on the PA rejection layer.

An increase in the ALD cycles had a strong effect on RO performance. Almost 65 % reduction of water permeability (*A)* was measured for the membrane with the thickest coating (c100_t70). This may be explained by the changes in the rejection layer, such as hydrophobicity and increase in the significant hydraulic resistance of the coating layer. Moreover, the salt permeability was reduced and the salt rejection was increased with increasing the coating thickness. This could be related to a tightening of the coating layer at increased coating thickness.

The trade-off between rejection and water permeability is typical for a coated membrane. For example, an additional ALD coating has been shown to form a hydraulic resistance layer on a porous polymeric membrane, which has typically reduced water permeability for 50–80 % and respectively, increased a solute retention for 10–30 % [78,80].

Table 9. Water permeability coefficient (*A*), salt (NaCl) rejection (*R*) and salt (NaCl) permeability coefficient (*B*) of the uncoated and the coated membranes.

Membrane	Water permeability coefficient (A) [L/m^2 h bar] [a]	Salt rejection (R) [%] [a]	Salt permeability coefficient (B) [L/m^2 h] [a]
Uncoated LE-400	4.20 ± 0.11	95.5 ± 2.8	5.50 ± 3.34
c10_t70	4.63 ± 0.42	89.7 ± 4.6	15.05 ± 8.56
c50_t70	4.17 ± 0.56	89.1 ± 2.8	14.24 ± 5.50
c100_t70	1.52 ± 0.37	93.6 ± 2.0	2.98 ± 1.67

[a] Water flux (J_v) and salt rejection (*R*) of the membranes were evaluated using 10 mM NaCl feed solution and applied pressure of 27.6 bar (400 psi) at 23 ºC.

8. Conclusions

In this thesis, thin-film composites (TFC) were fabricated and modified using various coating methods. Firstly, the aim was to create a TFC packaging film with tailored permeability [P1–P3]. It was essential to study the effect of atmospheric plasma pre-treatment and sol-gel coating layer on the oxygen (O_2) and water vapour (WV) permeability. In addition, the thesis investigated the effect of sol-gel coating composition on the O_2 permeability and oil repellence. Secondly, the aim was to investigate the effects of surface properties on the anti-fouling performance of coated polyamide (PA) TFC membranes [P4–P6]. Polyvinyl alcohol (PVA) and atomic-layer-deposition (ALD) were used to enhance the anti-fouling performance of TFC-PA membrane. Both antimicrobial and anti-adhesion approaches were studied so as to gain further understanding of the anti-fouling tendency. The main conclusions of the thesis are the following:

- SiOx coating was plasma-deposited on LDPE-boards. However, the SiOx coating did not improve the barrier performance of the LDPE-board. Therefore, a plasma-assisted sol-gel hybrid coating approach was considered for the LDPE-board. The composition of the two different sol-gel coatings (named SG204 and SG206) had an effect on barrier performances. The SG206 coating with more cross-linked 3D oligomer structure showed better O_2 barrier performance in comparison to the SG204 coating with 2D oligomer structure. Nevertheless, the SG204 coating enhanced the oleophobicity of the LDPE-board, indicating improved grease barrier performance. The wettability and adhesion of the sol-gel coatings were enhanced when using the atmospheric plasma pre-treatment. Therefore, the plasma-activation of LDPE ensured the enhancement of O_2 barrier performance for the SG206 coating and the grease barrier performance for the SG204 coating respectively. [P1–P2]
- The sol-gel coating (named SG200) was deposited on the PLA-board to form a smooth and hydrophilic primer layer. Besides the primer function, the SG200 coating showed a moderate improvement of O_2 and WV barrier. The ALD-Al_2O_3 layers were successfully deposited on top of the SG200 coating. The ALD coating further enhanced the O_2 and WV barrier performances. In

fact, the TFC structure based on the ALD and sol-gel coatings had a somewhat better barrier performance compared to a plain ALD coating. [P3]

- Surface characterisation of commercially available uncoated and coated TFC-PA membranes revealed that the coating layer had a significant effect on the hydrophobicity, surface energy and roughness. In addition, the surface characterisation of experimental PVA-, PVA-PHMG- and ALD-coated TFC-PA membranes revealed an increase in the hydrophilicity and surface polarity. [P4–P6]
- All the coated membranes had better anti-fouling performance in comparison to uncoated TFC-PA membranes. The experimental PVA and ALD coatings showed anti-adhesion performance, showing a decrease in the attachment of the three model bacteria. The surface polarity correlated with the attachment of bacteria. The antimicrobial coatings with a higher PHMG percentage tended to have a higher bacteria-repellence and antimicrobial performance. CFU and DIZ results proved the antimicrobial performance of PHMG. [P4–P6]
- The PVA-, PVA-PHMG and ALD coatings had an effect on permeability and rejection of the TFC-PA membranes. PVA and PVA-PHMG coatings reduced the water and salt permeability and also, increased the salt rejection. Furthermore, the increase of the PHMG content showed a decrease in salt rejection. The thinner ALD coatings increased the water and salt permeability and also, reduced the salt rejection. However, the thicker ALD coatings reduced the water and salt permeability, while the salt rejection was slightly increased. [P5–P6]

This study provides a basis for future development of TFC concepts with tailored permeability. Further research should focus on the effect of pre-treatment or primer layers to smooth the rough and heterogeneous polymer surfaces prior to the deposition of nanoscale inorganic coatings. In addition, the use of organic or inorganic-organic protective coatings could be considered, in order to improve the durability of an inorganic coating layer. Furthermore, tailoring of the coating compositions and combining of coating layer structures are expected to improve the barrier performance.

An optimal anti-fouling surface could be obtained by applying a coating, which is a combination of anti-adhesion and antimicrobial performances. However, further optimisation of the coating composition is needed in order to create the anti-fouling performance without sacrificing the RO performance. In addition, further studies should include long-term fouling studies of the coated TFC-PA membranes.

The ALD method has not been used for surface modification of RO membranes until now. Based on the first experiments, the ALD technology could be a promising candidate to modify RO membranes. In fact, even a low thickness of ALD coating could modify the surface properties of the RO membrane by increasing the hydrophilicity and polarity as well as by lowering the surface roughness. These properties are essential improvements, especially for anti-fouling and permeability.

Despite the promising results obtained in this study, the parameters of the Al_2O_3-based ALD process need further investigation in order to find the balance between improved anti-fouling and RO performance. Moreover, investigations of other inorganic ALD chemistries are expected to provide new functionalities.

References

[1] M.F. Ashby and Y.J.M Bréchet, Designing hybrid materials, Acta Mater. 51 (2003) 5801–5821.

[2] G. Choudalakis and A.D. Gotsis, Permeability of polymer/clay nanocomposites: A review, Eur. Polym. J. 45 (2009) 967–984.

[3] L. Valentini and J.M. Kenny, Novel approaches to developing carbon nanotube based polymer composites: fundamental studies and nanotech applications, Polymer 46 (2005) 6715–6718.

[4] L.W. McKeen, Permeability properties of polymers and elastomers, 3rd edition, Elsevier, USA, (2012).

[5] N.S. Sangaj and V.C. Malshe, Permeability of polymers in protective organic coatings, Prog. Org. Coat. 50 (2004) 28–39.

[6] H.M.C. de Azeredo, Nanocomposites for food packaging applications, Food Res. Int. 42 (2009) 1240–1253.

[7] J.-C. Schotter and B. Bozkaya-Schotter, Current and emerging membrane processes for water treatment, in: K.-V. Peinemann and S.P. Nunes, Membranes for water treatment, vol. 4., Wiley-VCH, Weinheim, (2010) 53–88.

[8] A.G. Fane, C.Y. Tang and R. Wang, Membrane technology for water: Microfiltration, ultrafiltration, nanofiltration and reverse Osmosis, Chapter 91, Elsevier, USA, (2010).

[9] R. Field, Fundamentals of fouling, in: K.-V. Peinemann and S.P. Nunes, Membranes for water treatment, vol. 4., Wiley-VCH, Weinheim, (2010) 1–23.

[10] D. Rana and T. Matsuura, Surface modifications for antifouling membranes, Chem. Rev. 110 (2010) 2448–2471.

[11] M. Ulbricht, Advanced functional polymer membranes, Polymer 47 (2006) 2217–2262.

[12] M. Stamm, Polymer surfaces and interfaces – characterization, modification and applications, First edition, Chapter 11 grafting on solid surfaces: “grafting to” and “grafting from” methods, Springer-Verlag Berlin Heidelberg, (2008).

[13] D. Hegemann, H. Brunner and C. Oehr, Plasma treatment of polymers for surface and adhesion improvement, Nucl. Instr. Meth. Phys. 208 (2003) 281–286.

[14] C. Tendero, C. Tixier, P. Tristant, J. Desmaison and P. Leprince, Atmospheric pressure plasmas: A review, Spectrochim. Acta B 61 (2006) 2–30.

[15] Y.M. Chung, M.J. Jung, J.G. Han, M.W. Lee and Y.M. Kim, Atmospheric RF plasma effects on the film adhesion property, Thin Solid Films 354 (2004) 447–448.

[16] D. Vangeneugden, S. Paulussen, O. Goossens, R. Rego and K. Rose, Aerosol-assisted plasma deposition of barrier coatings using organic-inorganic sol-gel precursor systems, Chem. Vap. Depositions 11 (2005) 491–496.

[17] M. Pykönen, H. Sundqvist, O.-V. Kaukoniemi, M. Tuominen, J. Lahti, P. Fardim and M. Toivakka, Ageing effect in atmospheric plasma activation of paper substrates, Surf. Coat. Technol. 202 (2008) 3777–3786.

[18] M.H. Blees, G.B. Winkelman, A.R. Balkenende and J.M.J. den Toonder, The effect of friction on scratch adhesion testing: application to a sol–gel coating on polypropylene, Thin Solid Films 359 (2000) 1–13.

[19] O.-J. Kwon, S. Tang, S.-W. Myung, N. Lu and H.S. Choi, Surface characteristics of polypropylene film treated by an atmospheric pressure plasma, Surf. Coat. Technol. 192 (2005) 1–10.

[20] M.F Dubreuil and E.M. Bongaers, Use of atmospheric pressure plasma technology for durable hydrophilicity enhancement of polymeric substrates, Surf. Coat. Technol. 202 (2008) 5036–5042.

[21] D. Hegemann, H. Brunner and C. Oehr, Evaluation of deposition conditions to design plasma coatings like SiOx and a-C:H on polymers, Surf. Coat. Technol., 174–175 (2003) 253–260.

[22] G.R. Nowling, M. Yajima, S.E. Babayan, M. Moravej, X. Yang, W. Hoffman and R.F. Hicks, Chamberless plasma deposition of glass coatings on plastic. Plasma Sources Sci. Technol. 14 (2005) 477–484.

[23] S. Paulussen, R. Rego, O. Goossens, D. Vangeneugden and K. Rose. Plasma polymerization of hybrid organic–inorganic monomers in an atmos-

pheric pressure dielectric barrier discharge. Surf. Coat. Technol. 200 (2005) 672–675.

[24] M.R. De Geyter, N. Van Vlierberghe, S. Dubruel, P. Leys and C. Schacht, Deposition of polymethyl methacrylate on polypropylene substrates using an atmospheric pressure dielectric barrier discharge. Surf. Coat. Technol. 203 (2009) 1366–1372.

[25] C.J. Brinker and G.W. Scherer, Sol-Gel Science: The Physics and Chemistry of Sol-Gel Processing. Academic Press, Inc., San Diego (1990).

[26] C. Sanchez, B. Julián, P. Belleville and M. Popall, Applications of hybrid organic–inorganic nanocomposites. J. Mater. Chem. 15 (2005) 3559–3592.

[27] R. Puurunen, Surface chemistry of atomic layer deposition: A case study for the trimethylaluminum / water process. J. Appl. Phys. 97 (2005) 121301–121352.

[28] S. M. George, Atomic Layer Deposition: An Overview, Chem. Rev. 110 (2010) 111–131.

[29] M. Kemell, E. Färm, M. Ritala and M. Leskelä, Surface modification of thermoplastics by atomic layer deposition of Al_2O_3 and TiO_2 thin films, Eur. Polym. J. 44 (2008) 3564–3570.

[30] G.K. Hyde, G. Scarel, J.C. Spagnola, Q. Peng, K. Lee, B. Gong, K.G. Roberts, K.M. Roth, C.A. Hanson, C. K. Devine, S.M. Stewart, D. Hojo, J. Na, J.S. Jur and G.N. Parsons, Atomic layer deposition and abrupt wetting transitions on nonwoven polypropylene and woven cotton fabrics, Langmuir 26 (2010) 2550–2558.

[31] J.C. Spagnola, B. Gong, S.A. Arvidson, J.S. Jur, S.A. Khan and G.N. Parsons, Surface and sub-surface reactions during low temperature aluminium oxide atomic layer deposition on fiber-forming polymers, J. Mater. Chem. 20 (2010) 4213–4222.

[32] B. Gong and G.N. Parsons, Quantitative in situ infrared analysis of reactions between trimethylaluminum and polymers during Al_2O_3 atomic layer deposition, J. Mater. Chem. 22 (2012) 15672–15682.

[33] B. Gong, J.C. Spagnola, S.A. Arvidson, S.A. Khan and G.N. Parsons, Directed inorganic modification of bi-component polymer fibers by selective vapor reaction and atomic layer deposition, Polymer 53 (2012) 4631–4636.

[34] T. Hirvikorpi, R. Laine, M. Vähä-Nissi, V. Kilpi, E. Salo,W.-M. Lia, S. Lindfors, J. Vartiainen, E. Kenttä, J. Nikkola, A. Harlin and J. Kostamo, Barrier properties of plastic films coated with Al_20_3 by roll-to-roll ALD, Thin Solid Films 550 (2014) 164–169.

[35] ASTM D 3985 Standard test method for oxygen gas transmission rate through plastic film and sheeting using a coulometric sensor, ASTM International: West Conshohocken, PA.

[36] ASTM E 96 Standard test methods for water vapor transmission of materials, ASTM International: West, Conshohocken, PA.

[37] ISO 2528 Sheet materials – Determination of water vapor transmission rate – Gravimetric (dish) method, International Organization for Standardization: Geneva, Switzerland.

[38] TAPPI T 448 Water vapor transmission rate of sheet materials at standard temperature and humidity, TAPPI Press, Atlanta, GA.

[39] L.H. Ledenbach and R.T. Marshall, Microbiological spoilage of dairy products, pp. 41–67, in W.H. Sperber, M.P. Doyle (eds) Compendium of the microbiological spoilage of foods and beverages, Food microbiology and safety. Springer Science + Business Media, LLC, (2009).

[40] B. Nowak, K. Sammet, G. Klein and T. Mueffling, Trends in the production and storage of fresh meat- the holistic approach to bacteriological meat quality, Int. J. Food Sci. Technol. 41 (2006) 303–310.

[41] C.J. Weber, V. Haugaard, R. Festersen and G. Bertelsen, Production and applications of biobased packaging materials for the food industry, Food Addit. Contam. 19 (2002) 172–177.

[42] H. Ayvaz, S. Schirmer, Y. Parulekar, V.M. Balasubramaniam, J.A. Somerville and H. Daryaei, Influence of selected packaging materials on some quality aspects of pressureassisted thermally processed carrots during storage, LWT-Food Sci. Technol. 46 (2012) 437–447.

[43] J. Breil, Chapter 16 - Multilayer oriented films, in: J.R. Wagner Jr., Multilayer flexible films, Elsevier, USA (2009) 231–237.

[44] T. Hirvikorpi, M. Vähä-Nissi, A. Harlin and M. Karppinen, Comparison of some coating techniques to fabricate barrier layers on packaging materials, Thin Solid Films 518 (2010) 5463–5466.

[45] T. Hirvikorpi, M. Vähä-Nissi, A. Harlin, J. Marles, V. Miikkulainen and M. Karppinen, Effect of corona pre-treatment on the performance of gas barrier layers applied by atomic layer deposition onto polymer-coated paperboard, Appl. Surf. Sci. 257 (2010) 736–740.

[46] C.F. Struller, P.J. Kelly, N.J. Copeland, V. Tobin, H.E. Assender, C.W. Holliday and S.J. Read, Aluminium oxide barrier films on polymeric web and their conversion for packaging applications, Thin Solid Films 553 (2014) 153–156.

[47] C.A. Bishop and E.M. Mount, Chapter 14 - Vacuum metallizing for flexible packaging, in J.R. Wagner Jr., Multilayer flexible films, Elsevier, USA, (2009) 185–202.

[48] K.-H. Haas, S. Amberg-Schwab, K. Rose and G. Schottner, Functionalized coatings based on inorganic-organic polymers (ORMOCER's) and their combination with vapor deposited inorganic thin films, Surf. Coat. Technol. 111 (1999) 72–79.

[49] J.A. Redondo, Development and experience with new FILMTEC reverse osmosis membrane elements for water treatment, Desalination 108 (1996) 59–66.

[50] M. Al-Ahmad, F.A. Abdul Aleem, A. Mutiri and A.Ubaisy, Biofuoling in RO membrane systems Part 1: Fundamentals and control, Desalination 132 (2000) 173–179.

[51] C.Y. Tang , Y.-N. Kwon and J.O. Leckie, Fouling of reverse osmosis and nanofiltration membranes by humic acid – Effects of solution composition and hydrodynamic conditions, J. Membr. Sci. 290 (2007) 86–94.

[52] Y.N. Wang and C.Y. Tang, Protein fouling of nanofiltration, reverse osmosis, and ultrafiltration membranes – The role of hydrodynamic conditions, solution chemistry, and membrane properties, J. Membr. Sci. 376 (2011) 275–282.

[53] D. Norberg, S. Hong, J. Taylor and Y. Zhao, Surface characterization and performance evaluation of commercial fouling resistant low-pressure RO membranes, Desalination 202 (2007) 45–52.

[54] H.-C. Hemming, Reverse osmosis membrane biofouling, Exp. Therm. Fluid Sci. 14 4 (1997) 382–391.

[55] M. Herzberg and M.Elimelech, Biofouling of reverse osmosis membranes: Role of biofilm-enhanced osmotic pressure, J. Membr. Sci. 295 (2007) 11–20.

[56] M. Klausen, A. Heydorn, P. Ragas, L. Lambertsen, A. Aaes-Jørgensen, S. Molin and T. Tolker-Nielsen, Biofilm formation by Pseudomonas aeruginosa wild type, flagella and type IV pili mutants. Mol. Microbiol. 48 6 (2003) 1511–1524.

[57] H-C. Flemming and J. Wingender, The biofilm matrix, Nat. Rev. Microbiol. 8 (2010) 623–633.

[58] S.B. Sadr Ghayeni, P.J. Beatson, R.P. Schneider and A.G. Fane, Adhesion of waste water bacteria to reverse osmosis membranes, J. Membr. Sci. 138 (1998) 29–42.

[59] A. Subramani and E.M.V. Hoek, Biofilm formation, cleaning, re-formation on polyamide composite membranes, Desalination 257 (2010) 73–79.

[60] S. Kang, E.M.V. Hoek, H. Choi and H. Shin, Effect of membrane surface properties during the fast evaluation of cell attachment, Sep. Sci. Technol. 41 (2006) 1475–1487.

[61] M.M.T. Khan, P.S. Stewart, D.J. Moll, W.E. Mickols, S.E. Nelson and A.K. Camper, Characterization and effect of biofouling on polyamide reverse osmosis and nanofiltration membrane surfaces, Biofouling 27 2 (2011) 173–183.

[62] V. Chen, J. Mansouri and T. Charlton, Biofouling in membrane systems, in: K.-V. Peinemann and S.P. Nunes, Membranes for water treatment, Wiley-VCH, Weinheim, 4 (2010) 25–48.

[63] T. Nguyen, F.A. Roddick and L. Fan, Biofouling of water treatment membranes: A review of the underlying causes, monitoring techniques and control measures, Membranes 2 (2012) 804–840.

[64] C.Y. Tang, Y.-N. Kwon and J.O. Leckie, Effect of membrane chemistry and coating layer on physiochemical properties of thin film composite polyamide RO and NF membranes: I. FTIR and XPS characterization of polyamide and coating layer chemistry, Desalination 242 (2009) 149–167.

[65] H-L. Yang, J. Chun-Te Lin and C. Huang, Application of nanosilver surface modification to RO membrane and spacer for mitigating biofouling in seawater desalination, Water Res. 42 (2009) 3777–3786.

[66] B.-H. Jeong, E.M.V. Hoeka, Y. Yan, A. Subramani, X. Huanga, G. Hurwitz, A.K. Ghosha and A. Jawor, Interfacial polymerization of thin film nanocomposites: a new concept for reverse osmosis membranes, J. Membr. Sci. 294 (2007) 1–7.

[67] S. Belfer, Y. Purinson, R. Fainshtein, Y. Radchenko, and O. Kedem, Surface modification of commercial composite polyamide reverse osmosis membranes, J. Membr. Sci. 139 (1998) 175–181.

[68] J. Gilron, S. Belfer, P. Väisänen and M. Nyström, Effects of surface modification on antifouling and performance properties of reverse osmosis membranes, Desalination 140 (2001) 167–179.

[69] Y. Zhou, S. Yub, C. Gaoc and X. Fenga, Surface modification of thin film composite polyamide membranes by electrostatic self-deposition of polycations for improved fouling resistance, Sep. Purif. Technol. 66 (2009) 287–294.

[70] G. Kang, M. Liu, B. Lin, Y. Cao and Q. Yuan, A novel method of surface modification on thin-film composite reverse osmosis membrane by grafting poly(ethylene glycol), Polymer 48 (2007) 1165–1170.

[71] J.S. Louie, I. Pinnau, I. Ciobanu, K. P. Ishida, A. Ng and M. Reinhard, The Effects of polyether-polyamide block copolymer coating on performance and fouling of reverse osmosis membranes, J. Membr. Sci. 280 (2006) 762–770.

[72] S. Yu, Z. Lü, Z. Chena, X. Liua, M. Liua and C. Gaoc, Surface modification of thin-film composite polyamide reverse osmosis membranes by coating N-isopropylacrylamide-co-acrylic acid copolymers for improved membrane properties, J. Membr. Sci. 371 (2011) 293–306.

[73] T.D. Tran, S. Mori and M. Suzuki, Characteristics of polyimide-based composite membranes fabricated by low-temperature plasma polymerization, Thin Solid Films 516 (2008) 4384–4390.

[74] L. Zou, I. Vidalis, D. Steele, A. Michelmore, S.P. Low and J.Q.J.C. Verberk, Surface hydrophilic modification of RO membranes by plasma polymerization for low organic fouling, J. Membr. Sci. 369 (2011) 420–428.

[75] N. Kim, D. Ho Shin and Y. Taek Lee, Effect of silane coupling agents on the performance of RO membranes, J. Membr. Sci. 300 (2007) 224–231.

[76] D. Ho Shin, N. Kim and Y. Taek Lee, Modification to the polyamide TFC RO membranes for improvement of chlorine-resistance, J. Membr. Sci. 376 (2011) 302–311.

[77] C. Kong, A. Koushima, T. Kamada, T. Shintani, M. Kanezashi, T. Yoshioka and T. Tsuru, Enhanced performance of inorganic-polyamide nanocomposite membranes prepared by metal-alkoxide-assisted interfacial polymerization, J. Membr. Sci. 366 (2011) 382–388.

[78] Q. Xu, Y. Yang, X. Wang, Z. Wang, W. Jin, J. Huang and Y. Wang, Atomic layer deposition of alumina on porous polytetrafluoroethylene membranes for enhanced hydrophilicity and separation performances, J. Membr. Sci. 415–416 (2012) 435–443.

[79] F. Li, L. Li, X. Liao and Y. Wang, Precise pore size tuning and surface modifications of polymeric membranes using the atomic layer deposition technique, J. Membr. Sci. 385–386 (2011) 1–9.

[80] Q. Wang, X. Wang, Z. Wang, J. Huang and Y. Wang, PVDF membranes with simultaneously enhanced permeability and selectivity by breaking the trade off effect via atomic layer deposition of TiO_2, J. Membr. Sci. 442 (2013) 57–64.

[81] F. Li, Y. Yang, Y. Fan, W. Xing and Y. Wang, Modification of ceramic membranes for pore structure tailoring: The atomic layer deposition route, J. Membr. Sci. 397–398 (2012) 17–23.

[82] M.A. Cameron, I.P. Gartland, J.A. Smith, S.F. Diaz and S.M. George, Atomic layer deposition of SiO_2 and TiO_2 in alumina tubular membranes:

Pore reduction and effect of surface species on gas transport, Langmuir 16 (2000) 7435–7444.

[83] CSID:6270, http://www.chemspider.com/Chemical-Structure.6270.html (accessed 07:43, Mar 16, 2014)

[84] CSID:16387, http://www.chemspider.com/Chemical-Structure.16387.html (accessed 08:04, Mar 16, 2014)

[85] CSID:68741, http://www.chemspider.com/Chemical-Structure.68741.html (accessed 07:39, Mar 16, 2014)

[86] CSID:14894, http://www.chemspider.com/Chemical-Structure.14894.html (accessed 07:37, Mar 16, 2014)

[87] B. Bolto, T. Tran, M. Hoang and Z. Xie, Crosslinked Poly(vinyl alcohol) Membranes, Progr. Polym. Sci. 34 (2009) 969–981.

[88] K. Grundke, Characterization of polymer surfaces by wetting and electrokinetic measurements – contact angle, interfacial tension, zeta potential, in: M. Stamm, Polymer surfaces and interfaces – Characterization, modification and applications, 1st Edition, Springer-Verlag Berlin Heidelberg (2008) 103–136.

[89] M. Klausen, A. Heydorn, P. Ragas, L. Lambertsen, A. Aaes-Jørgensen, S. Molin and T. Tolker-Nielsen, Biofilm formation by Pseudomonas aeruginosa wild type, Flagella and type IV Pili Mutants, Mol. Microbiol. 48 6 (2003) 1511–1524.

[90] D1141-98 Standard practise for the preparation of substitute ocean water, (2008).

[91] M. Schaechter, Escherichia Coli, in M. Schaechter, Encyclopedia of microbiology 3rd Edition, Elsevier, USA, (2009) 125–132.

[92] P.J. Piggot, Bacillus Subtilis, in M. Schaechter, Encyclopedia of microbiology 3rd Edition, Elsevier, USA, (2009) 45–56.

[93] Methods for dilution antimicrobial susceptibility tests for bacteria that grow aerobically, 9th ed. CLSI document M07-A9, Clinical Laboratory Standards Institute, Wayne, PA, 32 2 (2012).

[94] Performance standards for antimicrobial disk susceptibility tests; Approved standard, 9th ed, CLSI document M2-A9. Clinical Laboratory Standards Institute, Wayne, PA, 26 1 (2006).

[95] Y-N. Wang and C.Y. Tang, Protein fouling of nanofiltration, reverse osmosis, and ultrafiltration membranes – The role of hydrodynamic conditions, solution chemistry, and membrane properties, J. Membr. Sci., 376 (2011) 275–282.

[96] U. W. Gedde, Polymer physics, 1st ed., Kluwer Academic Publishers, Dordrecht, The Netherlands, 1995, 154–155.

[97] A. Grüniger, A. Bieder, A. Sonnenfeld, Ph. Rudolf von Rohr, U. Müller and R. Hauert, Influence of film structure and composition on diffusion barrier performance of SiOx thin films deposited by PECVD, Surf. Coat. Technol. 200 (2006) 4564–4571.

[98] R. Morent, N. De Geyter, Sandra Van Vlierberghe, P. Dubruel, C. Leys and E. Schacht, Organic-inorganic behaviour of HMDSO films plasma-polymerized at atmospheric pressure, Surf. Coat. Technol. 203 (2009) 1366–1372.

[99] I. Sawada, R. Fachrul, T. Ito, Y. Ohmukai, T. Maruyama and H. Matsuyama, Development of a hydrophilic polymer membrane containing silver nanoparticles with both organic antifouling and antibacterial properties, J. Membr. Sci. 387–388 (2012) 1–6.

[100] S. Balta, A. Sotto, P. Luisa, L. Benea, B. Van der Bruggena and J. Kim, A new outlook on membrane enhancement with nanoparticles: the alternative of ZnO, J. Membr. Sci. 389 (2012) 155–161.

[101] R.M. Silverstein and F.X. Webster, Spectrometric identification of organic compounds, 6th Edition, John Wiley & Sons, Inc. New York (1997).

[102] N.B. Colthup, L.H. Daly and S.E. Wiberley, Introduction to infrared and raman spectroscopy, Academic Press Inc. New York (1975).

[103] H.S. Mansur, C.M. Sadahira, A.N. Souza and A.A.P. Mansur, FTIR spectroscopy characterization of poly (vinyl alcohol) hydrogel with different hydrolysis degree and chemically crosslinked with glutaraldehyde, Mater. Sci. Eng. 28 (2008) 539–548.

[104] H. Hachisuka and K. Ikeda, Composite reverse osmosis membrane having a separation layer with polyvinyl alcohol coating and method of reverse osmosis treatment of water using the same. (2001) US Patent 6177011 B1.

[105] I.C. Kim and K.H. Lee, Dyeing process wastewater treatment using fouling resistant nanofiltration and reverse osmosis membranes, Desalination 192 (2006) 246–251.

[106] C.Y. Tang, Y.-N. Kwon and J.O. Leckie, Effect of membrane chemistry and coating layer on physiochemical properties of thin film composite polyamide RO and NF membranes II – Membrane physiochemical properties and their dependence on polyamide and coating layers, Desalination 242 (2009) 168–182.

[107] K.C. Khulbe, C.Y. Feng and T. Matsuura, Synthetic polymeric membranes – characterisation by atomic force microscopy, Springer-Verlag Berlin Heidelberg (2008) 157–167.

[108] O.J. Schmidt, A Schmidt and D. Toptchiev, Biocidal polymers based on guanidine salts. (2006) US Patent 7001606.

[109] Z.X. Zhou, D.F. Wei, Y. Guan, A.N. Zheng and J.J. Zhong, Damage of Escherichia coli membrane by bactericidal agent polyhexamethylene guanidine hydrochloride: Micrographic evidences, J. Appl. Microbiol. 108 (2010) 898–907.

[110] J.S. Louie, I. Pinnau, I. Ciobanu, K.P. Ishida, A. Ng and M. Reinhard, Effects of polyether-polyamide block copolymer coating on performance and fouling of reverse osmosis membranes, J. Membr. Sci. 280 (2006) 762–770.

[111] N.P. Kobayashi, C. L. Donley, S. Wang and R.S. Williams, Atomic layer deposition of aluminium oxide on hydrophobic and hydrophilic surfaces, J. Cryst. Growth 299 (2007) 218–222.

[112] S.D. Puckett, E. Taylor, T. Raimondo and T. J. Webster, The relationship between the nanostructure of titanium surfaces and bacterial attachment, Biomaterials 31 (2010) 706–713.

PUBLICATION P1

Reel-to-reel inline atmospheric plasma deposition of hydrophobic coatings

In: Journal of Coatings Technology and Research 8(2)2011, pp. 237–245.

Publication P1 of this publication is not included in the PDF version.

PUBLICATION P2

Raising the barriers

Nano-layer enhances resistance properties of polyethylene laminate

In: European Coatings Journal (1), pp. 41–47.

Raising the barriers

Nano-layer enhances resistance properties of polyethylene laminate

Juha Nikkola

Two sol-gel coatings were studied as barrier coatings on polyethylene-coated paper used in packaging applications. Smooth dense films were formed, but plasma pre-treatment was essential to ensure good adhesion and functional properties. Substantial performance differences were observed between the hydrophobically functionalised coating and the hydrophilically functionalised one.

The traditional packaging film materials, non-polar polypropylene (PP) and polyethylene (PE) are used in several industrial packaging applications. However, economic pressures and competition have created a trend towards a need for superior and multifunctional performances with even higher line speeds.

The ever-increasing demands on product properties combined with faster line speeds make it challenging to achieve the level of adhesion required for thin coatings in particular. In order to meet these challenges, new surface activation methods and functional coatings on paper, paperboard or plastic films have been developed to provide special or enhanced properties in the field of paper converting [1].

During the last ten years there has been general interest in studying the potential of organic-inorganic hybrid sol-gel thin films. The sol-gel process involves the development of nanoscale networks in a continuous liquid phase through the formation of a colloidal suspension and the subsequent gelation of the sol [2].

Sol-gel reactions summarised

Hydrolysis acts as a rapid initial reaction of the sol-gel process, where reactive alkoxide groups react with water molecules to form hydroxyl groups. *Equation (1)* represents the hydrolysis, where M is usually silicon, zirconium or titanium and n generally equals four.

(1) $M(OR)_n + H_2O \rightleftharpoons (OR)_{n-1}M(OH) + ROH$

After the initiation of the reaction, the hydrolysed alkoxides react easily with each other and produce the backbone of the sol-gel network. Water or alcohol is obtained as a by-product, depending on the reaction mechanism. The condensation reactions are explained by *Equations (2)* and *(3)*.

(2) $M(OH)(OR)_{n-1} + M(OR)_n \rightleftharpoons (OR)_{n-1}MOM(OR)_{n-1} + RO$

(3) $2M(OH)(OR)_{n-1} \rightleftharpoons (OR)_{n-1}MOM(OR)_{n-1} + H_2O$

Through these reactions the sol-gel technique offers opportunities to produce premium functional and transparent thin films.

Plasma technologies enhance coating adhesion

When using non-polar plastics such as polypropylene or polyethylene as the base material, it is necessary to increase the surface energy, by plasma pre-treatment for example, to obtain adhesion. One of the oldest industrial applications of plasma surface activation is corona treatment. The corona system does have certain limitations, though it has greatly evolved. For instance, the surface-activation effect of the corona is not stable and the use of plasma chemistry with different chemicals or gases is limited.

Dielectric barrier discharge (DBD) plasmas were originally created to eliminate the inhomogeneity of the surface treatment in the corona discharge [3]. The system is based on a dielectric layer covering at least one of the electrodes used. This generates a random distribution of streamers and a diffuse plasma, with a non-localised treatment effect. Other methods to generate the plasma include radio frequency (RF) plasma and microwave induced plasma (MIP).

RF plasma is based on a capacitive or inductive matching of the impedance in the system, with a time-varying magnetic field subsequently creating an electric ring field which excites the electrons and produces plasma [4]. In MIP, the plasma is produced in an electrodeless manner, by the microwaves which ionise the gas used and further support the propagation of the microwaves.

One of the main drawbacks of conventional DBD systems for surface modification is the risk of damage and/or back treatment of the substrate by direct plasma interaction. Due to these limitations in traditional corona or plasma techniques, cold or non-equilibrium atmospheric pressure plasmas have been studied and developed.

In addition, the search for new functionalities on paper surfaces has initiated research into novel atmospheric plasma applications for paper products. Recently, several authors have presented their studies on novel atmospheric plasma equipment and surface activation or deposition [5, 6, 7].

Plasma treatments tested in similar applications

The sol-gel technique with atmospheric plasma pre-treatment has proved to be a potential method to produce functional sol-gel thin films on reel-to-reel products [8, 9]. The use of atmospheric pressure plasma to obtain hybrid inorganic-organic barrier coatings on polyethylene terephthalate (PET) films has also been studied [10]. The

* **Corresponding author:**
Juha Nikkola
VTT Technical Research Centre of Finland
Juha,Nikkola@vtt.fi

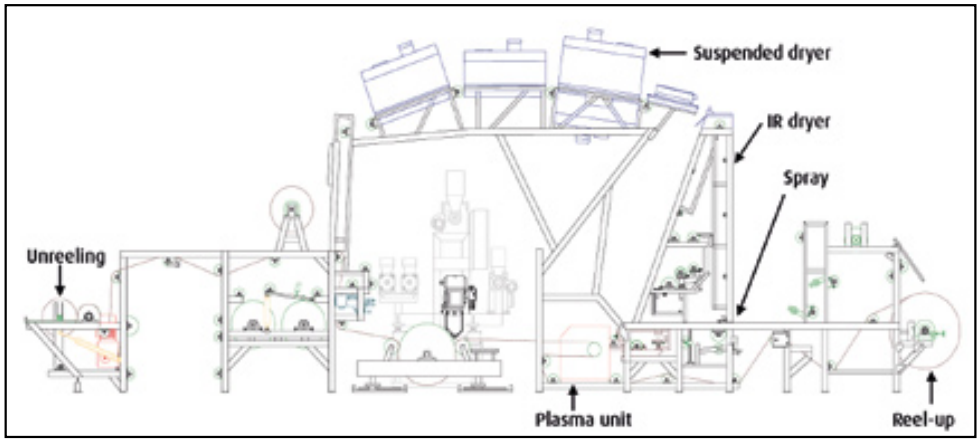

Figure 1: Extrusion coating line equipped with plasma activation unit

authors suggested that atmospheric plasma enhanced coatings could be an effective and environmentally friendly alternative to traditional barrier coatings such as polyvinylidene chloride (PVdC) lacquers.
In addition, durable hydrophilisation of PET, PP and PE films has been studied by Dubreuil et al [11]. They used acetic acid and ethyl acetate as precursors to deposit a hydrophilic layer on polymer surfaces with DBD atmospheric pressure plasma. Based on their experiments, these atmospheric pressure induced coatings can be used to produce durable hydrophilisation of polymer surfaces, which further improves the adhesion between polymer surfaces and coatings in certain applications.
In relation to this work, the pilot extrusion coating line (*Figure 1*) located at Tampere University of Technology was equipped with an atmospheric plasma pre-treatment unit. The main goal was to obtain high barrier effects to oxygen, grease etc with antimicrobial properties on the basis of PE-coated paper with different surface treatments.
Initially, multifunctional sol-gel based coatings were developed. Subsequently, the coatings thus developed were applied onto plasma pre-treated PE-coated paper in both laboratory and pilot scale on-line trials.

Experimental equipment and materials

The specifications of the plasma treatment unit on the coating line are shown in *Table 1*. Argon and helium may be used as treatment gases. In a typical experiment the atmospheric plasma pre-treatment unit is used to activate the substrate (e.g. plastic film) prior to coating or printing. In this study, the atmospheric plasma pre-treatment was used to pre-treat PE-coated paper prior to spraying on the sol-gel coating.
In the laboratory scale trials, thermal curing of the coatings was performed in a heating chamber at 110 °C for 10 minutes, whereas in pilot scale trials curing was by using IR and the suspended dryers of the pilot line.
The substrate material used in this work was "Lumiflex" (paper coated with polyethylene (PE) at 15 g/m^2) obtained from StoraEnso Oyj. Two silane based sol-gel coatings referred to as SG204 and SG206, developed by

Table 1: Plasma parameters in plasma activation

Parameter	Value
Treatment power	Max. 2000 W
Voltage	22.5–25.0 kV
Frequency	21.5–25.0 kHz
Treatment width	Max. 370 mm

Video interviews on packaging coatings: www.european-coatings.com/videos/

Results at a glance

›› Polyethylene and polypropylene are widely used as packaging materials. However, demands for both higher production speeds and enhanced performance are creating difficulties in applying coatings to these non-polar substrates to provide the desired performance.

›› Two different sol-gel coatings were studied as barrier coatings on polyethylene-coated paper. One coating was hydrophobically functionalised with long-chain hydrocarbon groups and the other hydrophilically functionalised with amino groups.

›› Surface characterisation by SEM and AFM showed that smooth dense layers were formed on the PE. Plasma pre-treatment greatly improved adhesion and performance of the coatings.

›› Only the hydrophobic coating provided effective grease barrier properties, whereas only the hydrophilic coating showed significant oxygen barrier properties and antibacterial activity.

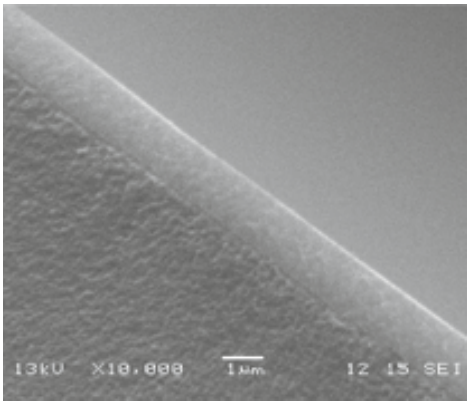

Figure 2: SEM cross-section image of amino-based sol-gel coating on PE-coated paper

VTT Technical Research Centre of Finland, were prepared through hydrolysis and condensation reactions.
SG204 was functionalised with long-chain hydrocarbon groups (hydrophobic coating) and SG206 with amino groups (hydrophilic coating), respectively. The sol-gel coatings were applied by spray coating and cured by heat as described above.

Test procedures summarised

The oil and grease resistance of the specimens was studied by contact angle measurements with oleic acid. In addition, the effect of abrasive wear on the oil repellency was studied by a standard paint washing tester apparatus (modified standard DIN 53778), where a brush was used as an abrasive material (1000 abrasion cycles). Abrasion resistance was evaluated by comparing the contact angle values before and after the test.
Oxygen transmission rate of the coated samples was measured with a "Model 8001" oxygen permeation analyser from Systech Instruments Ltd. The oxygen transmission rate was measured at room temperature (23 °C) and with three different relative humidities: 0, 50, and 80 % RH.
A "JEOL JSM-6360LV" scanning electron microscope (SEM) was used to characterise the surface structure of sol-gel coated samples. The surface topography was analysed by atomic force microscopy (AFM) with a Park Systems "XE-100" using non-contact mode.
Antimicrobial activity was determined as described in standard JIS Z 2801: 2000 "Antimicrobial products - test for antimicrobial activity and efficacy". Bacterial suspensions of gram positive *Staphylococcus aureus* and gram negative *Escherichia coli* containing approximately 1×10^6 colony forming units/ml of test bacteria were placed on the surface of the specimen and incubated for 24 h at 35 °C.
After incubation the bacteria were washed from the samples and the number of viable bacteria was measured by

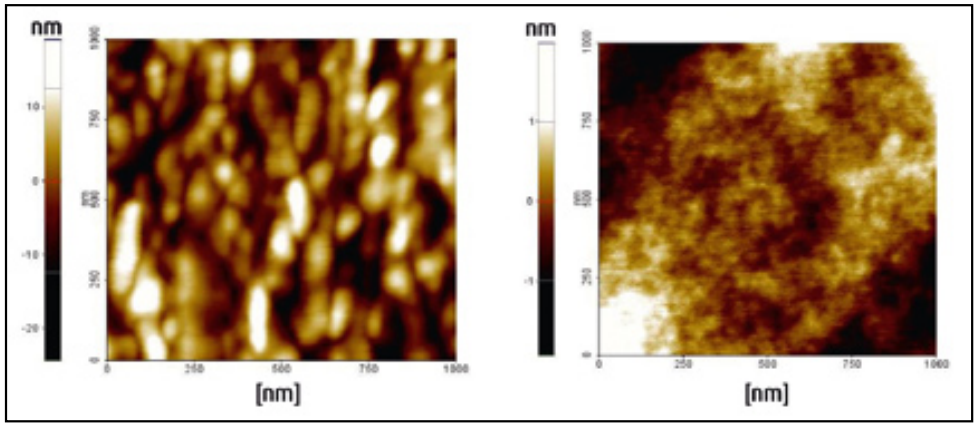

Figure 3: AFM images of untreated PE coated paper (left) and argon plasma enhanced amino-based coating on PE coated paper (right); image size is 1 µm x 1 µm

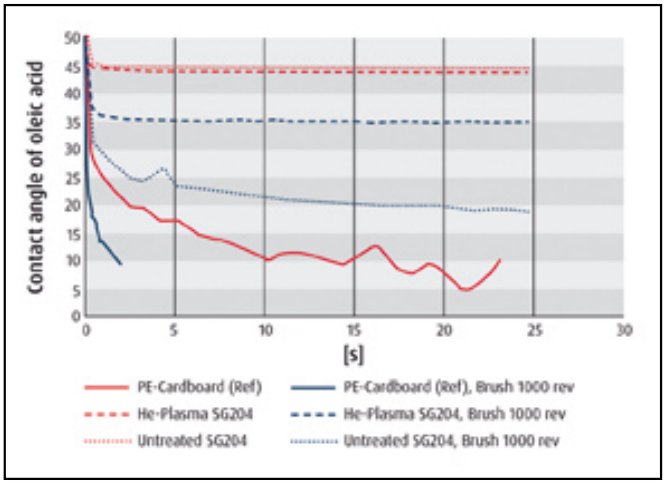

Figure 4: Contact angle values of oleic acid on test substrates before abrasive wearing

Figure 5: Contact angle values of oleic acid on test substrates after abrasive wearing.

plating. Antimicrobial activity was determined according to standard JIS Z 2801 using uncoated polyethylene as a reference sample.

Smooth, dense coatings are obtained

An example of the coating thickness and structure of the amino-based sol-gel coating is presented in an SEM cross-section image in *Figure 2*. The coating was applied by on-line spray coating on PE-coated paper after argon plasma pre-treatment in reel-to-reel paper converting at a line speed of 60 m/min.

The coating thickness determined from the SEM cross-section image is approximately 1.3 - 1.5 µm. Based on the SEM image, the coating has spread well and appears to be smooth and dense at the micro scale.

Figure 3 shows the AFM surface characterisation images of untreated PE-coated paper (left) and the amino-based sol-gel (right) coated sample. The R_a roughness values for untreated PE-coated paper are 5.1 nm and R_z is 43.0 nm. For sol-gel coated surfaces the roughness values are clearly lower. The R_a value is 0.4 nm and R_z is 3.8 nm. The measurement area was 1µm x 1µm.

These AFM results also show that the coating formed a smooth and dense layer on PE-coated paper in the nano scale.

Hydrophobic coating has good grease barrier properties

State-of-the-art coatings based on e.g. a fluorochemical [12] or on naturally-based chitosan [13] have been studied as grease barriers serving as an alternative or addition to polyolefin coatings on paper. For these fluorine-free coatings, the contact angles of oleic acid for untreated and sol-gel coated PE surfaces are presented in *Figure 4*. The rapid spreading of the oleic acid into the uncoated PE-coated paper took place during the measurement time of 25 seconds. The decrease of contact angle as a function of time also indicates possible absorption of oil into the specimen.

On the other hand, the stable contact angle over time shows that absorption of oil into the sol-gel coated surface did not occur. The sol-gel matrix with hydrophobic components displayed improved grease barrier performance. It should be noted that the hydrophobicity is not the only reason for these results, since the uncoated polyethylene surface is also relatively hydrophobic.

The improved performance may be due to the smooth and dense surface structure of the sol-gel coating together with the surface functionality introduced by long-chain hydrocarbon groups. However, it seems that the long-chain hydrocarbon groups also provide oil-repellent performance in addition to hydrophobicity. No effect of

plasma pre-treatment alone on the oil repellency of the coating in *Figure 4* was evident.
On the other hand, the effect of plasma pre-treatment on the adhesion of the sol-gel coating can be seen in *Figure 5*. The decrease of the oil repellency after abrasive wearing of the untreated and sol-gel coated specimen can be seen by the decrease of contact angle value.
The comparison between sol-gel coated samples with and without helium plasma pre-treatment showed that with the plasma pre-treated specimen the contact angle value decreased only slightly, whereas the value of the untreated sample decreased remarkably after wearing. This indicates that the adhesion of the coating to the PE surface was clearly enhanced by plasma pre-treatment and furthermore the durability of grease barrier was also improved.
With both specimens the contact angle value remained stable as a function of time, which means that absorption of the oil did not occur. The contact angle value for the untreated PE surface could not be measured after three seconds, indicating rapid absorption of the oil into the abraded PE surface.

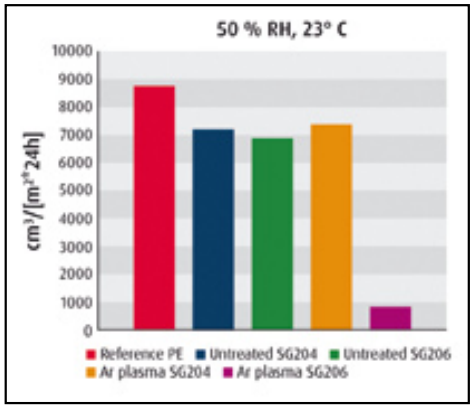

Figure 6: Oxygen transmission rates (OTR) of sol-gel coatings SG204 and SG206 with and without plasma pre-treatment on polyethylene coated paper (as reference)

Oxygen barrier performance can be enhanced

The oxygen transmission rates (OTR) of both sol-gel coatings with and without plasma pre-treatment are presented in *Figure 6*. The oxygen transmission rate for untreated polyethylene was approximately 8700 $cm^3/(m^2 \times 24\ h)$ at 23 °C, 50 % RH. The additional sol-gel coating layer on top of the polyethylene film improved the oxygen barrier levels.

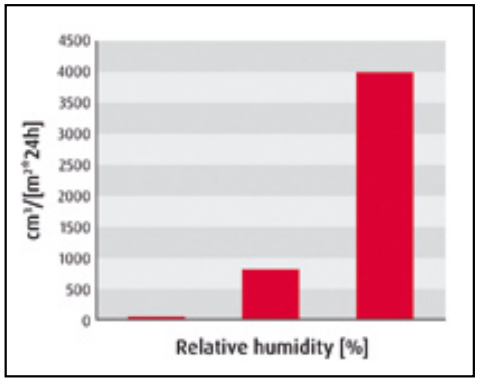

Figure 7: Oxygen transmission rates in different relative humidities for SG206 sol-gel coating on PE-coated paper with argon plasma activation

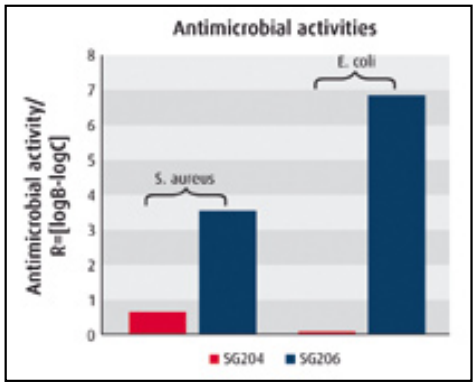

Figure 8: Antimicrobial activity of the SG204 and SG206 coatings against Staphylococcus aureus and Escherichia coli after 24 h at 35 °C

Additionally, the effect of plasma pre-treatment on the OTR value of SG206 can be seen. The comparison between untreated and argon plasma pre-treated SG206 coating shows that the OTR value is remarkably lower when using argon plasma pre-treatment. The improvement in oxygen barrier performance was most likely due to improved spreadability and uniformity of the coating.

In addition to the plasma pre-treatment, the chemistry of sol-gel coatings affects the oxygen barrier performance. It can be seen that even after plasma pre-treatment the hydrophobic SG204 coating did not have the same effect on oxygen barrier properties as the hydrophilic one. In addition to the differences in surface chemistry, it seemed that SG206 formed a denser inorganic network, as had been reported earlier for amino-based coatings [14], whereas the SG204 did not form a similar network.

Effects of relative humidity on hydrophilic coating

Figure 7 presents the OTR values of the SG206 coating on argon plasma pre-treated PE-coated paper as a function of different relative humidities. It was observed that when the relative humidity content was 0 % RH, the oxygen transmission rate of the sol-gel coated specimen was even lower than presented above. In addition, it was seen that the OTR value increased when the relative humidity content increased.

It seemed that the increase in moisture content adversely affected the uniformity and density of the sol-gel coating layer and therefore increased the OTR value. Also, this effect is most likely due to the hydrophilic nature of the SG206 coating, when it increasingly attracts H_2O molecules to the surface due to the increase of moisture content.

Therefore the hydrophilicity of the SG206 coating may further diminish its barrier effect against oxygen molecules at higher moisture levels. Similar behaviour has been noted when studying the oxygen barrier performance of hydrophilic chitosan coatings [15].

The further development of the sol-gel coating composition for better oxygen barrier in higher moisture content will be continued in future studies. However, the OTR value (4000 $cm^3/(m^2 \times 24\ h)$) in 80 % RH for sol-gel coated sample was still notably lower than the value (8700 $cm^3/(m^2 \times 24\ h)$) for the reference untreated polyethylene coated paper.

Amino functionalised coating shows antimicrobial properties

Antimicrobial properties were determined as described in standard JIS Z 2801. Activity was expressed using an R-value determined as shown in *Equation 4*:

$$R = \log B - \log C \quad (4)$$

Here, B indicates the viable cells on the reference after 24 hours and C the viable cells on the sample after 24 hours. Materials are evaluated as having antimicrobial properties if a calculated reduction of $R \geq 2$ is attained.

The antimicrobial activity of the two coatings against *S. aureus* and *E. coli* is presented in *Figure 8*. These indicate that SG206 showed antimicrobial activity against both bacteria, whereas SG204 did not.

This behaviour is again due to the difference in coating composition. However, neither of the coatings includes biocides for achieving the antimicrobial activity, which has been already studied elsewhere [16, 17]. In SG206 the antimicrobial activity is based on the direct interaction between the amino groups and bacteria, which inhibits their growth. A similar approach has already been presented in spacecraft solutions [18], but not in packaging coatings.

Even though the results are very promising, the use of this approach is limited in food contact applications, since the coating does not meet the requirements set by the European packaging legislation nor does it have

FDA (US Food and Drug Administration) acceptance. Therefore, at present these coatings should be used only in packaging applications where direct food contact can be avoided.

Surface chemistry is key to performance

In summary, two different kinds of sol-gel coatings for functional polyethylene packaging applications have been developed. The coatings were successfully applied onto PE by spray coating in a reel-to-reel paper converting process. The performance of the two coatings revealed that the surface chemistry had a remarkable effect on the desired properties.

Firstly, good grease barrier performance was obtained with the hydrophobic coating and secondly, oxygen barrier and antimicrobial performances were obtained with the hydrophilic coating. Apart from the surface chemistry, it is proposed that the coating composition, inorganic network density and surface functionality affected the performance.

The spreadability and adhesion of the coatings on the polyethylene surface was clearly improved by using atmospheric plasma pre-treatment, which also enhanced the barrier performance of the coatings.

REFERENCES

[1] *Lahti J.*, D.Sc.Thesis, Tampere University of Technology, 2005.
[2] *Brinker C. J., Scherer G. W.*, Sol-Gel Science: The Physics and Chemistry of Sol-Gel Processing, Academic Press, Inc., 1990.
[3] *Tendero C.et al*, Spectrochimica Acta Part B: Atomic Spectroscopy, 2006, Vol 61, pp 2-30.
[4] *Fauchais P., Vardelle A.*, Novelect (EDF R&D), 2003, 54 pp.
[5] *Vangeneugden D. et al*, Chem. Vap. Depositions, 2005, Vol. 11, pp 491-496.
[6] *Cernakova L.* et al, 9th TAPPI Advanced Coating Fundamentals Symposium, Turku, Finland, February 8th–10th 2006, pp 7–17.
[7] *Pykönen M. et al*, Surf. Coat. Technol., 2008, Vol. 202, pp 3777–3786.
[8] *Nikkola J. et al*, NETCOAT Annual Seminar, Tampere, Finland, 24 Oct. 2006.
[9] *Nikkola J. et al*, ISPC18, Kyoto, Japan, 26-31 Aug. 2007.
[10] *Paulussen S. et al*, Surf. Coat. Technol., 2005, Vol. 200, pp 672-675.
[11] *Dubreuil M. F., Bongaers E. M.*, Surf. Coat. Technol., 2008, Vol. 202, pp 5036-5042.
[12] *Deisenroth E. et al*, JOCCA-Surf. Coat. Intnl., 1998, Vol. 81, pp 440-447.
[13] *Kjellgren H. et al*, Carbohydrate Polymers, 2006, Vol. 65, pp 453-460.
[14] *Kyoungmi J., Hyunjoon K.*, Jnl. Sol-Gel Sci. Techn., 2007, Vol. 41, pp 19–24.
[15] *Vartiainen J., Tuominen M., Nättinen K.*, Jnl. Applied Polym. Sci., 2010, Vol. 116, No. 6, pp 3638–3647.
[16] *Marini M. et al*, Europ. Polym. Jnl., 2007, Vol. 43, pp 3621-3628.
[17] *Tatar P. et al*, Jnl. of Inorganic and Organometallic Polymers and Materials, 2007, Vol. 17, p 3.
[18] *Hodges M., Woodard D., Roberts M.*, SAE Technical Paper, International Conference on Environmental Systems, July 2007, Chicago, USA.

PUBLICATION P3

Thin Al_2O_3 barrier coatings onto temperature-sensitive packaging materials by atomic layer deposition

In: Surface and Coatings Technology (205),
pp. 5088–5092.

Surface & Coatings Technology 205 (2011) 5088–5092

Contents lists available at ScienceDirect

Surface & Coatings Technology

journal homepage: www.elsevier.com/locate/surfcoat

Thin Al_2O_3 barrier coatings onto temperature-sensitive packaging materials by atomic layer deposition

Terhi Hirvikorpi [a], Mika Vähä-Nissi [a,*], Juha Nikkola [b], Ali Harlin [a], Maarit Karppinen [c]

[a] VTT Technical Research Centre of Finland, Biologinkuja 7, Espoo, P.O. Box 1000, FI-02044 VTT, Finland
[b] VTT Technical Research Centre of Finland, P.O. Box 1300, FI-33101 Tampere, Finland
[c] Aalto University, School of Chemical Technology, Department of Chemistry, Laboratory of Inorganic Chemistry, P.O. Box 16100, FI-00076 AALTO, Finland

ARTICLE INFO

Article history:
Received 11 March 2011
Accepted in revised form 15 May 2011
Available online 23 May 2011

Keywords:
Atomic layer deposition
Barrier
Packaging material
Recyclability
Aluminum oxide
Biopolymer

ABSTRACT

Thin (25 nm) and highly uniform Al_2O_3 coatings have been deposited at relatively low temperature of 80 and 100 °C onto various bio-based polymeric materials employing the atomic layer deposition (ALD) technique. The work demonstrates that the ALD-grown Al_2O_3 coating significantly enhances the oxygen and water vapor barrier performance of these materials. Promising barrier properties were revealed for polylactide-coated board, hemicellulose-coated board as well as various biopolymer (polylactide, pectin and nano-fibrillated cellulose) films.

1. Introduction

Growing environmental concerns related to the use of synthetic polymers in the packaging industry have led to the need for new, especially bio-based, materials in such applications [1]. Currently synthetic polymers are widely used in packaging applications because of their relatively low cost and high performance. Bio-based packaging materials would have many advantages over their plastic competitors, such as sustainability and recyclability [2]. However, the sensitivity towards moisture restricts their extended use. One way to improve the water-sensitivity is to apply a surface coating.

"Barrier property" refers to a material's capability to resist the diffusion of a specific species (molecule, atom or ion) into and through the material. To be a good gas and vapor barrier, the material needs to be pore-free. When considering polymer-coated boards, the water vapor transmission rate (WVTR) is affected by e.g. the coating weight of the polymer as well as the temperature and humidity of the surroundings [3, 4]. The common polymers used in packages include low- and high-density polyethylene, polypropylene and polyethylene terephthalate [5]. Hygroscopic materials, such as many biopolymers, typically lose their barrier properties at high relative humidity due to water absorption [6]. There have been some efforts to improve the water vapor and oxygen barrier properties of polymer coatings with e.g. SiO_x layers [7]. Based on our recent studies [8–11] and studies by others [12–14], a thin Al_2O_3 coating layer grown by the atomic layer deposition (ALD) technique could work as a high-quality pore-free barrier film. The ALD technique is a surface-controlled layer-by-layer deposition process based on self-limiting gas-solid reactions [15]. It is well suited to produce inorganic gas barrier coatings on various materials.

Because of the covalent bonding, the adhesion of ALD-grown Al_2O_3 layer with the substrate is commonly excellent [16, 17]. Biopolymers typically have functional surface groups improving the bonding between the substrate and the Al_2O_3 layer. This makes biopolymeric materials, in our opinion, even more interesting substrates to create efficient gas and moisture barrier materials when combined with a thin Al_2O_3 coating than regular oil-based polymers, such as polyethylene, polypropylene or polyethylene terephthalate, for instance.

The ALD film growth characteristics on oil-based polymers have been previously studied by others [18–21]. Metal oxide films were found to grow on the native substrate surface. The basis for the initial film growth and nucleation was the hydroxyl groups on the polymer [15, 22]. The Al_2O_3 growth mechanism on porous polymeric substrates was demonstrated to occur through the adsorption of the trimethylaluminum (TMA) precursor onto the surface or by absorption into the porous material leading to the formation of Al_2O_3 clusters and further on to the linear film growth rate after the nucleation period [19]. The same mechanism has been demonstrated for many polymers. However, the initiation period differs depending on the polymer [18].

* Corresponding author.
E-mail addresses: Terhi.Hirvikorpi@vtt.fi (T. Hirvikorpi), mika.vaha-nissi@vtt.fi (M. Vähä-Nissi), juha.nikkola@vtt.fi (J. Nikkola), Ali.Harlin@vtt.fi (A. Harlin), maarit.karppinen@tkk.fi (M. Karppinen).

0257-8972/$ – see front matter © 2011 Elsevier B.V. All rights reserved.
doi:10.1016/j.surfcoat.2011.05.017

Here we demonstrate that ALD is indeed a promising technique to fabricate thin Al_2O_3 barrier layers on bio-based temperature-sensitive packaging materials. We moreover show that the barrier properties can be further improved by coating the materials with a pre-barrier layer prior to the ALD-Al_2O_3 coating.

2. Material and methods

The packaging materials investigated were commercial boards (provided by Stora Enso Oyj) coated with bio-based polylactide (PLA). In addition, several different biopolymer films were investigated. The materials tested are presented in Table 1. From our previous thermogravimetric study performed for most of the present substrate materials [8], we may conclude that the materials do not degrade thermally at temperatures employed in our low-temperature ALD-Al_2O_3 process.

The ALD-Al_2O_3 depositions were carried out at 80 or 100 °C in a Picosun SUNALE™ reactor on substrates that were *ca.* 10×10 cm^2 in size. Trimethylaluminum (TMA, electronic grade purity, SAFC Hitech) and H_2O or O_3 were used as precursors. Ozone was produced by feeding oxygen gas (99.9999%) into the reactor through an ozone generator (In USA Inc., model AC 2025). The concentration of ozone was ca. 8% and the gas flow rate during the pulse was about 200 sccm (standard cubic centimeters per minute). High purity nitrogen (99.9999% N_2) was used as a carrier and purge gas. The operating pressure was 1–2 kPa. The precursor pulsing sequence was: 0.1 s TMA pulse, 6 s N_2 purge, 0.1 s H_2O or O_3 pulse, and 6 s N_2 purge, and the number of ALD cycles was adjusted according to the targeted Al_2O_3 coating thickness of 25 nm (selected based on our previous works) [9–11]. The actual thicknesses of the Al_2O_3 films could not be directly measured. Instead, we estimated the thicknesses based on the growth rate determined to be appr. 0.1 nm/cycle with a Nanospec AFT4150 reflectometer from films grown on a Si(100) wafer. This was done for the TMA-H_2O process at both temperatures and for the TMA-O_3 process at 100 °C. Because of the different surface chemistries of different polymers, the actual thickness may somewhat deviate from that determined for the Al_2O_3-coated silicon wafer [20, 23]. It should also be mentioned that even though the aim was to deposit only on the polymer-coated side, film growth also on the uncoated side could not be totally prevented.

We also considered the possibility to coat the substrate material with a pre-barrier layer prior to the ALD-Al_2O_3 coating to block the largest pinholes in the porous substrates. For these experiments B2(PLA) substrates were used. Epoxy-based hybrid coatings with targeted coating weight of 2 g/m^2 were fabricated by a sol-gel (SG) method using 3-(trimethoxysilyl)propyl glycidyl (from Sigma-Aldrich) as an epoxy source, ethanol as a solvent and water to initiate the hydrolysis and condensation reactions. The coatings were sprayed on corona-treated substrates and dried at 120 °C for 10 min. The corona treatment unit (ET1 from Vetaphone) with treatment time of 60 s was used for better wetting and adhesion properties between the coating and the substrate. The SG-coated substrates were further coated with an Al_2O_3 layer at 80 °C using TMA and H_2O as precursors.

The Al_2O_3-coated samples were characterized by scanning electron microscopy (SEM; Hitachi S-3400 N VP-SEM, operating voltage 15 keV) for the microstructure. Prior to the imaging the samples were sputter-coated with Pt. The surface topography was analyzed with atomic force microscopy (AFM: Park Systems XE-100 equipment with cantilever 905-ACTA) using a non-contact "tapping" mode.

Contact angle (CA) and surface energy (SE) measurements (KSV CAM 200 Optical Contact Angle Meter) were carried out for some of the samples in a controlled atmosphere (relative humidity 50%, temperature 23 °C) with three to eight parallel measurements and expressed as degrees (°). The CA value was determined using water as solvent. For the SE measurements, water and di-iodomethane were used as solvents. The CA values of solvents were calculated at the time of 1 s from the moment the drop contacts. The SE values were calculated from the CA data by using the OWRK (ext. Fowkes) theory and expressed as mN/m.

For all the samples, the oxygen and water vapor transmission rate (OTR, WVTR) values were determined. The OTR values expressed as $cm^3/m^2/10^5$Pa/day were measured (Systech M8001 and Mocon Oxtran 2/20) from two to three parallel samples using humid gases at 23 °C and in 50% relative humidity. The WVTR values were measured from three to five parallel samples according to the modified gravimetric methods ISO 2528:1995 and SCAN P 22:68 and were expressed as g/m²/day in conditions of 23 °C and 75% relative humidity.

3. Results and discussion

Our first task was to optimize the ALD-Al_2O_3 process for temperature-sensitive bio-based substrates. In these preliminary experiments two PLA-coated board samples, B1(PLA) and B2(PLA), were investigated and the deposition parameters considered were the deposition temperature (80 or 100 °C) and the choice of the oxygen source (H_2O or O_3). Interestingly, the growth per cycle (GPC) values for the H_2O and O_3 processes were found to be nearly identical, i.e. 0.1 nm/cycle (as measured for films grown on silicon substrates). This somewhat disagrees with the work by Elliot et al. [22] reporting somewhat lower GPC values for the TMA-O_3 process compared to the TMA-H_2O process. It seems that in our case the O_3 gas might have been somewhat wet; note that the H_2O present may act as a catalyst for the reactions during the TMA-O_3 process, increasing the GPC value.

The results from the OTR and WVTR experiments for the B1(PLA) and B2(PLA) samples with differently grown Al_2O_3 coatings are shown in Table 2. Independent of the deposition parameters used, the 25-nm thick ALD-Al_2O_3 coating remarkably improves both the oxygen and water vapor barrier properties of our PLA-coated board samples. Previous studies have shown that the deposition temperature may have some impact on the surface topography and morphology as well on the adhesion of Al_2O_3 coating in the case of polymeric substrates [24]. Higher deposition temperature may increase crystallinity of the polymers and cause brittleness for polymer structures which could

Table 1
Packaging materials employed as substrates.

Code	Description
B1(PLA)	Polylactide-coated board; PLA 35 g/m^2, board 310 g/m^2
B2(PLA)	Polylactide-coated board; PLA 35 g/m^2, board 210 g/m^2
B3(PLA)	Polylactide-coated board; PLA 27 g/m^2, board 210 g/m^2
PLA1	Polylactide film, 20 μm
PLA2	Polylactide film, 75 μm
NFC	Nano-fibrillated cellulose film; NFC; appr. 60 g/m^2
B(GGM)	Galactoclugomannan-coated board; GGM appr. 9 g/m^2, board 200 g/m^2 pigment coated
PHB	Polyhydroxy butyrate film, 180 μm
Pectin	Pectin film made by solution casting, 160 μm

Table 2
OTR and WVTR values for plain and variously ALD-Al_2O_3-coated B1(PLA) and B2(PLA) samples. The ALD parameters investigated were the deposition temperature (80 or 100 °C) and the choice of the oxygen source (H_2O or O_3).

Sample	OTR ($cm^3/m^2/10^5$ Pa/day)	WVTR (g/m^2/day)
B1(PLA) uncoated	420 ± 10	65 ± 2
B1(PLA) + Al_2O_3 by H_2O (100 °C)	20 ± 3	1 ± 0.2
B1(PLA) + Al_2O_3 by O_3 (100 °C)	12 ± 1	5 ± 2
B2(PLA) uncoated	400 ± 9	75 ± 2
B2(PLA) + Al_2O_3 by H_2O (80 °C)	6 ± 1	3 ± 1
B2(PLA) + Al_2O_3 by O_3 (80 °C)	3 ± 1	7 ± 2
B2(PLA) + Al_2O_3 by O_3 (100 °C)	2 ± 0.2	1 ± 0.2

then lead to cracking of the polymer layer impairing the barrier properties. Here however, the choice of the deposition temperature (in the range investigated, i.e. 80–100 °C) may not be crucially important. In some cases even lower deposition temperatures might be advantageous. For extremely temperature-sensitive biopolymeric substrates the low deposition temperature could prevent the curling effect due to polymer shrinkage. Moreover, Lahtinen et al. [24], demonstrated that by using lower deposition temperatures it was possible to achieve better adhesion between the polymer surface and the Al_2O_3 coating.

Also, both the processes, TMA-H_2O and TMA-O_3, apparently work well at least for the PLA-coated boards. This could be due to the different fabrication methods of the pristine substrates. From Table 2, the OTR values achieved are somewhat better in the case of the TMA-O_3 process, while the opposite seems to be true for the WVTR values. During the water pulse, the absorbed H_2O may cause the polymer to swell, which should not be the case with O_3. OTR is generally regarded as more sensitive towards coating defects than WVTR. Hence, the TMA-O_3 process can be considered a highly potential alternative for depositing Al_2O_3 coatings on biopolymers except for the most sensitive materials not standing the strong oxidation power of O_3.

We should also consider the moisture within the polymer chains of the substrate material. Bio-based substrates tend to contain absorbed moisture and the removal of it could enhance the barrier properties because absorbed water may act as a plasticizer impairing the barrier properties. The possible benefits of the removal of the substrate moisture prior to the ALD-Al_2O_3 deposition were investigated by keeping a B1(PLA) sample in a heated (100 °C) ALD reactor chamber overnight before coating it with Al_2O_3 at 100 °C using the TMA-H_2O process. The overnight heat-treatment resulted in a slight improvement in the OTR value: the value decreased from 20 to 8 $cm^3/m^2/10^5$Pa/day. However, the effect on the WVTR value was just the opposite: it increased from 1 to 7 g/m^2/day. The removal of the moisture within the polymer chains made the sample brittle.

The main scope of the present work was to investigate whether the excellent results obtained for the PLA-coated boards with ALD-grown Al_2O_3 coatings could be extended to other bio-based materials. The oxygen and water vapor barrier results achieved for a variety of biopolymer substrates with a 25 nm-thick Al_2O_3 layer deposited by the TMA-H_2O process are summarized in Fig. 1. Note that H_2O was used as the oxygen source instead of O_3 to be sure that the results would not be distorted by the possible harmful effects of O_3 in the case of the most sensitive biopolymer film substrates. The depositions were performed at 80 or 100 °C depending on the expected temperature tolerance of the substrate material. From Fig. 1, it can be concluded that our ALD-Al_2O_3-coated PLA, pectin, NFC, B1(PLA) and B(GGM) samples are highly promising oxygen barriers with OTR values that are already close to the oxygen barrier level required for dry food applications. For example, for PLA1 and B1(PLA) the OTR values were improved from 702 to 43 $cm^3/m^2/10^5$Pa/day and from 420 to 20 $cm^3/m^2/10^5$Pa/day, respectively. Besides being a good oxygen barrier, the Al_2O_3-coated B1(PLA) sample is also a highly promising water vapor barrier as the WVTR value of it was improved from 65 to 1 g/m^2/day.

The NFC film investigated here is a highly interesting fiber network for various potential applications. Besides enhancing the oxygen barrier of NFC, the ALD-Al_2O_3 coating works as a kind of protective layer for the nanofibers (Fig. 2). Such materials are in the very focus of current research interest as examples of the controlled material integration of organic fibers and inorganic thin films [25]. This type of uniform coatings on single fibers are believed to open up new application possibilities e.g. in the area of filter development.

Despite the promising results achieved so far for the ALD-Al_2O_3 coated bio-based materials here and in our earlier studies [8–11], further improvements are still desired. A pre-barrier layer could close the larger pinholes on the surface of porous substrate making it denser and probably smoother and thus more favorable surface for the Al_2O_3 barrier layers to be grown on. The effect of a sol-gel coating between the substrate and the top ALD-Al_2O_3 coating was studied using B2(PLA) as a substrate material. In Fig. 3, AFM surface and phase images for plain, SG-coated and SG + Al_2O_3-coated B2(PLA) are presented. The observed average roughness (R_a) values are also given. From Fig. 3, the SG coating decreases the R_a value making the surface of the substrate smoother. The ALD-Al_2O_3 layer on top of the SG coating makes the surface even smoother. The total decrease in R_a was from 54 to 15 nm.

We also determined the contact angle (CA) and surface energy (SE) values for plain, SG-coated and SG + Al_2O_3-coated B2(PLA), see Table 3. The SG coating decreases the CA value indicating a more hydrophilic surface. The CA value drops even further with the additional Al_2O_3 coating. In Table 3, also given are the OTR and WVTR values for the same samples. The results show a moderate positive effect of SG coating on the barrier properties of B2(PLA). Only after the SG-coated B2(PLA) was additionally coated with Al_2O_3, the appreciably low OTR and WVTR values of 2 $cm^3/m^2/10^5$ Pa/day and 2 g/m^2/day, respectively, were reached. Most importantly, these

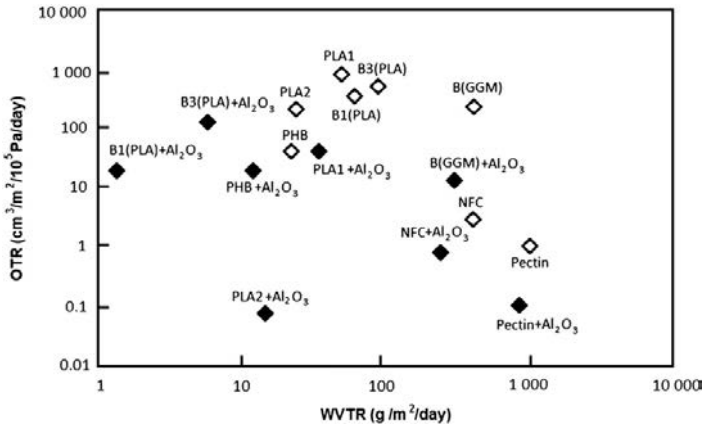

Fig. 1. Oxygen and water vapor barrier results achieved for various bio-based substrate materials (open markers) by means of a 25-nm thick ALD-Al_2O_3 coating (filled markers). The depositions were carried out at 80 or 100 °C using the TMA-H_2O process.

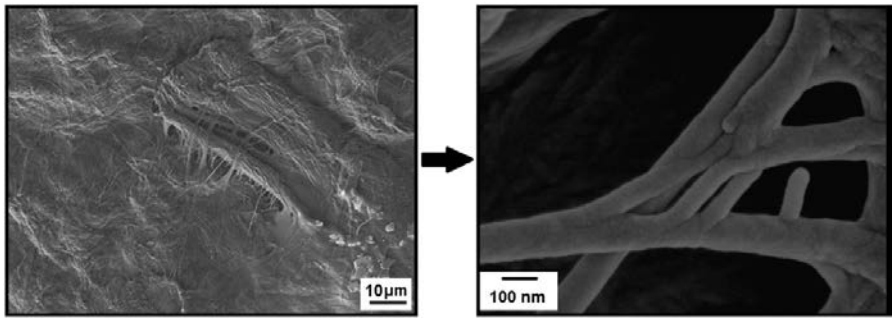

Fig. 2. SEM image (*left image*) with a magnification (*right image*) of NFC coated with a 25-nm thick Al_2O_3 layer, showing that the nano-fibrillated fibers are indeed uniformly coated with Al_2O_3. The smallest observed fiber thickness is *ca.* 50 nm and the curve radius from the fiber ends is appr. 25 nm.

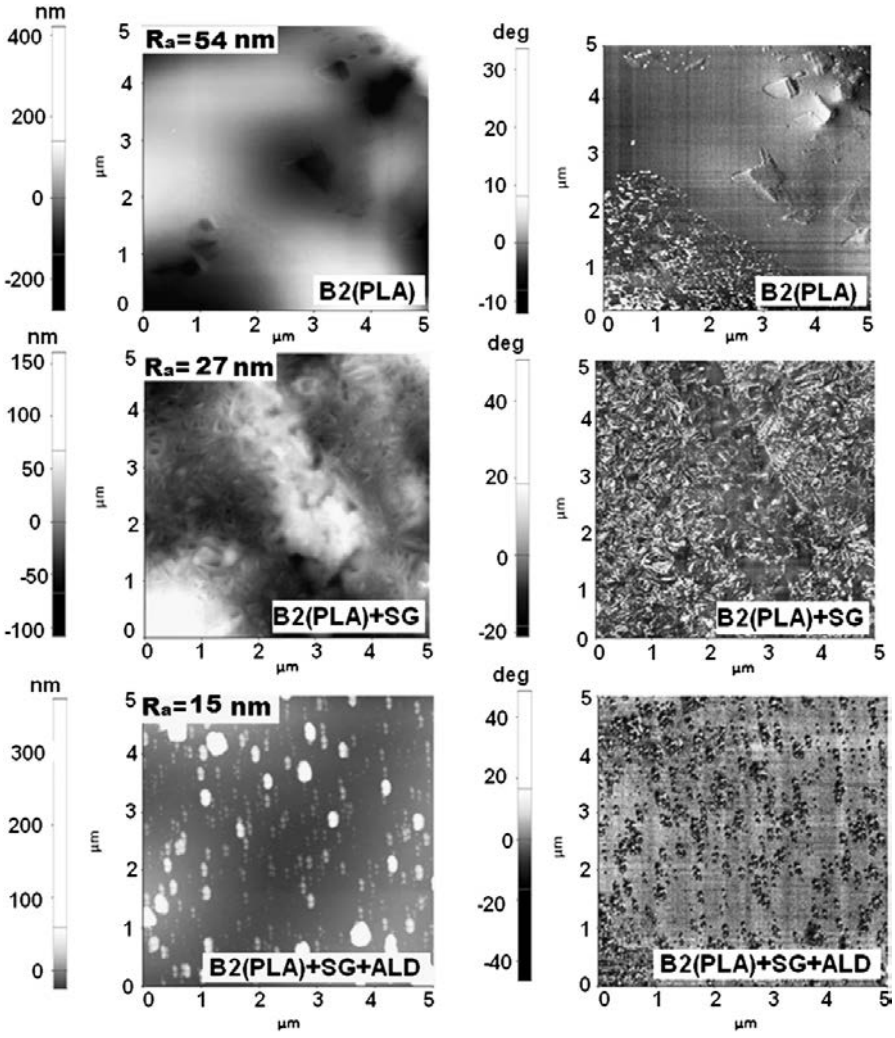

Fig. 3. AFM surface topography (*left image*) and phase (*right image*) images of plain, SG- and SG + Al_2O_3-coated B2(PLA).

Table 3
Contact angle (CA), surface energy (SE), OTR and WVTR values for plain, SG-, SG + Al_2O_3-, and Al_2O_3-coated B2(PLA). The total value of surface energy (SE) is the sum of dispersive (SE_d) and polar (SE_p) components.

Sample	CA (°)	SE_p (mN/m)	SE_d (mN/m)	SE (mN/m)	OTR ($cm^3/m^2/10^5$ Pa/day)	WVTR (g/m^2/day)
B2(PLA) uncoated	71	7.4	38.2	45.6	400 ± 9	75 ± 2
B2(PLA) + SG	58	13.2	40.6	53.8	310 ± 2	44 ± 2
B2(PLA) + SG + Al_2O_3	52	18.0	36.9	54.9	2 ± 1	2 ± 1
B2(PLA) + Al_2O_3	–	–	–	–	6 ± 1	3 ± 1

values are lower than those achieved for B2(PLA) with the ALD-Al_2O_3 coating only, i.e. 6 $cm^3/m^2/10^5$ Pa/day and 3 g/m^2/day, respectively.

4. Conclusions

We have demonstrated that the oxygen and water vapor barrier properties of various bio-based boards and films are significantly enhanced by coating them with a 25-nm thick ALD-grown Al_2O_3 film. Through careful process optimization excellent barrier properties were reached for some of the bio-based materials investigated such that the materials satisfy the basic requirements set for commercial barrier materials for dry food or pharmaceutical packaging applications. Also shown was that there are means to improve the barrier properties further by cheap and easy-to-make coatings applied on the substrate surface prior to the top ALD-Al_2O_3 coating. In the future these materials could be produced with a continuous ALD process. There are already research tools and several patent applications concerning the development of the continuous ALD process.

Acknowledgements

The authors thank VTT and the Academy of Finland (No: 126528) for funding. Stora Enso Oyj and polymer film suppliers are thanked for providing the substrates. The facilities of Nanomicroscopy Center, Aalto University were also used during this research.

References

[1] K. Khwaldia, E. Arab-Tehrany, S. Desobry, CRFSFS 1 (2010) 82–91.
[2] C. Andersson, Packag. Technol. Sci. 2 (2008) 339–372.
[3] J. Kuusipalo, K. Lahtinen, TAPPI J. 7 (2008) 8–15.
[4] A. Savolainen, J. Kuusipalo, E. Laiho, T. Penttinen, in: A. Savolainen (Ed.), Paper and Paperboard Converting, Fapet Oy, Helsinki Finland, 1998, pp. 123–187.
[5] J. Lange, Y. Wyser, Packag. Technol. Sci. 16 (2003) 149–158.
[6] Y. Leterrier, Prog. Mater. Sci. 48 (2003) 1–55.
[7] A. Sorrentino, M. Tortora, V.J. Vittoria, Polymer Sci. B 44 (2006) 265–274.
[8] T. Hirvikorpi, M. Vähä-Nissi, T. Mustonen, E. Iiskola, M. Karppinen, Thin Solid Films 518 (2010) 2654–2658.
[9] T. Hirvikorpi, M. Vähä-Nissi, A. Harlin, M. Karppinen, Thin Solid Films 518 (2010) 5463–5466.
[10] T. Hirvikorpi, M. Vähä-Nissi, A. Harlin, J. Marles, V. Miikkulainen, M. Karppinen, Appl. Surf. Sci. 257 (2010) 736–740.
[11] T. Hirvikorpi, M. Vähä-Nissi, J. Vartiainen, P. Penttilä, J. Nikkola, A. Harlin, R. Serimaa, M. Karppinen, J. Appl. Polymer Sci. (2011) in press.
[12] M.D. Groner, S.M. George, R.S. McLean, P.F. Carcia, Appl. Phys. Lett. 88 (051907) (2006) 1–3.
[13] P.F. Carcia, R.S. McLean, M.H. Reilly, M.D. Groner, S.M. George, Appl. Phys. Lett. 89 (031915) (2006) 1–3.
[14] S.H.K. Park, J. Oh, C.S. Hwang, J.I. Lee, Y.S. Yang, H.Y. Chu, H.Y. Electrochem, Solid-State Lett. 8 (2005) H21–H23.
[15] R.L. Puurunen, J. Appl. Phys. 97 (121301) (2005) 1–52.
[16] T.O. Kääriäinen, D.C. Cameron, M. Tanttari, Plasma Process. Polym. 6 (2009) 631–641.
[17] D.C. Miller, R.R. Foster, Y. Zhang, S.-H. Jen, J.A. Bertrand, Z. Lu, D. Seghete, J.L. O'Patchen, R. Yang, Y.-C. Lee, S.M. George, M.L. Dunn, J. Appl. Phys. 105 (2009) 093527-12.
[18] M.D. Groner, F.H. Fabreguette, J.W. Elam, S.M. George, Chem. Mater. 16 (2004) 639–645.
[19] C.A. Wilson, R.K. Grubbs, S.M. George, Chem. Mater 17 (2005) 5625–5634.
[20] J.D. Ferguson, A.W. Weimer, S.M. George, Chem. Mater. 16 (2004) 5602–5609.
[21] C.A. Wilson, J.A. McCormick, A.S. Cavanagh, D.N. Goldstein, A.W. Weimer, S.M. George, Thin Solid Films 516 (2008) 6175–6185.
[22] S.D. Elliot, G. Scarel, C. Wiemer, M. Fanciulli, G. Pavia, Chem. Mater. 18 (2006) 3764–3773.
[23] X.H. Liang, L.F. Hakim, G.D. Zhan, J.A. McCormick, S.M. George, A.W. Weimer, J.A. Spencer, K.J. Buechler, J. Blackson, C.J. Wood, J.R. Dorgan, J. Am. Ceram. Soc. 90 (2007) 57–63.
[24] K. Lahtinen, P. Maydannik, P. Johansson, T. Kääriäinen, D.C. Cameron, J. Kuusipalo, Surf. Coat. Technol. 205 (2011) 3916–3922.
[25] J.S. Jur, J.C. Spagnola, K. Lee, B. Gong, Q. Peng, G.N. Parsons, Langmuir 26 (2010) 8239–8244.

PUBLICATION P4

Bacterial anti-adhesion of coated and uncoated thin film composite (TFC) polyamide (PA) membranes

In: Journal of Coating Science and Technology
(1), pp. 1–7.

Publication P4 of this publication is not included in the PDF version.

PUBLICATION P5

Surface modification of thin film composite RO membrane for enhanced anti-biofouling performance

In: Journal of Membrane Science (444),
pp. 192–200.

Journal of Membrane Science 444 (2013) 192–200

Contents lists available at SciVerse ScienceDirect

Journal of Membrane Science

journal homepage: www.elsevier.com/locate/memsci

Surface modification of thin film composite RO membrane for enhanced anti-biofouling performance

Juha Nikkola [a,*], Xin Liu [c,d], Ye Li [c,d], Mari Raulio [b], Hanna-Leena Alakomi [b], Jing Wei [c,d], Chuyang Y. Tang [c,d]

[a] VTT Technical Research Centre of Finland, PO Box 1300, 33101 Tampere, Finland
[b] VTT Technical Research Centre of Finland, PO Box 1000, 02044 Espoo, Finland
[c] School of Civil and Environmental Engineering, Nanyang Technological University, Singapore 639798, Singapore
[d] Singapore Membrane Technology Centre, Nanyang Technological University, Singapore 637141, Singapore

ARTICLE INFO

Article history:
Received 14 March 2013
Received in revised form
15 May 2013
Accepted 16 May 2013
Available online 24 May 2013

Keywords:
Thin film composite (TFC) polyamide (PA)
Reverse osmosis (RO) membrane
Anti-adhesion
Antimicrobial

ABSTRACT

Anti-adhesion and antimicrobial coatings were prepared and applied on commercial thin-film-composite (TFC) polyamide (PA) membrane to enhance anti-biofouling performance. Polyvinyl alcohol (PVA) coating was modified with cationic polyhexamethylene guanidine hydrochloride (PHMG) polymer to obtain antimicrobial performance. ATR-FTIR, SEM and AFM investigated the surface chemistry and morphology of the coated membranes. The contact angle measurement was used to determine hydrophilicity and surface energy. All coated membranes revealed more hydrophilic and lower surface roughness compared to uncoated membrane. Lower number of adhered *Pseudomonas aeruginosa* (*P. aeruginosa*) bacteria was detected on coated membranes, indicating anti-adhesion performance. The colony forming unit (CFU) and diffusion inhibition zone (DIZ) tests determined antimicrobial activity of the coated membranes against *Escherichia coli* (*E. coli*) and *Bacillus subtilis* (*B. subtilis*), showing the antimicrobial performance of PHMG. The results suggested that an optimal anti-fouling surface could be obtained applying a coating, which combines anti-adhesion and antimicrobial performance.

1. Introduction

Reverse osmosis (RO) membranes are widely applied for seawater desalination and wastewater reclamation. However, biofouling of RO membranes remains as a critical challenge in these applications. Biofouling is initiated by the adhesion and accumulation of planktonic microorganisms followed by their primary colonization and growth [1]. The attachment of microorganisms together with their extracellular polymeric substance (EPS) decreases membrane permeability and therefore, increases the energy consumption of RO processes [2].

Biofouling can be affected by various factors, including feed water characteristics, hydrodynamic conditions, and membrane surface properties. Pre-treatment of feed water with disinfection, coagulation, filtration and/or adsorption are adopted to remove/inactivate microorganisms and to reduce organic/nutrient loading [2,3]. In addition, operating at moderate flux level seems to be effective in preventing severe biofouling at the initial fouling stage [4]. However, the growth and colonization of micro-organisms on membranes after initial attachment remains an unsolved issue [3]. Membrane surface properties play also a key role in affecting biofilm formation. In many cases, anti-fouling membrane is achieved as combination of the surface physiochemical properties, such as increased hydrophilicity, lowered surface roughness and neutralised surface charge [5]. It has been shown that surfaces are more easily fouled for membranes with high peaks or deep valleys [2,5]. Furthermore, the type of surface texture has essentially affected to the biofouling tendency [6,7].

Recently, surface modification of RO membranes has gained increasing attention [8]. For example, some of the commercial thin-film-composite (TFC) polyamide (PA) membranes are coated by additional thin PVA layer to introduce hydroxyl groups to the PA surface [9]. In the laboratory experiments, the surface modification of commercial TFC PA membrane has been carried out by depositing or grafting various hydrophilic polymeric substances on PA surface, such as hydrogels, surfactants or monomers [10–12]. Furthermore, these anti-adhesion surfaces can be prepared using contact active amphiphilic, microbe-repelling or anti-adhesive polymers [13–15]. In addition, active antimicrobial coatings with bactericidal effects have been prepared using heavy metal nanoparticles, such as silver, copper and zinc [16,17]. However, the heavy metal based antimicrobial coatings may have certain disadvantages: (1) uncontrolled leaching of the metal ions to the

* Correspondence to: VTT Technical Research Centre of Finland; Sinitaival 6, 33101 Tampere, Finland. Tel.: +358 207223672; fax: +358 207223498.
E-mail address: juha.nikkola@vtt.fi (J. Nikkola).

0376-7388/$ - see front matter © 2013 Elsevier B.V. All rights reserved.
http://dx.doi.org/10.1016/j.memsci.2013.05.032

surroundings decreases the self-life of the anti-fouling membrane [18], and (2) these metal ions may raise questions concerning their safety to environment [19]. In this regard, polymer based antimicrobial coatings may be favoured.

The current study aimed to develop surface coating method to enhance anti-biofouling performance of RO membranes. Polyvinyl alcohol (PVA) and cationic polyhexamethylene guanidine hydrochloride (PHMG) coatings were used to obtain hydrophilic and smooth surfaces to enhance membrane anti-adhesion properties. In addition, the PHMG coating was shown to have antimicrobial effect.

2. Experimental

2.1. Materials and chemicals

The commercial TFC PA membrane DOW™ FILMTEC™ LE-400, purchased from HOH Separtec Oy (Finland), was used as a substrate for the coatings. The following chemicals were used for the membrane surface modification. PVA (Mw 9000–10,000 g/mol, 80% hydrolysed) was purchased from Sigma-aldrich. PHMG, polyhexamethylene guanidine hydrochloride ($C_7N_3H_{15}\cdot HCl$, Mw=8000–10,000 g/mol) was provided by Soft Protector Oy. The chemical structures are presented in Scheme 1.

2.2. Membrane surface modification

The preparation of PVA coatings was done by mixing 2 wt% of PVA into milliQ water at 60 °C. After a complete mixing, the solution was cooled down to room temperature. The PVA–PHMG solutions were similarly prepared as described above, by adding PHMG to the PVA solution after the cooling step. PVA–PHMG solutions were prepared in ratios 95:5 and 99:1 (PVA:PHMG) with a total polymer content of 2 wt%. The pure PHMG solution (2 wt%) was prepared by mixing PHMG with milliQ water to reach the targeted concentration. PVA, PVA–PHMG and PHMG solutions were applied on the membrane coupons using dispersion coating method with K Control Coater K202 device (R K Print-Coat Instruments Ltd.). The device was equipped with glass bed and close wound K202 meter bar No. 0 was used to apply wet films with a thickness of 4 μm. The applied coatings were heat-treated at 110 °C for 2 min to evaporate the water and to increase the coating stability using thermal cross-linking [20].

2.3. Membrane characterizations

ATR-FTIR measurement was carried out to analyse the surface chemistry of uncoated and coated membranes. Perkin Elmer spectrum BX II FT-IR (Fourier transform IR) system was equipped with vertical-ATR (Attenuated total reflectance) and KRS-5 crystal. In a typical analysis 50 scans were collected from 500 to 4000 cm^{-1} at 4 cm^{-1} resolution. A background spectrum of pure KRS-5 was collected before running the samples.

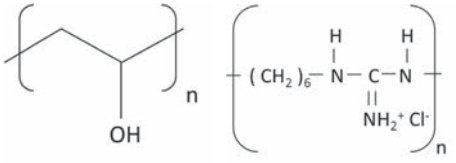

Polyvinyl alcohol (PVA) Polyhexamethylene guanidine hydrochloride (PHMG)

Scheme 1. Chemical structure of polyvinyl alcohol (PVA) and polyhexamethylene guanidine hydrochloride (PHMG).

The microscopic imaging of uncoated and coated membranes was conducted using scanning electron microscope (SEM) JEOL JSM-6360 LV 11 kV on high vacuum mode. Membrane cross sections were prepared by fracturing samples in liquid nitrogen. All SEM samples were sputter coated with gold before imaging.

The surface topography of uncoated and coated membrane samples was characterised using non-contact mode atomic force microscopy (NC-AFM). The NC-AFM analysis was performed using Park Systems XE-100 AFM equipment with cantilever 905M-ACTA (purchased from ST Instruments B.V.). Typically, the scan rate was 0.4–0.6 Hz and the measured area was 5×5 μm^2. Six replicate measurements were performed to determine the roughness value root-mean-square roughness R_{RMS}.

The measurements of the static contact angle were conducted by using Optical Tensiometer Theta T200 device (Attension, Biolin Scientific). The measurements were performed in a controlled atmosphere (RH 50%, temperature 23 °C) and the results are given as an average of five parallel measurements. The water contact angle values, expressed as °, are presented at the time of 30 s from the moment the drop contacts the surface. The surface energy values were obtained by measuring the contact angle of three different probe liquids, including water (H_2O, γ=72.80 mN/m), di-iodomethane (CH_2I_2, γ=50.80 mN/m) and formamide (CH_3NO, γ=58.20 mN/m). The total surface energy values, as summary of polar and dispersive surface energies, were determined from the measured contact angle data using the Fowkes theory [21].

2.4. Membrane anti-adhesion performance

Biofilm formation was demonstrated by analysing the attachment of *Pseudomonas aeruginosa* on uncoated and coated membranes. *P. aeruginosa* is Gram-negative, aerobic, rod-shaped bacterium, which is widely used as the model microbe for biofilm formation study [22–25]. Therefore, *P. aeruginosa* was selected as model bacterium in our study to provide comparable data related to the attachment of bacteria.

Bacteria attachment test was conducted by submerging the membranes (Ø4.7 cm) in bacterial suspension consisted of standard seawater ASTM D1141-98 (2008) [26]. Furthermore, the suspension was inoculated with overnight culture of *P. aeruginosa* (VTT E-96726) cultivated in 37 °C Trypticase soy broth solution, harvested by centrifugation (3000 rpm, 10 min) and washed with PBS (10 mM). The cell density was approximately 1×10^8 CFU/mL determined by plate count on TSA (37 °C, 1 d). The exposure of membranes was conducted in a rotary shaker (75 rpm) at room temperature for 1 d. The number of adhered cells on the membranes was determined after swabbing by plate count on TSA (37 °C, 1 d). It was aimed to describe the anti-adhesion performance. Results are presented as colony forming units per membrane area (CFU/cm^2). Three replicate membrane samples were examined for each membrane type.

2.5. Membrane antimicrobial performance

2.5.1. Colony forming unit (CFU) test

Antimicrobial performance of uncoated and coated membranes were analysed using colony forming unit (CFU) test for the two rod shaped model microorganisms, Gram-positive bacteria *Bacillus subtilis* (ATCC 6633) and Gram-negative bacteria *Escherichia coli* (ATCC 8739). These bacteria are extensively used to investigate surface antimicrobiality [27,28].

Bacteria cultivation was conducted by following the instruction of the producer, ATCC (24 h cultivation for *B. subtilis* in 30 °C nutrient broth solution and 12 h cultivation for *E. coli* in 37 °C

nutrient broth solution, respectively). Bacterial cells were harvested by centrifugation (3000 rpm, 10 min) and washed twice with 0.9% NaCl solution. Harvested bacterial cells were suspended in 0.9 % NaCl solution to achieve a cell density of 1.0×10^7 CFU/mL.

The membrane samples (Ø1.27 cm) were immersed in Milli-Q water for 24 h before the actual exposure to bacteria suspension. Bacterial suspensions were contacted with the respective membranes specimens for 24 h. A serial dilution of bacterial suspensions was performed for CFU test according to CLSI M07-A9 [29]. In the CFU test, 0.1 mL volume of diluents was inoculated and spread on a nutrient agar plate, and incubated for another 24 h. CFU results were obtained from 3 measurements of 3 independent membranes, and each measurement was based on the results of 3 replicate agar plates. Results are presented as colony forming units per membrane area (CFU/cm^2).

2.5.2. Diffusion inhibition zone (DIZ) method

Diffusion inhibition zone (DIZ) method was conducted to analyse the antimicrobial performance of the coatings in more detail. DIZ test of surface modified membranes were performed by following the CLSI document M2-A9 26:1 [30]. 100 μL bacterial inoculums were spread on the agar plates. Punched membrane discs (Ø12.7 mm) were placed on the agar plates and incubated at 24 h cultivation for *B. subtilis* at 30 °C and 12 h cultivation for *E. coli* at 37 °C. The diffusion inhibition zones formed around membranes were determined by visual observation.

2.6. Water permeability and salt rejection

Uncoated and coated membranes were tested in a lab-scale crossflow filtration setup to evaluate their water permeability and NaCl rejection according to Wang et al. [31]. Briefly, membranes were tested at a feed pressure of 27.6 bar (400 psi) using a feed water containing 10 mM NaCl. The temperature of feed water was maintained at 23 °C. Water flux of the membranes was determined by gravimetric method. Membrane NaCl rejection (R) was determined by:

$$R = \frac{C_f - C_p}{C_p} \times 100\%$$

where C_f and C_p are the concentrations (via conductivity measurements) of feed and permeate solutions, respectively.

3. Results and discussion

3.1. ATR-FTIR measurements

Fig. 1 present the ATR-FTIR spectra of uncoated membrane and PVA, PVA–PHMG and PHMG coated membranes. Fig. 1a shows the peaks in the range of 2000–600 cm^{-1}, and Table 1 summarises the corresponding peak assignments. Uncoated membrane showed typical FTIR spectra of fully aromatic PA membranes formed from *m*-phenylenediamine and trimesoyl chloride on top of a polysulfone support layer [9]. The peak at 1608 cm^{-1} was assigned to the C=O stretching (amide I band), and the peak at 1540 cm^{-1} was assigned to N–H bending (amide II band) known typical for a secondary amide group. The latter peak is due to the interaction between N–H bending and C–N stretching of the –CO–N–H group. The peak at 1590 cm^{-1} was assigned as C=C stretching of the aromatic ring. The characteristic peaks for the polysulfone was detected at 1324 cm^{-1} (SO_2 asymmetric stretching), 1244 cm^{-1} (C–O–C stretching) and 1150 cm^{-1} (SO_2 symmetric stretching) [32,33]. Also, the coated membrane samples revealed the characteristic peaks of the polysulfone layer and some of the peaks originated from the aromatic polyamide layer. Furthermore, PVA

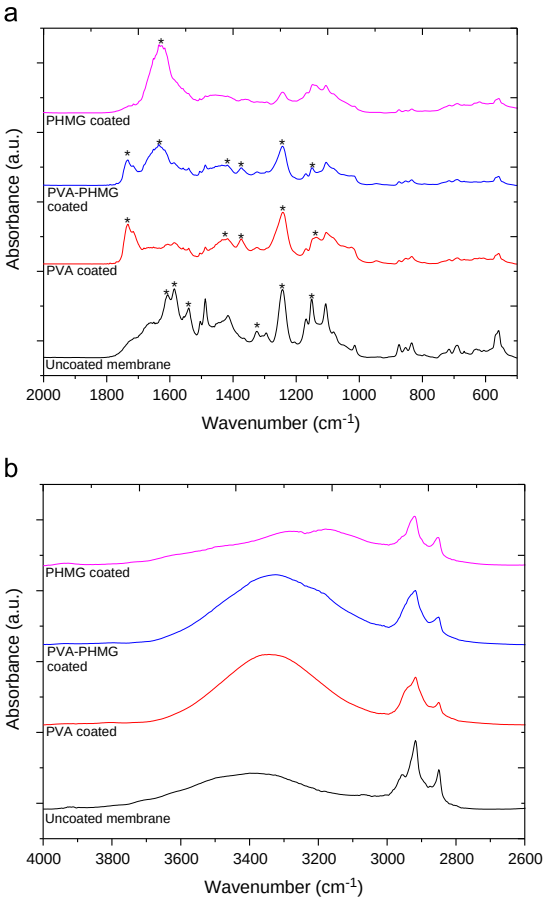

Fig. 1. (a) ATR-FTIR spectra of uncoated membrane and coated with PVA, PVA–PHMG (95:5) and PHMG. The peaks in the range of 2000–600 cm^{-1}. (b) ATR-FTIR spectra of uncoated Membrane and coated with PVA, PVA–PHMG (95:5) and PHMG. The peaks in the range of 4000–2600 cm^{-1}.

Table 1
Summary of the ATR-FTIR peak assignments.

Origin of the peaks	Wavenumber cm^{-1}	Peak assignment [9,32–34]
Polysulfone	3620–3200	O–H stretching
	2980–2820	Aromatic and aliphatic C–H stretching
	1324	SO_2 asymmetric stretching
	1244	C–O–C stretching of aryl group
	1150	SO_2 symmetric stretching
Aromatic polyamide	1608	C=O stretching (amide I band)
	1586	C=C stretching of the aromatic ring
	1540	N–H bending (amide II band)
PVA	3550–3100	O–H stretching
	2980–2850	aliphatic C–H stretching
	1720	C=O stretching
	1450–1420	C–O–H in-plane bending and C–H bending vibrations (CH_2, CH_3)
	1392	symmetric bending of CH_3 group
	1150–1070	aliphatic C–O and C–C stretching
PHMG	3300–3000	N–H stretching of primary amine
	1650	N–H bending (scissoring) of primary amine

coated membranes showed all the major peaks related to hydroxyl and acetate groups of the PVA precursor. Both of PVA and PVA–PHMG coated membranes showed strong peak at 1710 cm^{-1}, which was assigned as carbonyl peak's C=O stretching [32,33]. The slightly broadened peak at around 1450–1420 cm^{-1} was due to the overlapping C–O–H in-plane bending and C–H bending vibrations. The minor broadening of the peaks at 1150–1070 cm^{-1} may be attributed to aliphatic C–O and C–C stretching. The peak at 1392 cm^{-1} was assigned as symmetric bending of CH_3 group [34]. The most evident peak of PHMG was the strong peak at 1650 cm^{-1}, which was identified as N–H bending (scissoring) [32,33]. Similar low intensity peak was noticed in PVA–PHMG coating, although PHMG was added into PVA using relatively low amount.

Fig. 1b includes the characteristic peaks in the range of 4000–2600 cm^{-1} and Table 1 summarises the peak assignments for the same wavenumber range. The spectrum of uncoated membrane showed the low intensity peak at 3600–3200 cm^{-1}, indicating O–H stretching. Respectively, the evident peaks can be seen at around 3000–2900 cm^{-1} indicating aromatic and aliphatic C–H stretching. PVA and PVA–PHMG coated membrane showed strong increase in the O–H stretching peak at 3550–3100 cm^{-1}. Furthermore, the peak intensity of aliphatic C–H stretching at 2980–2850 cm^{-1} was more dominant compared to uncoated membrane. The pure PHMG coating showed strong and broad double peak at 3260 and 3130 cm^{-1}. These were assigned as asymmetrical and symmetrical N–H stretching vibrations, which are a typical for primary amine [32]. PVA–PHMG coating showed very weak broadening of the O–H stretching peak. However, the intensity was too low to be assigned as N–H stretching.

3.2. SEM characterization

The SEM characterization was performed to determine the coating thickness and to verify how the coatings were formed on the membrane. Fig. 2 presents the SEM cross-section images of uncoated and coated membranes. The SEM images show clearly the polysulfone support layer (~150 μm). In addition, the SEM images show either the polyamide selective layer or the coatings applied on the PA. The SEM cross-section (Fig. 2a) of the uncoated membrane revealed typical structure of PA TFC membrane [5,14]. Among the coated membranes, the SEM images (Fig. 2b–d) revealed that the coating thickness varied approximately from 80 nm to 250 nm (marked in the SEM images). The detected coating thicknesses were within the optimal range (1–1000 nm) reported in the literature [35,36].

3.3. AFM characterization

Fig. 3 presents AFM images of uncoated and coated membranes. The uncoated membrane showed the ridge-and-valley as well as nodular surface texture, which is typical for TFC PA membranes [37,38]. The AFM image of PVA coated membrane showed covering and smoothening of the nodular structure of TFC PA membrane. PVA–PHMG and PHMG coatings showed similarly smoothening effects, in good agreement with SEM observations (Fig. 2).

Table 2 presents the roughness parameter R_{RMS}. Comparison of the R_{RMS} values indicated the smoothening of uncoated membrane surface (67.8 nm) appeared with all the coatings. PVA coating showed the lowest RMS value (42.5 nm) among the coatings. Furthermore, the results indicated that PVA–PHMG (57.5 nm) and PHMG (53.4 nm) coatings had slightly rougher surface. The clear smoothening effect of PVA coating is most likely due to the film forming capability [36,37]. The combination of PHMG with PVA revealed little increase in the roughness values compared to pure PVA. This may be due to slight incompatibility between the PVA and PHMG polymers.

3.4. Water contact angle and surface energy

Table 2 summarises the results on the water contact angle and the surface energies. The results revealed that the water contact

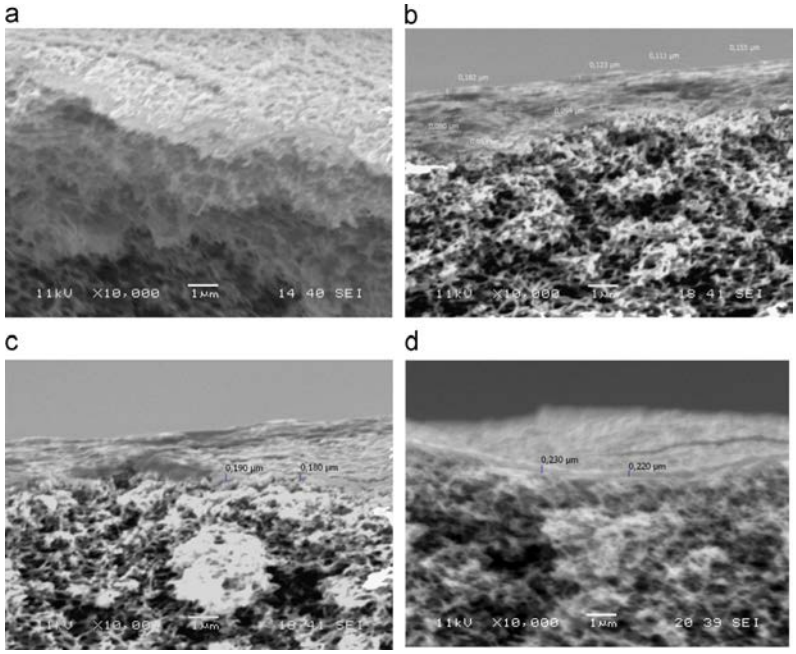

Fig. 2. SEM cross-section images (× 10,000 magnification) of the (a) uncoated membrane and coated membranes: (b) PVA, (c) PVA–PHMG (95:5) and (d) PHMG. The coatings thicknesses (80–250 nm) are marked in the specific SEM image.

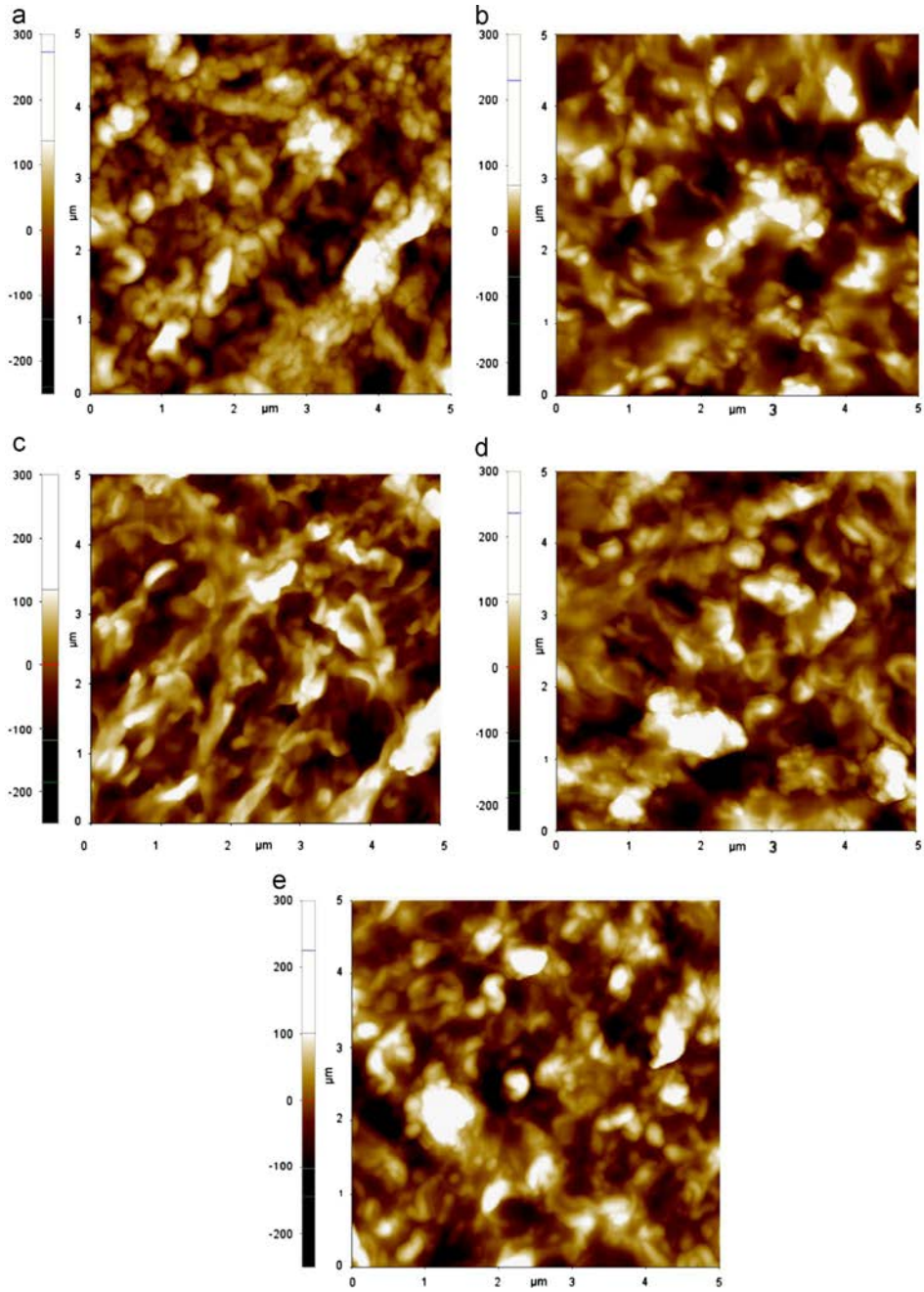

Fig. 3. AFM images of (a) uncoated membrane and coated membranes: (b) PVA, (c) PVA–PHMG (99:1) (d) PVA–PHMG (95:5) and (e) PHMG.

value of uncoated membrane (53.2°) was clearly decreased and, respectively, the surface energy values were increased after applying the coatings. In addition, the surface polarity of coated membranes was higher compared to uncoated membrane. The water contact angle values of PVA (21.5°) and PVA–PHMG (25.2 and 20.7°) coatings indicated formation of hydrophilic surface. The hydrophilic character of PVA based coatings was due to the dominant amount of hydroxyl groups as well as some residues of acetyl groups (see ATR-FTIR analysis in Section 3.1). The similar founding has been concluded for the commercial fully aromatic TFC PA membrane coated with PVA coating [38]. Nevertheless, the water contact angle value 15.9° of PHMG was the lowest among the coatings. The hydrophilicity was increased due to the primary amine groups of the PHMG (see ATR-FTIR analysis in Section 3.1).

Table 2
Summary of the results on water contact angle, surface energies and R_{RMS} roughness.

Membrane	Water contact angle [o]	Surface energy			Roughness R_{RMS} [nm]
		Total [mN/m]	Polar [mN/m]	Dispersive [mN/m]	
Uncoated	53.2 ± 9.2	54.6	11.3	43.3	67.8 ± 3.3
PVA	21.5 ± 1.9	60.2	20.7	39.5	42.5 ± 5.9
PVA–PHMG (99:1)	25.2 ± 2.8	59.4	18.7	40.7	54.6 ± 5.6
PVA–PHMG (95:5)	20.7 ± 2.4	60.2	21.9	38.3	57.6 ± 6.2
PHMG	15.9 ± 1.1	64.9	26.0	38.9	53.4 ± 2.2

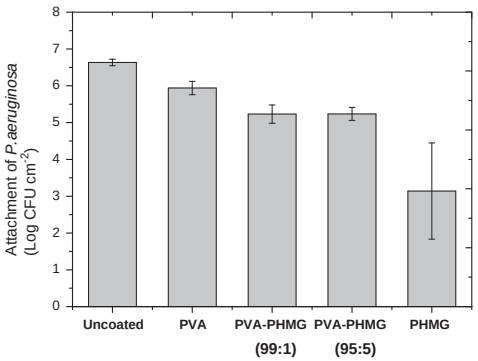

Fig. 4. Attachment of *Pseudomonas aeruginosa* on uncoated and coated membranes.

3.5. Anti-adhesion performance of membranes

The attachment of model biofilm forming microorganism, *P. aeruginosa*, was studied in order to demonstrate bacteria repellence performance of uncoated and coated membranes. The lower CFU values should indicate stronger bactericidal effects or bacteria repellence (anti-adhesion). Fig. 4 presents the attachment of *P. aeruginosa* on uncoated and coated membranes. In general, the CFU test detected lower number of the adhered *P. aeruginosa* on coated membrane surfaces. In fact, the CFU results revealed that the attachment of *P. aeruginosa* were significantly different between the specimens. Therefore, the CFU results are presented in logarithmic scale for the *P. aeruginosa* (Fig. 4).

Among the colony counts of the coated membranes, the PHMG coating showed evidently the lowest number of viable cells of bacteria. It was also observed that PVA–PHMG coated membranes attracted lower number of the bacteria compared to PVA coated membrane. Apparently, the unmodified PVA coating showed only minor bacteria repellence effect compared to PHMG modified coatings. Nevertheless, the CFU results evidently showed that the PVA coated membrane attracted less bacteria compared to the uncoated membrane. The effect of the surface properties can be seen on the attachment of bacteria, because of a clear correlation between the increase in hydrophilicity (see Table 2) and correspondingly, decrease in the attachment of the bacteria. Furthermore, the lowered surface roughness may have affected on the attachment of the bacteria. Therefore, PVA coating revealed anti-adhesion and bacteria repellence performance, due to the physiochemical anti-fouling performance. However, PVA–PHMG and PHMG coatings showed also hydrophilic and smooth surface roughness. In fact, the attachment of the bacteria decreased by the increase in the PHMG content in the surface. This suggested that the strongest effect on the attachment of bacteria was obtained by combining the antimicrobial activity with the physiochemical anti-adhesion surface properties.

3.6. Antimicrobial performance of membranes

The membrane antimicrobial performance was studied by determining the number of the viable model bacteria, *E. coli* and *B. subtilis*, found on uncoated and coated membrane specimens. Figs. 5 and 6 present the CFU results of *E. coli* and *B. subtilis*, respectively. In Fig. 5, the number of *E. coli* cells of coated membranes was lower compared to the uncoated membrane. In addition, CFU test results of *B. subtilis* indicated similar behaviour, although the differences were not as significant. Nevertheless, the trend of CFU changes was consisted between the specimens. In addition, these CFU results showed similar behaviour of the membrane specimens compared to the study of *P. aeruginosa*. PHMG coating showed repeatedly the lowest number of viable cells of the bacteria, among the coated membranes. It was similarly observed that PVA–PHMG coated membranes attracted lower number of the both bacteria compared to PVA coated membrane. The results indicated that PHMG was somewhat more efficient against the Gram-negative *E. coli*. Apparently, the unmodified PVA coating showed only minor repellence effect on these bacteria compared to PHMG modified coatings. However, the CFU results showed that the PVA coated membrane attracted less bacteria to some extent, in comparison to the uncoated membrane, indicating enhanced anti-adhesion performance.

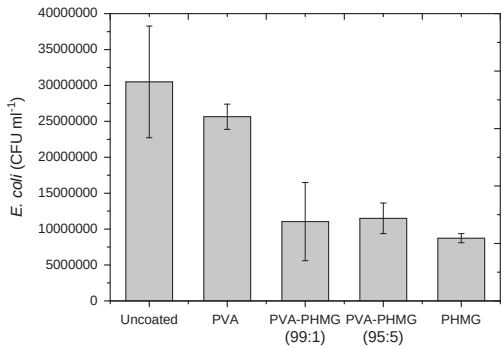

Fig. 5. CFU results of *Escherichia coli* on uncoated and coated membranes.

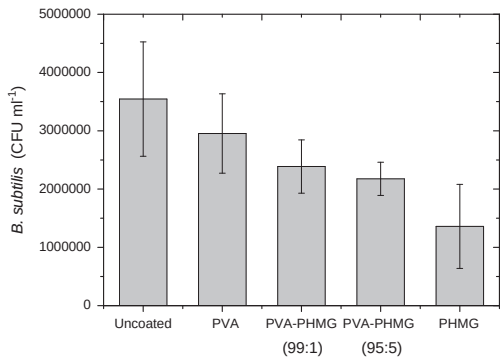

Fig. 6. CFU results of *Bacillus subtilis* on uncoated and coated membranes.

The diffusion inhibition zone (DIZ) test was conducted to further investigate the antimicrobial activity of the membrane specimens. An inhibition circle should form around a specimen, indicating antimicrobial activity and in addition, the leaching effect of the antimicrobial substance. Fig. 7 presents DIZ test results for Gram-negative *E. coli* bacteria and for Gram-positive *B. subtilis* bacteria. As expected, uncoated and PVA coated membranes did not show the formation of the inhibition circle toward *E. coli* and *B. subtilis*, indicating no observation of antimicrobial effect. The CFU results suggested that antimicrobial activity is obtained using PHMG. According to these results, the antimicrobial activity was more effective when the PHMG content was increased. However, PVA–PHMG coated membranes did not show the inhibition circle against the bacteria. Nevertheless, the results showed evidently that the pure PHMG coating formed the inhibition circle toward both of *E. coli* and *B. subtilis* bacteria, indicating the antimicrobial activity. In general, PHMG is known to have antimicrobial performance, as indicated in the literature [39,40]. The formation of strong inhibition zone may also indicate leaching of the PHMG polymer. Therefore, the lack of inhibition circle might be explained in the case of PVA–PHMG coatings. In fact, the decrease in the attachment of bacteria was obtained by adding low amount of PHMG in PVA coating. In addition, the FTIR spectra revealed only low intensity peaks assigned for PHMG (Section 3.1). Furthermore, the SEM and the AFM analysis as well as the contact angle measurements suggested that PHMG had minor effect on the PVA coating morphology, surface texture and hydrophilicity (Sections 3.2–3.4). In that respect, PHMG might be somehow consolidated into the PVA coating matrix. This could explain the stability of the PVA–PHMG coating, allowing PHMG to be active against bacteria. In particular, our aim was to prevent biofilm formation by developing bacteria repellent anti-adhesion surface with a contact killing antimicrobial property, without leaching of the antimicrobial agent.

3.7. RO performance

The data obtained from the water flux (J_v) and the salt rejection (R) measurements was used to calculate water (A) and solute (B) permeability. These were used to analyse the effect of coatings on the membrane separation performance. Water permeability (A) was calculated using the equation $A=(J_v \times \Delta P)/(\Delta P-\Delta \pi)$ [41].

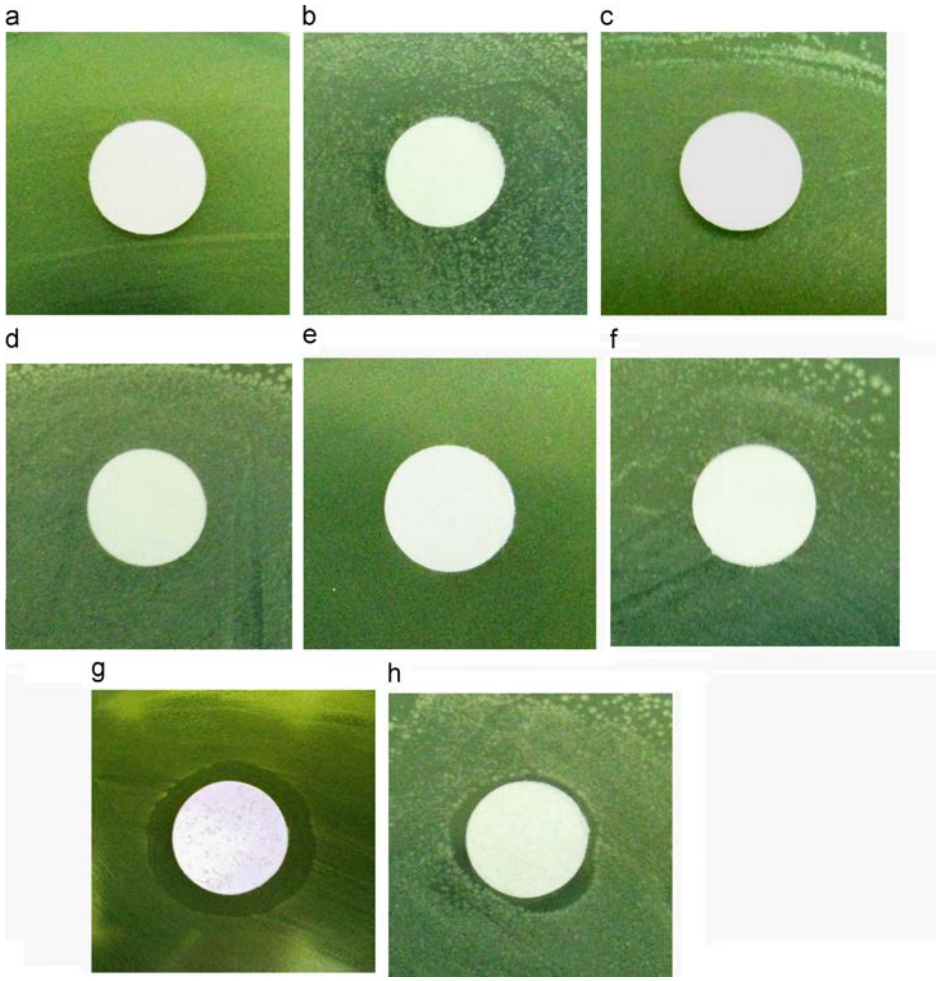

Fig. 7. Gram negative *E. coli* DIZ photos of the (a) uncoated and coated membranes: (c) PVA, (e) PVA–PHMG (95:5), (f,g) PHMG. Respectively, gram positive *B. subtilis* DIZ photos of the (b) uncoated and coated membranes: (d) PVA, (f) PVA–PHMG (95:5) and (h) PHMG.

Table 3
Water permeability coefficient (A), salt rejection (R) and salt permeability coefficient (B) of uncoated and coated membranes.

Membrane	Water permeability coefficient (A) [L/m^2/h/bar][a]	Salt rejection (R) [%][a]	Salt permeability coefficient (B) [L/m^2/h][a]
Uncoated membrane	4.35 ± 0.48	97.2 ± 1.2	3.47 ± 1.87
PVA	3.71 ± 0.31	98.5 ± 0.6	1.53 ± 0.51
PVA–PHMG (99:1)	2.39 ± 0.60	98.2 ± 0.6	1.26 ± 0.70
PVA–PHMG (95:5)	1.67 ± 0.25	95.8 ± 2.2	2.17 ± 1.28
PHMG	0.76 ± 0.48	91.6 ± 0.3	2.30 ± 1.29

[a] Water flux (J_v) and salt rejection (R) of the membranes were evaluated using 10 mM NaCl feed solution and applied pressure of 27.6 bar (400 psi) at 23 °C. The experimental errors represent the standard deviation of three repeated measurements.

Solute permeability (B) was correspondingly calculated according to the equation $B=(J_v \times \Delta P) \times (1/R-1)$ [41]. Table 3 summarises the values of the water permeability (A), the salt (NaCl) rejection (R) and the salt (NaCl) permeability of uncoated and coated membranes. The coating layers reduced the permeability properties compared to uncoated membrane. Among the coated membranes, the PVA coating reduced the water permeability approximately 15%, and correspondingly the salt rejection showed minor increase. However, PVA coating decreased the NaCl permeability almost 55%. In comparison, PVA–PHMG coatings led to 45% and 58% decline in the water permeability. Their salt rejection was within the error bars in comparison to uncoated or PVA coated membrane. In addition, PHMG content did not have much effect on NaCl permeability of PVA coating. The pure PHMG coated membrane showed 78% decline in water permeability. In fact, membranes with higher PHMG percentage tended to decrease water permeability. Furthermore, the pure PHMG coating significantly decreased the salt rejection and, respectively, slightly increased NaCl permeability. According to the calculation of NaCl permeability, the lower salt rejection could be contributed to the lower water flux (low water permeability or low pressure). It explains the decrease in salt permeability of the membrane with lower water permeability. Furthermore, some other investigations have typically shown 50–80 % decrease in the water and salt permeability of coated membranes [11,42]. Therefore, in conditions where higher pressure is applied or the membrane with reasonable permeability combination, the membrane is preferred in view of the better anti-fouling performance.

4. Conclusions

Polymeric thin coatings were successfully applied on TFC PA membrane. The coating thicknesses varied from 100 to 250 nm. All the coatings increased the hydrophilicity and decreased the surface roughness compared to uncoated membrane. In addition, all the coated membranes decreased the attachment of bacteria on the surface. PVA coating showed anti-adhesion performance, showing decrease in the attachment of all the model bacteria. Coated membranes with higher PHMG percentage tended to have higher bacteria repellent and antimicrobial performance. CFU and DIZ results proved the antimicrobial performance of PHMG. Therefore, an optimal anti-fouling surface could be obtained applying a coating, which consists of anti-adhesion and antimicrobial performance. However, further optimisation of PVA–PHMG composition is needed in order to maintain the anti-fouling performance, without sacrificing the RO performance. In addition, the further studies will include long-term fouling studies of PVA–PHMG coated RO membranes.

Acknowledgements

The authors acknowledge Tekes (the Finnish Funding Agency for Technology and Innovation) and VTT Technical Research Centre of Finland due to the financial support of project. Skilful technical assistances of Niina Torttila, Sini Eskonniemi and Marjo Ketonen are acknowledged in the microbiological part, the contact angle measurements and SEM imaging.

References

[1] H.-C. Hemming, Reverse osmosis membrane biofouling, Exp. Therm Fluid Sci. 14 (4) (1997) 382–391.
[2] T. Nguyen, F.A. Roddick, L. Fan, Biofouling of water treatment membranes: a review of the underlying causes, monitoring techniques and control measures, Membranes 2 (2012) 804–840.
[3] V. Chen, J. Mansouri, T. Charlton, Biofouling in membrane systems, in: K.-V. Peinemann, S.P. Nunes (Eds.), Membranes for Water Treatment, vol. 4, Wiley-VCH, Weinheim, 2010, pp. 25–48.
[4] R. Field, Fundamentals of fouling, in: K.-V. Peinemann, S.P. Nunes (Eds.), Membranes for Water Treatment, vol. 4, Wiley-VCH, Weinheim, 2010, pp. 1–23.
[5] D. Rana, T. Matsuura, Surface modifications for antifouling membranes, Chem. Rev. 110 (2010) 2448–2471.
[6] K. Bazaka, R.J. Crawford, E.P. Ivanova, Review: do bacteria differentiate between degrees of nanoscale surface roughness? Biotechnol. J. 6 (2011) 1103–1114.
[7] S.D. Puckett, E. Taylor, T. Raimondo, T.J. Webster, The relationship between the nanostructure of titanium surfaces and bacterial attachment, Biomaterials 31 (2010) 706–713.
[8] M. Ulbricht, Advanced functional polymer membranes, Polymer 47 (2006) 2217–2262.
[9] C.Y. Tang, Y.-N. Kwon, J.O. Leckie, Effect of membrane chemistry and coating layer on physiochemical properties of thin film composite polyamide RO and NF membranes: I. FTIR and XPS characterization of polyamide and coating layer chemistry, Desalination 242 (2009) 149–167.
[10] R. Bernstein, S. Belfer, V. Freger, Bacterial attachment to RO membranes surface-modified by concentration-polarization-enhanced graft polymerization, Environ. Sci. Technol. 45 (2011) 5973–5980.
[11] A.C. Sagle, E.M. VanWagner, H. Ju, B.D. McCloskey, B.D. Freeman, M.M. Sharma, PEG-coated reverse osmosis membranes: desalination properties and fouling resistance, J. Membr. Sci. 340 (2009) 92–108.
[12] E.M. Van Wagner, A.C. Sagle, M.M. Sharma, Y.-H. La, B.D. Freeman, Surface modification of commercial polyamide desalination membranes using poly (ethylene glycol) diglycidyl ether to enhance membrane fouling resistance, J. Membr. Sci. 367 (2011) 273–287.
[13] S. Belfer, Y. Purinson, R. Fainshtein, Y. Radchenko, O. Kedem, Surface modification of commercial composite polyamide reverse osmosis membranes, J. Membr. Sci. 139 (1998) 175–181.
[14] S. Yu, Z. Lü, Z. Chen, X. Liu, M. Liu, C. Gao, Surface modification of thin-film composite polyamide reverse osmosis membranes by coating *N*-isopropylacrylamide-co-acrylic acid copolymers for improved membrane properties, J. Membr. Sci. 371 (2011) 293–306.
[15] J. Gilron, S. Belfer, P. Väisänen, M. Nyström, Effects of surface modification on antifouling and performance properties of reverse osmosis membranes, Desalination 140 (2001) 167–179.
[16] I. Sawada, R. Fachrul, T. Ito, Y. Ohmukai, T. Maruyama, H. Matsuyama, Development of a hydrophilic polymer membrane containing silver nanoparticles with both organic antifouling and antibacterial properties, J. Membr. Sci. 387–388 (2012) 1–6.
[17] S. Balta, A. Sotto, P. Luisa, L. Benea, B. Van der Bruggena, J. Kim, A. New, Outlook on membrane enhancement with nanoparticles: the alternative of ZnO, J. Membr. Sci. 389 (2012) 155–161.
[18] F. Diagne, R. Malaisamy, V. Boddie, R.D. Holbrook, B. Eribo, K.L. Jones, Polyelectrolyte and silver nanoparticle modification of microfiltration membranes to mitigate organic and bacterial fouling, Environ. Sci. Technol. 3 (46) (2012) 4025–4033.
[19] A. Zago, S. Chugani, Pseudomonas, in: M. Schaechter (Ed.), Encyclopedia of Microbiology, third ed.,Elsevier Inc., 2009, pp. 245–260.
[20] B. Bolto, T. Tran, M. Hoang, Z. Xie, Crosslinked poly(vinyl alcohol) membranes, Progr. Polym. Sci 34 (2009) 969–981.
[21] K. Grundke, Characterization of polymer surfaces by wetting and electrokinetic measurements—contact angle, interfacial tension, zeta potential, in: M. Stamm (Ed.), Polymer Surfaces and Interfaces—Characterization, Modification and Applications, first ed.,Springer-Verlag, Berlin Heidelberg, 2008, pp. 103–136.

[22] M. Herzberg, M. Elimelech, Biofouling of reverse osmosis membranes: role of biofilm-enhanced osmotic pressure, J. Membr. Sci. 295 (2007) 11–20.
[23] S.B. Sadr Ghayeni, P.J. Beatson, R.P. Schneider, A.G. Fane, Adhesion of waste water bacteria to reverse osmosis membranes, J. Membr. Sci. 138 (1998) 29–42.
[24] M. Klausen, A. Heydorn, P. Ragas, L. Lambertsen, A. Aaes-Jørgensen, S. Molin, T. Tolker-Nielsen, Biofilm formation by *Pseudomonas aeruginosa* wild type, flagella and type IV pili mutants, Mol. Microbiol. 48 (6) (2003) 1511–1524.
[25] H.-C. Flemming, J. Wingender, The biofilm matrix, Nat. Rev. Microbiol. 8 (2010) 623–633.
[26] D1141-98 Standard Practise for the Preparation of Substitute Ocean Water, (2008).
[27] M. Schaechter, Escherichia coli, in: M. Schaechter (Ed.), Encyclopedia of Microbiology, third ed., Elsevier Inc., 2009, pp. 125–132.
[28] P.J. Piggot, Bacillus subtilis, in: M. Schaechter (Ed.), Encyclopedia of Microbiology, third ed., Elsevier Inc., 2009, pp. 45–56.
[29] Clinical Laboratory Standards Institute, Methods for Dilution Antimicrobial Susceptibility Tests for Bacteria that Grow Aerobically, ninth ed. CLSI document M07-A9 vol. 32 no. 2, Clinical Laboratory Standards Institute, Wayne, PA, 2012.
[30] Clinical Laboratory Standards Institute, Performance Standards for Antimicrobial Disk Susceptibility Tests; Approved standard, ninth ed., CLSI document M2-A9. 26:1, Clinical Laboratory Standards Institute, Wayne, PA, 2006.
[31] Y.-N. Wang, C.Y. Tang, Protein fouling of nanofiltration, reverse osmosis, and ultrafiltration membranes—the role of hydrodynamic conditions, solution chemistry, and membrane properties, J. Membr. Sci. 376 (2011) 275–282.
[32] R.M. Silverstein, F.X. Webster, Spectrometric Identification of Organic Compounds, sixth ed., John Wiley & Sons, Inc., New York, 1997.
[33] N.B. Colthup, L.H. Daly, S.E. Wiberley, Introduction to Infrared and Raman Spectroscopy, Academic Press Inc., New York, 1975.
[34] H.S. Mansur, C.M. Sadahira, A.N. Souza, A.A.P. Mansur, FTIR spectroscopy characterization of poly (vinyl alcohol) hydrogel with different hydrolysis degree and chemically crosslinked with glutaraldehyde, Mater. Sci. Eng., C 28 (2008) 539–548.
[35] H. Hachisuka, K. Ikeda, Composite Reverse Osmosis Membrane Having a Separation layer with Polyvinyl Alcohol Coating and Method of Reverse Osmosis Treatment of Water Using the Same. (2001) US Patent 6177011 B1.
[36] I.C. Kim, K.H. Lee, Dyeing process wastewater treatment using fouling resistant nanofiltration and reverse osmosis membranes, Desalination 192 (2006) 246–251.
[37] C.Y. Tang, Y.-N. Kwon, J.O. Leckie, Effect of membrane chemistry and coating layer on physiochemical properties of thin film composite polyamide RO and NF membranes II. Membrane physiochemical properties and their dependence on polyamide and coating layers, Desalination 242 (2009) 168–182.
[38] K.C. Khulbe, C.Y. Feng, T. Matsuura, Synthetic polymeric membranes—characterisation by atomic force microscopy, Springer-Verlag, Berlin Heidelberg 157–167.
[39] O.J. Schmidt, A. Schmidt, D. Toptchiev, Biocidal Polymers Based on Guanidine Salts. (2006) US Patent 7001606.
[40] Z.X. Zhou, D.F. Wei, Y. Guan, A.N. Zheng, J.J. Zhong, Damage of *Escherichia coli* membrane by bactericidal agent polyhexamethylene guanidine hydrochloride: micrographic evidences, J. Appl. Microbiol. 108 (2010) 898–907.
[41] A.G. Fane, C.Y. Tang, R. Wang, Membrane Technology for Water: Microfiltration, Ultrafiltration, Nanofiltration and Reverse Osmosis, Elsevier, USA, 2010, chapter 91.
[42] J.S. Louie, I. Pinnau, I. Ciobanu, K.P. Ishida, A. Ng, M. Reinhard, Effects of polyether–polyamide block copolymer coating on performance and fouling of reverse osmosis membranes, J. Membr. Sci. 280 (2006) 762–770.

PUBLICATION P6

Surface modification of thin film composite polyamide membrane using atomic layer deposition method

In: Journal of Membrane Science (450) 2014,
pp. 174–180.

Journal of Membrane Science 450 (2014) 174–180

Contents lists available at ScienceDirect

Journal of Membrane Science

journal homepage: www.elsevier.com/locate/memsci

Surface modification of thin film composite polyamide membrane using atomic layer deposition method

Juha Nikkola [a,*], Jenni Sievänen [b], Mari Raulio [b], Jing Wei [c,d], Jyrki Vuorinen [e], Chuyang Y. Tang [c,d]

[a] VTT Technical Research Centre of Finland, PO Box 1300, 33101 Tampere, Finland
[b] VTT Technical Research Centre of Finland, PO Box 1000, 02044 Espoo, Finland
[c] School of Civil and Environmental Engineering, Nanyang Technological University, Singapore 639798, Singapore
[d] Singapore Membrane Technology Centre, Nanyang Technological University, Singapore 639798, Singapore
[e] Department of Materials Science, Tampere University of Technology, PO Box 589, 33101 Tampere, Finland

ARTICLE INFO

Article history:
Received 14 June 2013
Received in revised form
30 August 2013
Accepted 4 September 2013
Available online 10 September 2013

Keywords:
Thin-film-composite (TFC) polyamide (PA)
Reverse osmosis membrane
Inorganic surface modification
Atomic layer deposition (ALD)
Aluminium oxide (Al_2O_3)

ABSTRACT

We present surface modification of thin-film-composite (TFC) polyamide (PA) reverse osmosis (RO) membrane by atomic layer deposition (ALD) process using trimethylaluminium ($AlMe_3$). The aim of the inorganic ALD coating is to improve the anti-fouling performance of TFC PA membranes. The ALD processing parameters were systematically studied because of the lack of previous investigations of the ALD coated RO membranes. Two different processing temperatures (70 °C and 100 °C) and three different ALD cycles (10, 50 and 100) were used to deposit the Al_2O_3 ALD coatings on TFC PA membranes. The ALD process parameters affected on the hydrophilicity and the surface polarity as well as on the surface roughness of the coated membranes. The bacteria attachment test results indicated that the lowest number of *Pseudomonas aeruginosa* cells was adhered on the most hydrophilic and polar surface, among the ALD coated membranes. RO tests showed the effect of ALD coating on the water and salt permeability as well as on the salt rejection of the membranes.

1. Introduction

Membrane fouling, such as scaling, colloidal fouling (inorganic and organic) and biofouling, has remained a critical issue in the reverse osmosis (RO) process [1]. For example, thin-film-composite (TFC) polyamide (PA) membranes have shown to be vulnerable to fouling in the RO process. Several surface properties of TFC PA membranes, including hydrophilicity and low surface roughness, have shown to play a key role in reducing the membrane fouling [2]. Researchers have developed various approaches to modify the surfaces of TFC PA membranes to introduce anti-adhesion and antimicrobial surface [3]. Indeed, many commercial "low fouling" TFC PA membranes contain an additional polymeric coating layer to enhance their anti-fouling performance [4]. Compared to the vast literature on organic/polymeric surface coatings or modifications, there are few studies on inorganic coatings as a surface modification of RO membranes [5], despite their great potential to increase the mechanical and the chemical stability as well as to decrease the fouling tendency.

Atomic layer deposition (ALD) technology has been used almost four decades for manufacturing inorganic coating layers, such as oxides, nitrides and sulphides, with thickness down to the nanometre range [6]. Manufacturing of Al_2O_3 thin films using the self-terminating reaction of trimethylaluminium ($AlMe_3$, Me=CH), with water or ozone, is considered as an ideal example of the ALD process [7]. Recent advancement in ALD technology has increased its potential to produce functional thin films on flexible and temperature-sensitive polymeric materials [8,9]. The technology has also been applied to coat various fibrous polymers [10–13].

In recent years, a few research groups have investigated ALD technology as surface modification of porous microfiltration and ultrafiltration, including both polymeric and ceramic membranes [14–18]. These studies suggested that ALD processing parameters, such as temperature and number of ALD cycles, have clear impact on membrane performance. For example, they have shown an effect on the pore size of membrane, which have affected on solute permeability and rejection properties [16,17]. Furthermore, hydrophilic and smooth polymeric membranes have been obtained using $AlMe_3$ based ALD technology [15], which increases its potentiality to create low-fouling membrane surface. However, hydrophilicity and low surface roughness have been typically obtained using a relatively thick ALD coating, such as 300–500 ALD cycles [14,16]. In addition, the change in the ALD processing

* Corresponding author. Tel.: +358 405358169; fax: +358 207223498.
E-mail address: juha.nikkola@vtt.fi (J. Nikkola).

0376-7388/$ - see front matter © 2013 Elsevier B.V. All rights reserved.
http://dx.doi.org/10.1016/j.memsci.2013.09.005

temperature has affected on reactivity of $AlMe_3$ [11]. For example, the most hydrophilic membrane surface has been obtained at 150 °C [14]. The increase of ALD coating thickness and temperature may negatively affect the RO membrane performance by tightening the rejection layer of temperature-sensitive polymeric membrane. Therefore, further understanding of the ALD process is needed in order to overcome the current drawbacks and to develop new low-fouling RO membrane using the ALD technology. To the best knowledge of the authors, the ALD method has not been applied for modifying RO membranes, and therefore systematic study is needed to introduce ALD technology to the RO membranes.

Our aim was to investigate the surface modification of TFC PA membrane using the $AlMe_3$ based ALD process. Two different processing temperatures (70 °C and 100 °C) and three different number of ALD cycles (10, 50 and 100) were used to apply the ALD coatings on TFC PA membranes. The ALD process parameters were shown to have effect on the surface roughness as well as on the hydrophilicity and surface polarity of TFC PA membranes. The bacterial attachment test simulated the effect of ALD coating on the biofouling tendency. Furthermore, RO tests showed their effect on the water permeability and salt rejection.

2. Experimental

2.1. Materials

The commercial TFC PA membrane DOW™ FILMTEC™ LE-400 (The Dow Chemical Company, Midland, MI, USA) was used as-received as a substrate for the ALD coatings. Trimethylaluminum ($AlMe_3$) was purchased from Sigma-Aldrich (St. Louis, MO, USA) and it was used as received.

2.2. ALD coatings

The ALD-Al_2O_3 depositions were carried out in a Picosun SUNALE™ reactor (Picosun, Espoo, Finland) on substrates that were 10×10 cm^2 in size. $AlMe_3$ and H_2O were used as precursors. The ALD process parameters were selected according to our previous investigations on low-temperature ALD process for temperature-sensitive substrates [9,19,20]. Two different processing temperatures (70 °C and 100 °C) and three different ALD cycles (10, 50 and 100) were used to deposit the ALD coatings on the TFC PA membranes. Table 1 summarises the ALD coated specimens with their processing parameters. The coated membranes are named according to the coating cycles and temperature (e.g., c10_t70 denotes a membrane with 10 coating cycles at 70 °C).

Furthermore, our previous investigations have shown the effect of physical and chemical pre-treatment on the ALD layer growth, which has occurred due to the changes in surface morphology and chemistry of temperature-sensitive substrate [9]. Because RO membrane is sensitive to the changes in its surface morphology, it was decided to deposit the ALD coatings on virgin TFC PA membranes without further pre-treatment.

Table 1
Summary of the ALD coated specimens with their processing parameters.

Sample ID[a]	Number of cycles	Processing temp. (°C)	Nominal coating thickness[b] (nm)
c10_t70	10	70	1
c50_t70	50	70	5
c100_t70	100	70	10
c10_t100	10	100	1
c50_t100	50	100	5
c100_t100	100	100	10

[a] Al_2O_3 coating.
[b] Nominal thickness according to the growth rate 0.1 nm/cycle [19,20].

The precursor pulsing sequence was 0.1 s $AlMe_3$ pulse, 10 s N_2 purge, 0.1 s H_2O, 10 s N_2 purge and the number of ALD cycles was adjusted according to the targeted Al_2O_3 coating thickness. The nominal thicknesses of the coating was estimated based on the growth rate 0.1 nm/cycle measured from films grown on a silicon wafer with a Nanospec AFT 4150 reflectometer [19,20]. ALD coatings have shown a minor variation of the actual film thickness, because of the difference in surface chemistry and roughness of different polymers, in comparison to a silicon wafer. Although, the aim was to deposit the ALD film on PA side, the film growth cannot be totally prevented on reverse side of the membrane.

2.3. Membrane characterisations

ATR-FTIR measurement was carried out to analyse the surface chemistry of uncoated and coated membranes. Perkin Elmer spectrum BX II FT-IR (Fourier transform IR) system was equipped with vertical-Attenuated total reflectance (ATR) and KRS-5 (Thallium Bromoiodide) crystal. In a typical analysis 50 scans were collected from 500 to 4000 cm^{-1} at 4 cm^{-1} resolution. A background spectrum of pure KRS-5 was collected before running the samples.

The microscopic imaging of uncoated and coated membranes was conducted using scanning electron microscope (SEM) JEOL JSM-6360 LV 11 kV on high vacuum mode. All SEM samples were sputter coated with gold before imaging.

The surface topography of uncoated and coated membrane samples were characterised using non-contact mode atomic force microscopy (NC-AFM). The NC-AFM analysis was performed using Park Systems XE-100 AFM equipment (Suwon, South-Korea), with cantilever 905M-ACTA (AppNano Inc., Santa Clara, CA, USA). Typically, the scan rate was 0.4–0.6 Hz and the measured area was 5×5 μm^2. Six replicate measurements were performed to determine the root-mean-square roughness value, R_{RMS}.

The contact angle measurements were conducted by using Optical Tensiometer Theta T200 device (Attension, Biolin Scientific). The measurements were performed in a controlled atmosphere (RH 50%, temperature 23 °C) and the results are given as an average of five parallel measurements. The water contact angle values, expressed as deg, are presented at the time of 30 s from the moment the drop contacts the surface. The surface energy values were obtained by measuring the contact angle of three different probe liquids, including water (H_2O, $\gamma = 72.80$ mN/m), diiodomethane (CH_2I_2, $\gamma = 50.80$ mN/m) and formamide (CH_3NO, $\gamma = 58.20$ mN/m). The total surface energy values, as summary of polar and dispersive surface energies, were determined from the measured contact angle data using the Fowkes theory [21].

2.4. Bacterial anti-adhesion performance

Biofilm formation was demonstrated by analysing the attachment of *Pseudomonas aeruginosa* on uncoated and coated membranes. *P. aeruginosa* is Gram-negative, aerobic, rod-shaped bacterium, which is widely used as the model microbe for biofilm formation studies [22–25]. Therefore, *P. aeruginosa* was selected as model bacterium in our study to provide comparable data related to the attachment of bacteria.

Bacteria attachment test was conducted according to our previous studies [3]. The membranes (⌀ 4.7 cm) were submerged in bacterial suspension consisting of standard seawater ASTM D1141-98 (2008) [26]. Furthermore, the suspension was inoculated with overnight culture of *P. aeruginosa* (VTT E-96726) cultivated in 37 °C Trypticase soy broth solution, harvested by centrifugation

(3000 rpm, 10 min) and washed with phosphate buffered saline (PBS) (10 mM). The cell density was approximately 1×10^8 CFU mL^{-1} determined by plate count on Trypticase soy agar (TSA) (37 °C, 1 d). The exposure of membranes was conducted in a rotary shaker (75 rpm) at room temperature for 1 d. The number of adhered cells on the membranes was determined after swabbing by plate count on TSA (37 °C, 1 d). Results are presented as colony forming units per membrane area (CFU cm^{-2}). Three replicate membrane samples were examined for each membrane type.

2.5. Water permeability and salt rejection

Uncoated and coated membranes were tested in a lab-scale crossflow filtration setup to evaluate their water permeability and NaCl rejection according to Wang et al. [27]. Membranes were tested at a feed pressure of 27.6 bar (400 psi) using a feed water containing 10 mM NaCl. The temperature of feed water was maintained at 23 °C. Water flux of the membranes was determined by the gravimetric method. Membrane NaCl rejection (R) was determined by

$$R = \frac{C_f - C_p}{C_p} 100\%$$

where C_f and C_p are the concentrations (via conductivity measurements) of feed and permeate solutions, respectively.

Water permeability (A) was calculated using the equation $A = (J_v \times \Delta P)/(\Delta P - \Delta \pi)$ [28]. Solute permeability (B) was correspondingly calculated according to the equation $B = (J_v \times \Delta P) \times (1/R - 1)$ [28].

3. Results and discussion

3.1. ATR-FTIR measurements

Fig. 1 presents the FTIR spectra of uncoated and ALD coated membranes in the range of 2000–500 cm^{-1}, and Table 2 summarises the corresponding peak assignments. The uncoated membrane showed typical FTIR spectra of fully aromatic PA membranes formed from m-phenylenediamine and trimesoyl chloride on top of a polysulfone (PSf) support layer [29]. The peak at 1660 cm^{-1} was assigned to the C=O stretching (amide I band), and the peak at 1540 cm^{-1} was assigned to the N–H bending (amide II band), which are known to be typical for a secondary amide group [30,31]. The latter peak is due to the interaction between N–H bending and

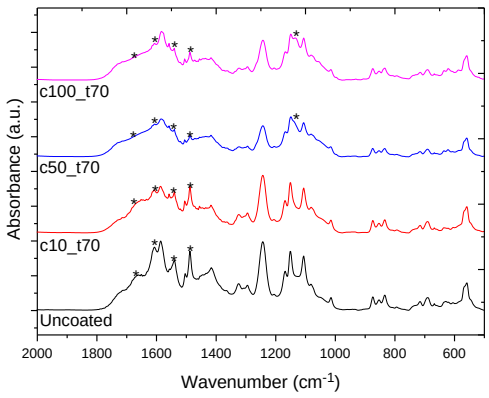

Fig. 1. FTIR spectra of uncoated and ALD coated (at 70 °C) specimens. The most essential peaks are marked with *.

Table 2
Summary of the peak assignments.

Origin of the peaks	Wavenumber (cm^{-1})	Peak assignment
Polysulfone	1324	SO_2 asymmetric stretching [29–31]
	1244	C–O–C stretching of aryl group [29–31]
	1180	SO_2 symmetric stretching [29–31]
Aromatic polyamide	1660	C=O stretching (amide I band) [29–31]
	1610	C=C stretching of the aromatic ring [29–31]
ALD coating	1540	N–H bending (amide II band) [29–31]
	1150	Al–CH_3 [11,12]

C–N stretching of the –CO–N–H group [30,31]. The peak at 1610 cm^{-1} was assigned as C=C stretching of the aromatic ring. The characteristic peaks for the PSf support layer were detected at 1324 cm^{-1} (SO_2 asymmetric stretching), 1244 cm^{-1} (C–O–C stretching) and 1180 cm^{-1} (SO_2 symmetric stretching) [29].

The FTIR spectra of the ALD coated membranes showed most of the significant peaks assigned for PA (1660, 1610, and 1540 cm^{-1}) and PSf (1324, 1244 and 1180 cm^{-1}), although the intensities of these peaks were reduced compared to the uncoated membrane. The decrease of the peak intensities was more prominent for thicker coating layers, which can be explained by the dilution effect due to the presence of the coating material. In addition, the decrease in the peak intensity at 1660 cm^{-1} and 1540 cm^{-1} might be partially attributed to the reaction of $AlMe_3$ precursors with C=O groups of PA (to produce C–O–Al bonds) [11,12] and N–H groups (to form Al–-N bonds) [11,12], respectively. In addition, the coated membranes showed the appearance of a new low intensity peak at 1150 cm^{-1}, which may originate from residues of unreacted Al–CH_3 group of the $AlMe_3$ precursor [11,12].

3.2. SEM characterisation

The SEM characterisation was performed to determine the surface morphology of the ALD coated membranes. Fig. 2 presents the SEM images of uncoated and coated membranes. SEM images of the ALD coated membranes (Fig. 2b–g) indicated some changes in the surface morphology compared to virgin membrane. The membranes coated at 100 °C looked generally tighter compared to those coated at 70 °C. Moreover, a tightening of the ALD coating layer can be noticed due to increase in the coating thickness. The tightening could cause significant hydraulic resistance of the coating layer and decrease in RO performance.

3.3. AFM characterisation

Fig. 3 presents AFM images of uncoated and ALD coated TFC PA membranes. The uncoated membrane (Fig. 3a) showed a ridge-and-valley as well as nodular surface texture, which is typical for TFC PA membranes [4,32]. Furthermore, its RMS roughness value (Table 3) was comparable to previous investigations [4].

The AFM images of the coated membranes indicated a particle-like topography of ALD coating (Fig. 3), which is typically obtained using low number of ALD cycles [14,33]. Furthermore, the number of the ALD cycles seemed to have an effect on the surface topography, as shown in Fig. 3.

Table 3 summarises the roughness values. The R_{RMS} roughness value of coated membranes reduced significantly after 10 cycles of ALD coating, which may be due to the deposition of a few particles on the surface filling the valley areas. However, increase of the coating layer thickness significantly increased the R_{RMS} roughness of the coated membranes. Moreover, ALD coating layer with 100

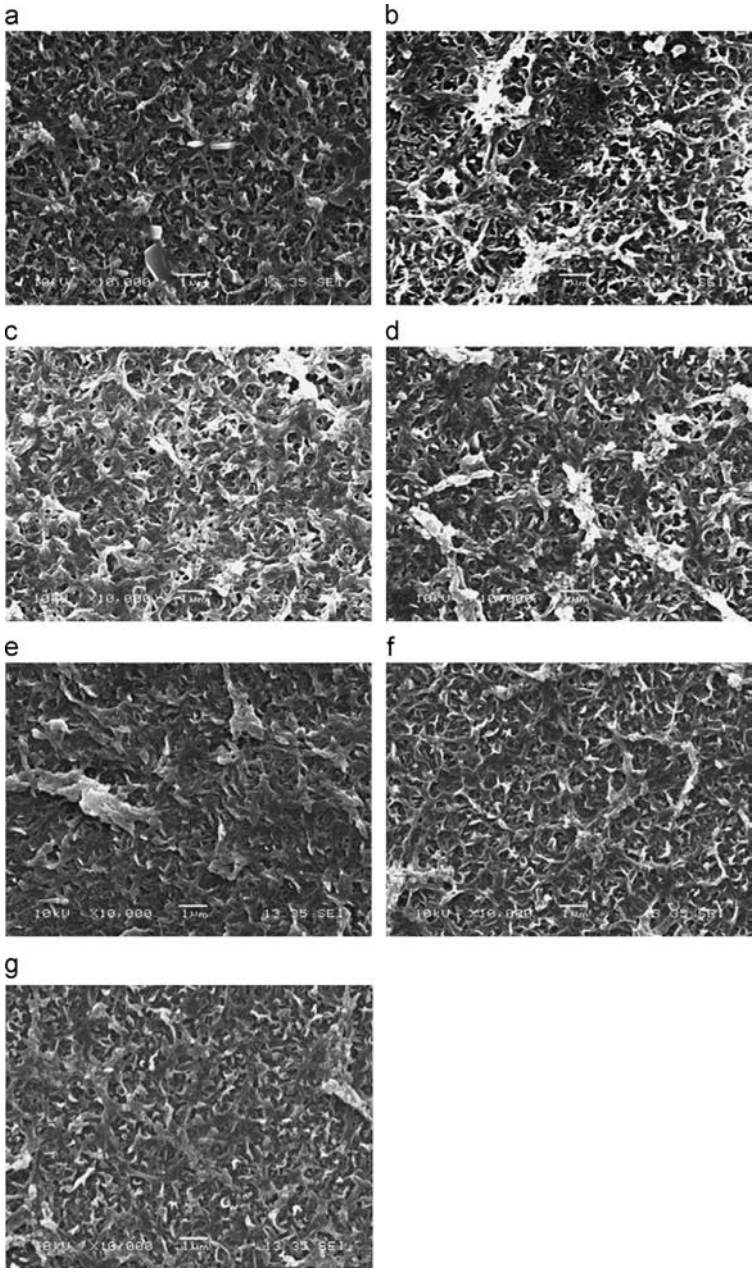

Fig. 2. SEM images of the uncoated (image (a)) and ALD coated TFC PA membranes using processing temperatures 70 °C (images (b)–(d)) and 100 °C (images (e)–(g)). (a) Uncoated, (b) c10_t70, (c) c50_t70, (d) c100_t70, (e) c10_t100, (f) c50_t100, and (g) c100_t100.

cycles showed R_{RMS} values that were nearly identical to that of the uncoated membrane. Similar trend was observed with both of the temperatures. Indeed, the increase in surface roughness may be due to the particle-like ALD layers. Furthermore, the particle-like ALD layers may have grown on the ridges of the membrane surface, which could then promote the surface roughness. Similar roughness increase has been also noticed when applying other type of ALD coatings [33].

3.4. Hydrophilic properties of ALD coated TFC PA membrane

Hydrophilic properties of uncoated and ALD coated TFC PA membranes were studied using the water contact angle measurements and the results are summarised in Table 3. The membranes became more hydrophilic, when a thin ALD coating layer was deposited on the membrane surface. Indeed, the most hydrophilic membrane surface was obtained using 10 and 50 ALD cycles at

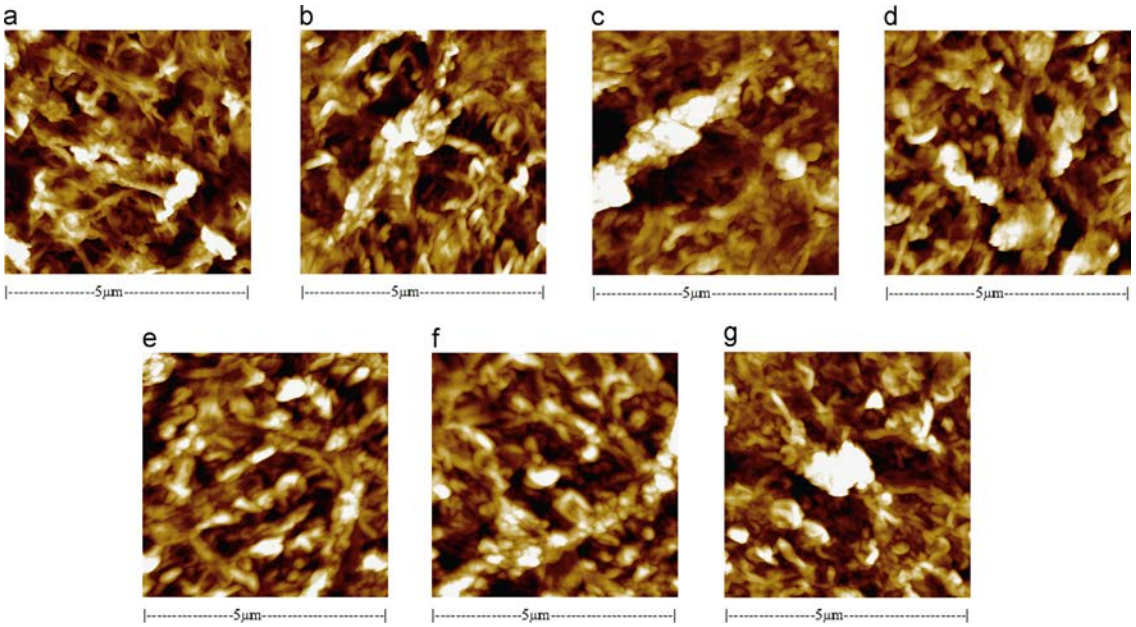

Fig. 3. AFM images of the uncoated (image (a)) and ALD coated TFC PA membranes using processing temperatures 70 °C (images (b)–(d)) and 100 °C (images (e)–(g)). Scan size 5 μm and *Z*-range 250 nm. (a) Uncoated (*Z*-scale 250 nm), (b) c10_t70 (*Z*-scale 250 nm), (c) c50_t70 (*Z*-scale 250 nm), (d) c100_t70 (*Z*-scale 250 nm), (e) c10_t100 (*Z*-scale 250 nm), (f) c50_t100 (*Z*-scale 250 nm), and (g) c100_t100 (*Z*-scale 250 nm).

Table 3
Surface properties of ALD coated TFC PA membrane including water contact angle, surface energy and surface roughness results.

Membrane	Water contact angle [deg]	Total surface energy [mN/m]	Polar surface energy [mN/m]	Dispersive surface energy [mN/m]	R_{RMS} [nm]
Uncoated	53 ± 9	54.6	11.3	43.3	73 ± 7
c10_t70	16 ± 4	66.9	33.4	33.5	50 ± 5
c50_t70	27 ± 1	57.3	21.7	35.6	56 ± 4
c100_t70	66 ± 2	38.0	10.2	27.8	75 ± 1
c10_t100	27 ± 5	44.8	11.4	33.4	54 ± 3
c50_t100	84 ± 4	38.8	0.8	38.0	69 ± 2
c100_t100	92 ± 1	34.2	0.9	33.3	71 ± 2

70 °C or 10 ALD cycles at 100 °C, having the water contact angles ~15–30° compared to 53° for the uncoated membrane. This reduction in water contact angle can be attributed to the formation of a hydrophilic coating layer of Al_2O_3 with some residues of Al–OH groups [33]. The membranes coated at 100 °C were generally less hydrophilic compared to those coated at 70 °C under otherwise identical conditions. This was probably due to the increase in reactivity and therefore, conversion of Al–OH to Al–O–Al at higher temperature. Previous investigations have shown the increase in the reactivity of $AlMe_3$ precursor and formation, when raising the temperature [11].

On the other hand, the number of ALD cycles was seen to have effect on water contact angle. Further increasing the coating layer thickness significantly increased the water contact angles of the coated membranes regardless of the temperatures. For example, a nominal coating thickness of 10 nm, the contact angle was 66° for c100_t70 and 92° for c100_t100, indicating the formation of more hydrophobic surfaces compared to the uncoated membrane. The increase in hydrophobicity with the coating thickness might be due to the accumulation of hydrophobic alkyl residues ($-CH_3$) as the ALD precursor $AlMe_3$ was not completely converted to Al_2O_3. The existence of Al–CH_3 groups can be seen in FTIR spectra (Section 3.1). Furthermore, the increase of surface roughness is known to promote the hydrophobicity of a non-polar surface.

Table 3 presents the surface energy measurement values. It was found that the surface energy was highly correlated to the contact angle – higher surface energy values were observed for membranes with lower contact angles. A closer analysis of the polar and non-polar components of the surface energy revealed that the increase in surface energy for the more hydrophilic membranes was mainly due to their larger polar contribution, whereas the non-polar contribution remained relatively constant. Once again, the increase in polarity may be attributed to the formation of Al–O–Al and Al–OH groups. The decrease in polarity for thicker coating layers may be due to the presence of significant amount of Al–CH_3 groups.

3.5. Bacterial anti-adhesion performance

The attachment of model biofilm forming microorganism, *P. aeruginosa*, onto uncoated and coated membranes was studied in order to demonstrate bacteria repellence performance. The test was only performed for the ALD coated membranes processed at 70 °C because of their more promising surface properties, in comparison to the membranes coated at 100 °C. Fig. 4 presents the number of adhered *P. aeruginosa* cells on uncoated and coated membranes. In general, lower number of the adhered *P. aeruginosa* was detected on ALD coated membrane surfaces compared to the uncoated.

Up to two log units reduction in the number of adhered *P. aeruginosa* was detected on thinner c10_t70 and c50_t70 ALD coatings compared to the uncoated membrane. The thicker ALD coating c100_t70 contained almost equal number of viable cells as it was detected from the uncoated membrane.

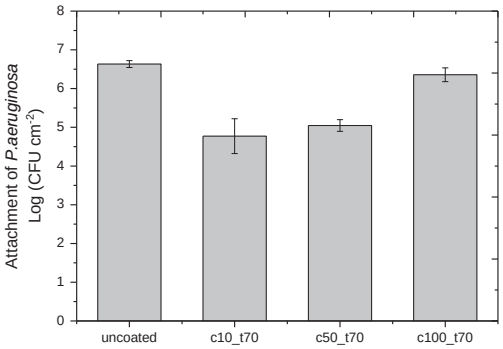

Fig. 4. Attachment of *P. aeruginosa* bacteria on uncoated and ALD coated (70 °C) membranes.

Table 4
Water permeability coefficient (A), salt rejection (R) and salt permeability coefficient (B) of uncoated and coated membranes.

Membrane	Water permeability coefficient (A) [L/m^2 h bar][a]	Salt rejection (R) [%][a]	Salt permeability coefficient (B) [L/m^2 h][a]
Uncoated membrane	4.20 ± 0.11	95.5 ± 2.8	5.50 ± 3.34
c10_t70	4.63 ± 0.42	89.7 ± 4.6	15.05 ± 8.56
c50_t70	4.17 ± 0.56	89.1 ± 2.8	14.24 ± 5.50
c100_t70	1.52 ± 0.37	93.6 ± 2.0	2.98 ± 1.67

[a] Water flux (J_v) and salt rejection (R) of the membranes were evaluated using 10 mM NaCl feed solution and applied pressure of 27.6 bar (400 psi) at 23 °C. The experimental errors represent the standard deviation of three repeated measurements.

ALD coating on the membrane created surface with bacteria repellence performance, most likely due to the altered physiochemical properties of the membrane surface. The decrease in the number of adhered bacteria showed strong correlation between the increase in surface hydrophilicity (Table 3) and the increase in the surface polarity. For example, c10_t70 coating had higher polarity compared (33.4 mN/m) to c50_t70 coating (21.7 mN/m) and, fewer bacteria attached on c10_t70 coating. Moreover, c100_t70 coating and uncoated membrane attracted bacteria in similar quantities and the surface polarity values of these were somewhat equal. In addition, the lower surface roughness of the thinner ALD coatings may have contributed on the attachment of the bacteria as well.

3.6. RO performance

The data obtained from the water flux (J_v) and the salt rejection (R) measurements were used to calculate water (A) and solute (B) permeability. These were used to analyse the effect of coatings on the membrane separation performance. The results are only presented for the ALD coated membranes processed at 70 °C because of their more promising surface properties, in comparison to the membranes coated at 100 °C. Table 4 summarises the values of the water permeability (A), the salt (NaCl) rejection (R) and the salt (NaCl) permeability (B) of uncoated and coated membranes.

Among the ALD coated membranes, the thinner coatings c10_t70 and c50_t70 did not show significant effect on the water permeability. Indeed, c10_t70 was marginally more permeable compared to the uncoated membrane. The sufficient water permeability of c10_t70 membranes could be explained by their hydrophilic character (Table 3) in addition to the low hydraulic resistance due to the thin coating thickness. However, the rejection of these membranes was reduced and their B values were increased as a result of ALD coating. This may indicate possible cake enhanced concentration polarisation in the loose coating layer [34]. Alternatively, the ALD coating may have adversely impacted the rejection layer of the polyamide substrate.

Increase of ALD cycles had a strong effect on RO performance. Almost 65% reduction of A value was measured for the membrane with a much thicker coating (c100_t70). This may be explained by the changes in the rejection layer, such as increase of hydrophobicity and the significant hydraulic resistance of the coating layer. Moreover, the salt permeability was decreased and the salt rejection was increased by the increase of coating thickness. This could be related to a tightening of the coating layer at increased coating thickness.

The trade-off between rejection and water permeability is typical for membrane coating. For example, an additional ALD coating has shown to form a hydraulic resistance layer on a porous polymeric membrane, which has typically decreased water permeability for 50–80% and respectively, increased a solute retention for 10–30% [14,16].

3.7. Implementation of ALD technology into RO membrane manufacturing

In recent years, several research groups have reported investigations on ALD based surface modification of both polymeric membranes and ceramic membranes. The studies have mainly aimed to modify the surface of porous ultrafiltration or microfiltration membranes [14–17]. However, the ALD method has not been applied for modifying RO membranes. Here we determined whether ALD could be a suitable method for the surface modification of RO membrane. In particular, the effect of processing parameters was our interest. Our systematic study investigated the typical Al_2O_3 based ALD process for TFC PA membrane. We deposited Al_2O_3 coating layers with three different ALD cycles (10, 50 and 100) and two different processing temperatures (70 °C and 100 °C).

It was shown that the ALD processing parameters had influence on the membrane performance. In fact, even a low thickness of ALD coating could modify the surface properties of RO membrane by increasing the hydrophilicity and polarity as well as lowering the surface roughness. These properties are essential improvements, especially for anti-fouling and permeability. Based on our first experiments, the ALD technology could be a promising candidate to modify RO membranes. However, the parameters of Al_2O_3 based ALD need further investigations to find the balance between improved anti-fouling and RO performance.

Although the ALD process is mainly carried out in batches in its current state, the development of a slow-speed roll-to-roll ALD technology is underway [35]. Due to the promising results obtained with lower thickness and processing temperature, we expect that the continuous slow-speed roll-to-roll ALD technology could be industrially implemented into the membrane manufacturing.

4. Conclusions

Inorganic $AlMe_3$ based ALD coatings were successfully applied on TFC PA membranes using two different processing temperatures (70 °C and 100 °C) and three different number of ALD cycles (10, 50 and 100). The ALD process parameters had effect on the surface roughness as well as on the hydrophilicity and surface polarity of TFC PA membrane. In general, low temperature and less

ALD cycles provided better RO membrane performance in terms of anti-fouling and permeability. The most hydrophilic surface was obtained with 10 and 50 ALD cycles at temperature 70 °C and 10 ALD cycles at 100 °C. The anti-fouling performance of the membrane was improved by the ALD coatings. The CFU test results indicated that the lowest number of *P. aeruginosa* cells was adhered on the most hydrophilic and polar surface, among the ALD coated membranes. RO tests indicated some effect on the water and salt permeability as well as the salt rejection of the ALD coated membrane. Indeed, RO performance of the TFC PA membrane was affected by the number of ALD cycles (i.e. layer thickness) and the processing temperature. Our further investigations aim to optimise the processing parameters for improved RO performance.

Acknowledgements

The authors acknowledge Tekes (the Finnish Funding Agency for Technology and Innovation) and the VTT Technical Research Centre of Finland due to the financial support of project. Skilful technical assistances of Niina Torttila, Marjo Ketonen and Sini Eskonniemi are acknowledged in the microbiological part, SEM characterisation and the contact angle measurements.

References

[1] H.C. Hemming, Reverse osmosis membrane biofouling, Exp. Therm. Fluid Sci. 14 (4) (1997) 382–391.
[2] C.Y. Tang, T.H. Chong, A.G. Fane, Colloidal interactions and fouling of NF and RO membranes: a review, Adv. Colloid Interface Sci. 164 (2011) 126–143.
[3] J. Nikkola, X. Liu, Y. Li, M. Raulio, H.-L. Alakomi, J. Wei, C.Y. Tang, Surface modification of thin film composite RO membrane for enhanced anti-biofouling performance, J. Membr. Sci. 444 (2013) 192–200.
[4] C.Y. Tang, Y.-N. Kwon, J.O. Leckie, Effect of membrane chemistry and coating layer on physiochemical properties of thin film composite polyamide RO and NF membranes II. Membrane physiochemical properties and their dependence on polyamide and coating layers, Desalination 242 (2009) 168–182.
[5] M. Ulbricht, Advanced functional polymer membranes, Polymer 47 (2006) 2217–2262.
[6] S.M. George, Atomic layer deposition: an overview, Chem. Rev. 110 (2010) 111–131.
[7] R. Puurunen, Surface chemistry of atomic layer deposition: a case study for the trimethylaluminum/water process, J. Appl. Phys. 97 (2005) 121301.
[8] M. Kemell, E. Färm, M. Ritala, M. Leskelä, Surface modification of thermoplastics by atomic layer deposition of Al_2O_3 and TiO_2 thin films, Eur. Polym. J. 44 (2008) 3564–3570.
[9] T. Hirvikorpi, M. Vähä-Nissi, J. Nikkola, A. Harlin, M. Karppinen, Thin Al_2O_3 barrier coatings onto temperature-sensitive packaging materials by atomic layer deposition, Surf. Coat. Technol. 205 (2011) 5088–5092.
[10] G.K. Hyde, G. Scarel, J.C. Spagnola, Q. Peng, K. Lee, B. Gong, K.G. Roberts, K. M. Roth, C.A. Hanson, C.K. Devine, S.M. Stewart, D. Hojo, J. Na, J.S. Jur, G. N. Parsons, Atomic layer deposition and abrupt wetting transitions on nonwoven polypropylene and woven cotton fabrics, Langmuir 26 (2010) 2550–2558.
[11] J.C. Spagnola, B. Gong, S.A. Arvidson, J.S. Jur, S.A. Khan, G.N. Parsons, Surface and sub-surface reactions during low temperature aluminium oxide atomic layer deposition on fiber-forming polymers, J. Mater. Chem. 20 (2010) 4213–4222.
[12] B. Gong, G.N. Parsons, Quantitative in situ infrared analysis of reactions between trimethylaluminum and polymers during Al_2O_3 atomic layer deposition, J. Mater. Chem. 22 (2012) 15672–15682.
[13] B. Gong, J.C. Spagnola, S.A. Arvidson, S.A. Khan, G.N. Parsons, Directed inorganic modification of bi-component polymer fibers by selective vapor reaction and atomic layer deposition, Polymer 53 (2012) 4631–4636.
[14] Q. Xu, Y. Yang, X. Wang, Z. Wang, W. Jin, J. Huang, Y. Wang, Atomic layer deposition of alumina on porous polytetrafluoroethylene membranes for enhanced hydrophilicity and separation performances, J. Membr. Sci. 415–416 (2012) 435–443.
[15] F. Li, L. Li, X. Liao, Y. Wang, Precise pore size tuning and surface modifications of polymeric membranes using the atomic layer deposition technique, J. Membr. Sci. 385–386 (2011) 1–9.
[16] Q. Wang, X. Wang, Z. Wang, J. Huang, Y. Wang, PVDF membranes with simultaneously enhanced permeability and selectivity by breaking the trade off effect via atomic layer deposition of TiO_2, J. Membr. Sci. 442 (2013) 57–64.
[17] F. Li, Y. Yang, Y. Fan, W. Xing, Y. Wang, Modification of ceramic membranes for pore structure tailoring: the atomic layer deposition route, J. Membr. Sci. 397–398 (2012) 17–23.
[18] M.A. Cameron, I.P. Gartland, J.A. Smith, S.F. Diaz, S.M. George, Atomic layer deposition of SiO_2 and TiO_2 in alumina tubular membranes: pore reduction and effect of surface species on gas transport, Langmuir, 16, 2000, 7435–7444.
[19] T. Hirvikorpi, M. Vähä-Nissi, A. Harlin, M. Karppinen, Comparison of some coating techniques to fabricate barrier layers on packaging materials, Thin Solid Films 518 (2010) 5463–5466.
[20] T. Hirvikorpi, M. Vähä-Nissi, A. Harlin, J. Marles, V. Miikkulainen, M. Karppinen, Effect of corona pre-treatment on the performance of gas barrier layers applied by atomic layer deposition onto polymer-coated paperboard, Appl. Surf. Sci. 257 (2010) 736–740.
[21] K. Grundke, Characterization of polymer surfaces by wetting and electrokinetic measurements—contact angle, interfacial tension, zeta potential, in: M. Stamn (Ed.), Polymer Surfaces and Interfaces—Characterisation, Modification and Applications, 1st edition,Springer-Verlag, Berlin Heidelberg, 2008, pp. 103–136.
[22] M. Herzberg, M Elimelech, Biofouling of reverse osmosis membranes: role of biofilm-enhanced osmotic pressure, J. Membr. Sci. 295 (2007) 11–20.
[23] S.B. Sadr Ghayeni, P.J. Beatson, R.P. Schneider, A.G. Fane, Adhesion of waste water bacteria to reverse osmosis membranes, J. Membr. Sci. 138 (1998) 29–42.
[24] M. Klausen, A. Heydorn, P. Ragas, L. Lambertsen, A. Aaes-Jørgensen, S. Molin, T. Tolker-Nielsen, Biofilm formation by *Pseudomonas aeruginosa* wild type, Flagella and type IV Pili Mutants, Mol. Microbiol. 48 (6) (2003) 1511–1524.
[25] H-C. Flemming, J. Wingender, The biofilm matrix, Nat. Rev. Microbiol. 8 (2010) 623–633.
[26] D1141-98 Standard Practise for the Preparation of Substitute Ocean Water, 2008.
[27] Y.N. Wang, C.Y. Tang, Protein fouling of nanofiltration, reverse osmosis, and ultrafiltration membranes—the role of hydrodynamic conditions, solution chemistry, and membrane properties, J. Membr. Sci. 376 (2011) 275–282.
[28] A.G. Fane, C.Y. Tang, R. Wang, Membrane technology for water: microfiltration, ultrafiltration, nanofiltration and reverse osmosis, in: P. Wilderer (Ed.), Treatise on Water Science, Elsevier B.V., USA, 2011, pp. 301–333. (Chapter 4.11).
[29] C.Y. Tang, Y.-N. Kwon, J.O. Leckie, Effect of membrane chemistry and coating layer on physiochemical properties of thin film composite polyamide RO and NF membranes: I. FTIR and XPS characterization of polyamide and coating layer chemistry, Desalination 242 (2009) 149–167.
[30] R.M. Silverstein, F.X. Webster, Spectrometric Identification of Organic Compounds, 6th ed., John Wiley & Sons, Inc., New York, 1997.
[31] N.B. Colthup, L.H. Daly, S.E. Wiberley, Introduction to Infrared and Raman spectroscopy, Academic Press Inc., New York, 1975.
[32] K.C. Khulbe, C.Y. Feng, T. Matsuura, Synthetic Polymeric Membranes—Characterisation by Atomic Force Microscopy, Springer-Verlag, Berlin Heidelberg (2008) 157–167.
[33] N.P. Kobayashi, C.L. Donley, S. Wang, R.S. Williams, Atomic layer deposition of aluminium oxide on hydrophobic and hydrophilic surfaces, J. Cryst. Growth 299 (2007) 218–222.
[34] E.M.V. Hoek, M. Elimelech, Cake-enhanced concentration polarization: a new fouling mechanism for salt-rejecting membranes, Environ. Sci. Technol. 37 (2003) 5581.
[35] T. Hirvikorpi, R. Laine, R.W.M Li, M. Vähä-Nissi, E. Salo, V. Kilpi, S. Lindfors, J. Vartiainen, E. Kenttä, J. Nikkola, A. Harlin, J. Kostamo, Barrier properties of plastic films coated with Al_2O_3 by roll-to-roll ALD, 50th Nordic Polymer Days, NPD 2013, 29–31 May 2013, Book of Abstracts, Society for Wood and Polymer Chemistry in Finland, Helsinki, Finland, 2013, p. 46.

Series title and number

VTT Science 66

Title	**Polymer hybrid thin-film composites with tailored permeability and anti-fouling performance**
Author(s)	Juha Nikkola
Abstract	Composites and hybrid materials are new material combinations which can provide added value for existing products or create novel multifunctional properties. This thesis aimed at fabricating and modifying thin-film composites (TFC) by using various coating technologies. Moreover, the target was to tailor the permeability or to create anti-fouling performance. Inorganic, inorganic-organic and organic coating layers were made by atmospheric plasma deposition (APD), sol-gel (SG), atomic-layer-deposition (ALD) or polyvinyl alcohol (PVA) dispersion coating methods. Coatings were deposited using either roll-to-roll or batch process. APD method was used to create an inorganic silicon oxide (SiOx) coating layer on a low-density polyethylene (LDPE) coated board. In addition, atmospheric plasma was used for pre-treatment of LPDE surface prior SG coatings. The SiOx coatings did not show a significant improvement in barrier performance using the specific roll-to-roll process. Therefore, SG coating method was studied instead in order to form a barrier layer on LDPE-board by using the roll-to-roll process. SG coatings reduced the surface roughness and made the polymer surfaces either hydrophilic or hydrophobic. In addition, the coating chemistry had an effect on the oxygen and grease barrier performances. The highly cross-linked SG coating gave a better oxygen barrier performance, while the other SG coating revealed an enhancement in the grease barrier. Plasma activation of the LDPE surface enhanced the wettability and adhesion of both SG coatings. In addition, SG coating was applied on a polylactic acid (PLA) coated board. The SG coating created favourable, smooth and hydrophilic primer layer on PLA-board, which was further coated with an inorganic aluminium oxide (Al_2O_3) skin layer by using ALD. The particular TFC structure based on ALD and SG coatings gave a slightly better barrier performance compared to a plain ALD coating. PVA and ALD based anti-fouling coatings increased the hydrophilicity and surface polarity of the polyamide (PA) TFC membranes. All the coated membranes indicated an enhancement in bacteria-repellence. Indeed, the improvement in the bacterial anti-adhesion performance of coated membranes was due to an increase in surface polarity. The biocide-modified PVA coatings enhanced further the anti-fouling performance due to their antimicrobial activity. As expected, in comparison to the uncoated membrane, the PVA-coated membranes tend to increase the salt rejection and to reduce the water and salt permeability. However, the biocide-modified PVA coatings decreased the water permeability and showed also a minor decline on the salt rejection. The ALD coatings increased the water and salt permeability and furthermore, reduced the salt rejection.
ISBN, ISSN	ISBN 978-951-38-8163-4 (Soft back ed.) ISBN 978-951-38-8164-1 (URL: http://www.vtt.fi/publications/index.jsp) ISSN-L 2242-119X ISSN 2242-119X (Print) ISSN 2242-1203 (Online)
Date	October 2014
Language	English
Pages	84 p. + app. 56 p.
Name of the project	
Commissioned by	
Keywords	Thin-film composite, hybrid, permeability, anti-fouling
Publisher	VTT Technical Research Centre of Finland P.O. Box 1000, FI-02044 VTT, Finland, Tel. 020 722 111

Polymer hybrid thin-film composites with tailored permeability and anti-fouling performance

Economic pressures and competition have created a need for superior performance and multifunctional properties of materials. The ever-increasing demand for new product properties makes it challenging to achieve the required features when using traditional materials. Therefore, new material combinations (i.e. hybrid or composite materials) are intended to meet these challenges. Composites and hybrid materials are new material combinations which can provide added value for existing products or create novel multifunctional properties.

This thesis aimed at fabricating and modifying thin-film composites (TFC) by using various coating technologies. Moreover, the target was to tailor the permeability or to create anti-fouling performance. Inorganic, inorganic-organic and organic coating layers were made by atmospheric plasma deposition, sol-gel, atomic-layer-deposition (ALD) or polyvinyl alcohol (PVA) dispersion coating methods. Coatings were deposited using either roll-to-roll or batch process.

The scientifically novel contribution of this thesis is as follows. The thesis contributes to the development of novel TFC structures using various coating methods. The novel TFC structures provide new alternatives or improvements for the existing barrier materials in food packaging. In addition, the developed anti-fouling coatings tackle the critical challenge of membrane fouling and introduce new low-fouling TFC membranes for water treatment.

ISBN 978-951-38-8163-4 (Soft back ed.)
ISBN 978-951-38-8164-1 (URL: http://www.vtt.fi/publications/index.jsp)
ISSN-L 2242-119X
ISSN 2242-119X (Print)
ISSN 2242-1203 (Online)